NASA-CR-175665

NASA-CR-175665
19850015958

N85 24269

COMET

LIBRARY COPY

JUN - 2 1997

LANGLEY RESEARCH CENTER
LIBRARY NASA
HAMPTON, VIRGINIA

NF00723

A Service of:

National Aeronautics and Space Administration

Scientific and Technical Information Program Office
Center for AeroSpace Information

NOTICE

THIS REPRODUCTION WAS MADE FROM THE BEST AVAILABLE COPY OF WHICH A NUMBER OF PAGES WERE OF POOR REPRODUCTION QUALITY.

JPL PUBLICATION 85-2

(NASA-CR-175665) GEOMETRIC ERROR ANALYSIS FOR SHUTTLE IMAGING SPECTROMETER EXPERIMENT (Jet Propulsion Lab.) 172 p EC A08/MF A01 CSCL 14B
N85-24269
Unclas
G3/35 14802

Geometric Error Analysis for Shuttle Imaging Spectrometer Experiment

Shyh Jong Wang
Che-Hang Charles Ih

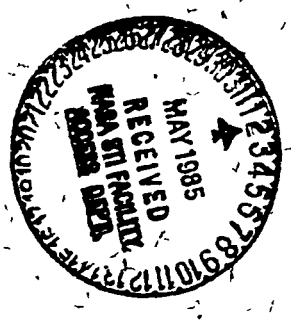

December 15, 1984

National Aeronautics and Space Administration

Jet Propulsion Laboratory
California Institute of Technology
Pasadena, California

JPL PUBLICATION 85-2

Geometric Error Analysis for Shuttle Imaging Spectrometer Experiment

Shyh Jong Wang
Che-Hang Charles Ih

December 15, 1984

National Aeronautics and
Space Administration

Jet Propulsion Laboratory
California Institute of Technology
Pasadena, California

The research described in this publication was carried out by the Jet Propulsion Laboratory, California Institute of Technology, under a contract with the National Aeronautics and Space Administration

Reference herein to any specific commercial product, process, or service by trade name, trademark, manufacturer, or otherwise, does not constitute or imply its endorsement by the United States Government or the Jet Propulsion Laboratory, California Institute of Technology

Acknowledgements

The authors wish to express their gratitude to Y. H. Lin and J. M. Cameron for their contributions at the early stage of this work, and to M. Herring, P. N. Kupferman, and J. B. Wellman for their support.

ABSTRACT

The demand of more powerful tools for remote sensing and management of earth resources has been steadily increasing over the last decade. With the recent advancement of area array detectors, high resolution multichannel imaging spectrometers can be realistically constructed.

This report documents the error analysis study for the Shuttle Imaging Spectrometer Experiment system for the purpose of providing information for design, tradeoff, and performance prediction.

Error sources including the Shuttle attitude determination and control system, instrument pointing and misalignment, disturbances, ephemeris, earth rotation, etc., have been investigated. Geometric error mapping functions were developed, characterized, and illustrated extensively with tables and charts. Selected ground patterns and the corresponding image distortions have been generated for direct visual inspection of how the various error sources affect the appearance of the ground object images.

TABLE OF CONTENTS

List of Illustrations

Page

List of Tables

I. INTRODUCTION

A. BACKGROUND

Earth resource management and utilization have experienced great success over the last decade through the Landsat programs. In more recent years, both NASA and user communities have envisioned the need for development of better and more powerful instruments for surveying and managing earth resources. The Landsat D's new sensor, Thematic Mapper (TM), the proposed utilization of Tracking and Data Relay Satellite System (TDRSS), and a more advanced ground system represent an advancement in the earth resource satellite development [1].

The Thematic Mapper of the Landsat D (launched in 1982) has seven spectral bands, two more than those of the Multispectral Scanner associated with the earlier Landsats. However, study shows that the reflectance spectrum of earth surface materials contains a significant amount of information which can only be identified with spectral resolution much finer than those of the Thematic Mapper [2]. With the advancement of area array detectors, a push broom imaging spectrometer can be realistically constructed for simultaneous imaging and registration of hundreds of spectral bands. For the case of Shuttle Imaging Spectrometer Experiment, 128 spectral channels have been proposed to cover the spectral range of 0.4 to 1.0 μm for VNIR (visible and near infrared) and 1.0 to 2.5 μm for SWIR (short-wavelength infrared) with instantaneous field of view of 30m. Table 1 shows the required sensor performance [2].

The purpose of this report is to document the error analysis study for the imaging spectrometer experiment. Error analysis is an important aspect of the overall remote sensing system, since errors from many sources, including

the spectrometer itself, the spacecraft that carries the instrument, knowledge limitations on the true spacecraft attitude and locations, earth rotation, curvature, and terrain variations, etc., will all contribute to image distortion, shift, rotation, and misregistration. Error correction or compensation are necessary and are an integral part of the image processing. This work covers the analysis of fundamental and geometric errors and error sensitivities, the development of geometric mapping functions, and the computation of ground

Table 1. Sensor Performance Requirements

Parameter	Value	Comments
Spectral Coverage	0.4 to 2.5 μm	Although the entire spectrum is probably not required for any one discipline, in the aggregate of all remote sensing disciplines, the entire region is required
Spectral Sampling Interval		
VNIR (0.4 to 1.0 μm)	0.01 μm or better	
SWIR (1.0 to 2.5 μm)	0.02 μm or better	
Instantaneous Field of View	30 m	Adequate for most research topics
Swath Width	at least 10-12 km	This is adequate for research if pointing capability is provided to assure target access
Pointing Mirror Range		
Along track	at least $\pm$ 45 deg	Essential for atmospheric and BRDF (Bidirectional Reflectance Distribution Function) Studies
Cross track	not more than $\pm$ 25 deg	
Radiometric Performance (NEdR)		
VNIR	$\leq$ 0.5%	
SWIR	$\leq$ 1.0%	

pattern distortions. The results are translated into many tables, plots, and patterns for visual apprehension. It is believed that the results reported here are important for design, trade-off, and performance prediction.

B. APPROACH

This study has been performed in four progressive stages as shown in block diagram form in Fig. 1. In Stage I, the error sources were identified, dynamic disturbances and the Space Shuttle error dynamics were modeled, and the error power spectral densities for two in-orbit configurations were developed. Stage II of this study concentrated on the development of geometric error mapping functions and error sensitivity analysis. Geometric errors due to ephemeris uncertainties, attitude deviations, earth rotation, etc., were studied. In Stage III, ground pattern image distortions caused by various error effects and forward and side looking angular offsets, altitude change, and effect of earth rotation were generated. Stage IV consists of the analysis of the imaging spectrometer instrument errors. These errors include optical jitter, nonlinearities, processing errors, and repeatability. The study of Stages I, II, and III has been completed and the results are included in this report. The study called for by Stage IV has not been planned. It is emphasized here that the imaging spectrometer error model development is an important step for the overall performance prediction and design of the imaging spectrometer system.

Major findings of this work are summarized in the following subsection. In Section II, the orbital and imaging spectrometer configurations are described. The attitude dynamics and error power spectral densities are documented in Section III; and parametric analysis of geometric errors are treated in Section IV. Section V deals with the ground pattern image distortions. Conclusions are summarized in Section VI.

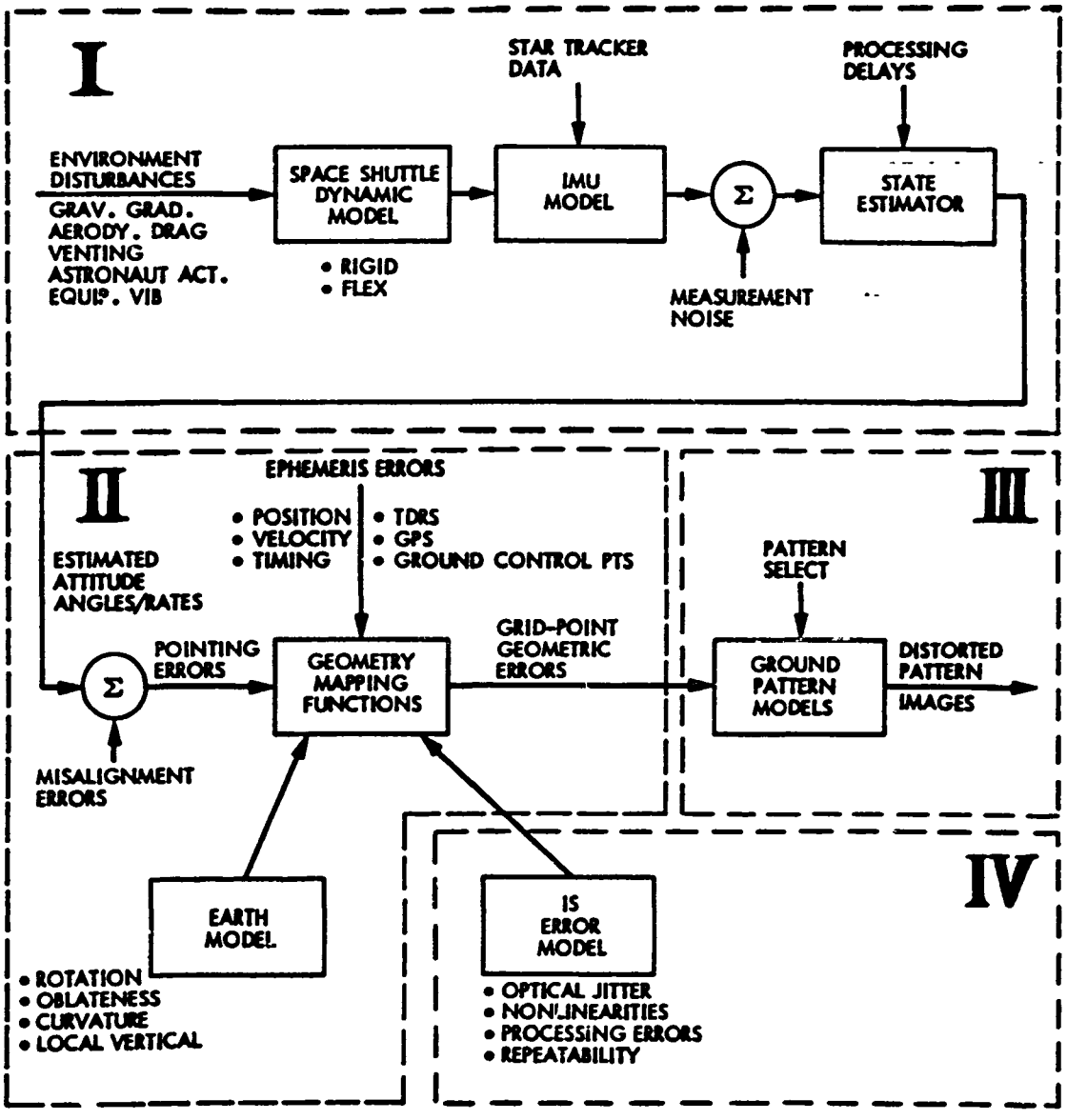

Figure 1. IS Error Analysis System Block Diagram

C. SUMMARY OF MAJOR FINDINGS

The following is a summary of major findings. The details of these are treated in the sections to follow.

1. The results show that the IS Experiment with image pickup period of 20 seconds at a time is feasible with the shuttle properly phased inside the control deadband. The error PSD (power spectral density) characteristic reveals that the system resonates at very low frequencies (in the 10^{-5} to 10^{-2} Hz region). Excitations at these frequencies must be avoided through design precautions. The analysis also showed that errors below 0.01 Hz are dominated by the shuttle dynamics reacting to disturbances, whereas those above 0.01 Hz are dominated by the shuttle inertial measurement system uncertainties and its inherent noise. These high frequency errors limit pointing performance and result in a one-sigma ground track error of 54.8 meters per axis. One-sigma rate errors are shown to be less than 4 meters per second per axis in the frequency range of 10^{-5} to 4×10^{-2} Hz. The image smear is not significant because of the short millisecond-level line time.
2. The effects of earth curvature are very small for the application here (see Fig. 42).
3. Altitude uncertainties cause only moderate geometric errors. The worst 1σ geometric errors are 11.71 m in position and 0.133 m/sec in rate with STDN and large unmodeled perturbations at 200 km orbit. The performance improves with TDRSS. For the 300 km orbit and with small unmodeled perturbations, the 1σ geometric errors will reduce to 0.22m and 0.0032 m/sec (see Table 11).

4. The effects of other navigation errors are significantly greater. The 1σ downtrack errors range from 203m (300 km orbit) to 8128m (200 km orbit); and those for the crosstrack are 152m to 508m (see Table 12).

5. The effects of roll and pitch attitude errors are relatively large compared with, for instance, those caused by yaw errors and altitude uncertainties. The error sensitivity is 1.94 m/arc sec or approximately 7000 m/degree. The yaw sensitivity is 0 for 0° view angle and 0.028 m/arc sec for the maximum view angle of $\pm 0.825^{\circ}$ (see Table 13).

6. The error sensitivities of attitude errors increase significantly for large attitude offsets. For 20° side looking, the sensitivity increases to 2.28 m/arc sec for roll errors and to 0.75 m/arc sec for yaw errors and the pitch error sensitivity is almost unaffected. For the 45° forward looking case, the sensitivities for the pitch, roll, and yaw errors increase to 2.83, 4.36, and 1.97 m/arc sec, respectively (see Table 13).

7. The performance of the Shuttle Imaging Spectrometer is limited by the Shuttle IMU (Inertial Measuring Unit) accuracy, instrument misalignment, etc., Shuttle RCS (Reaction Control Subsystem) deadband, etc. unless some means of error reduction are employed. For instance, ground control points may be used to reduce navigation prediction errors; and precision point mounts, such as AGS (ASPS* Gimbal System) and IPS (Instrument Pointing System), may be used to reduce the

*Annular Suspension Pointing System

attitude errors.

The single axis geometric errors due to the combined Shuttle/IS misalignment, for instance, for normal nadir pointing, 20° side looking, and 45° forward looking are 169m, 198m, and 379m, respectively (refer to Table 10 for detailed breakdowns).

8. Earth rotation causes shifts of images toward the direction of rotation. The magnitude of this shift depends on the latitude of the object. For instance, at the equator the object moves approximately 462m in one second (for 400 km orbit), and at 60° latitude it moves only 231m in one second.

II. ORBITAL AND IMAGING SPECTROMETER CONFIGURATIONS

A. SHUTTLE NOMINAL FLIGHT CONFIGURATIONS

Two shuttle in-orbit configurations have been considered, the Payload-Bay Nadir and the Nose-Down Nadir, as illustrated in Figures 2 and 3, respectively. It will be shown later that the Nose-Down Configuration is gravity gradient stabilized and the Payload-Bay Nadir Configuration is not. However, the Payload-Bay Nadir Configuration offers simpler instrument mounting and less aerodynamic drag. Besides, for certain experiments that require large forward looking angles, the Nose-Down Configuration will be unsuitable.

A circular orbit of 400 km altitude has been selected for this analysis. This selection is consistent with the SIS-B parameters.*

There are a number of possible instrument mounting options that will affect the pointing and the geometric errors of the instrument. These options include:

a) Direct mount

b) AGS (ASPS Gimbal System) mount

c) IPS (Instrument Pointing System) mount

Since both the AGS and IPS systems are capable of providing precision payload pointing and measurements, the system performance will be improved at the expense of significant extra cost. The direct mount approach is the least complex and most cost effective, provided that the errors are within the tolerance. In this report the direct mount approach is considered. Furthermore, the shuttle IMU

*During the period when this part of the work was performed, SIS-B (Shuttle Imaging Spectrometer-Configuration B) was considered. However, the methods used here are mostly generic, and hence, can be applied to systems of similar configurations.

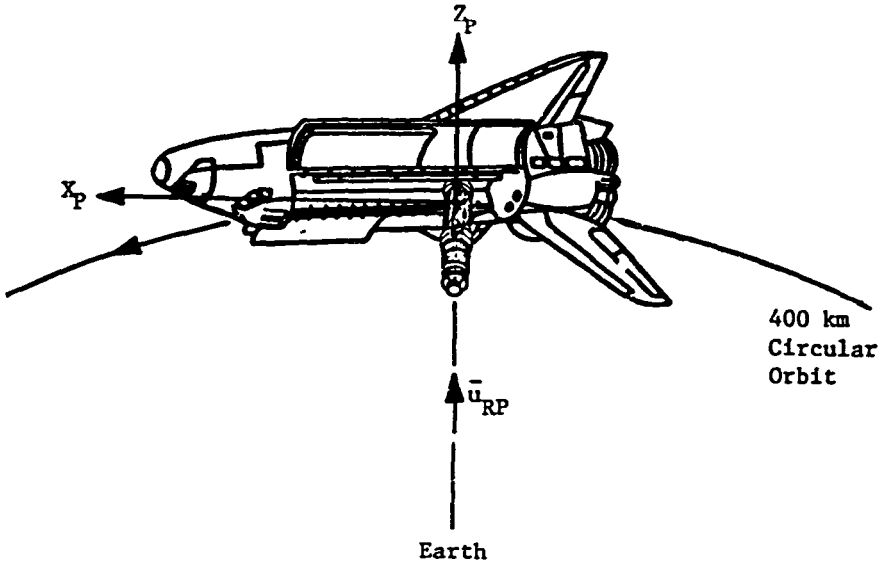

Figure 2. Payload-Bay Nadir Pointing Configuration (A)

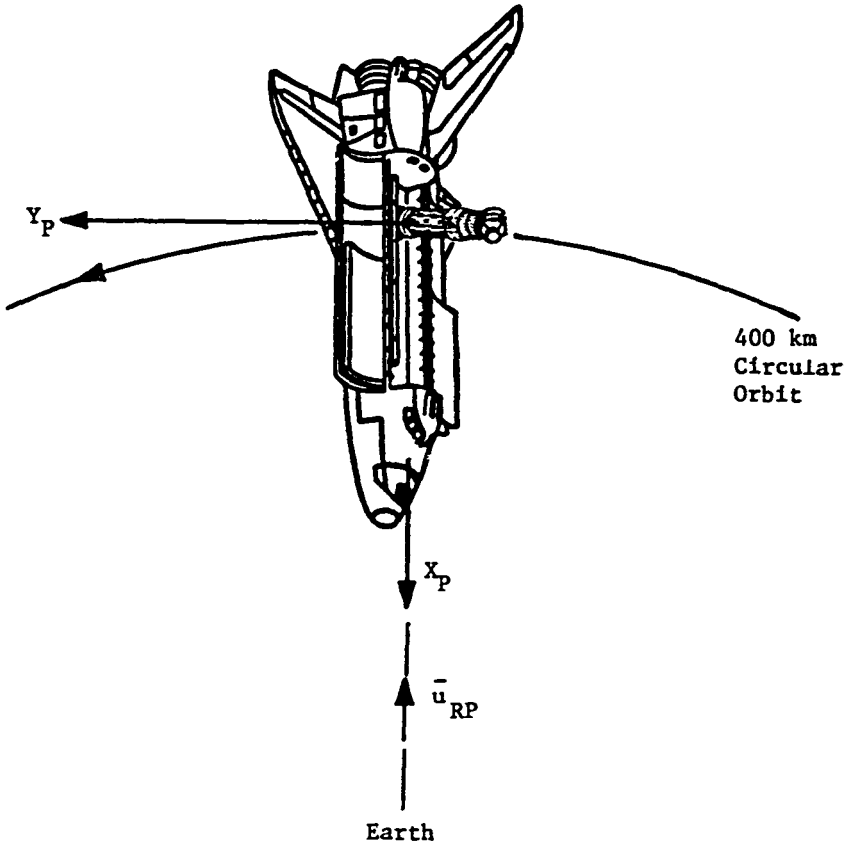

Figure 3. Nose-Down Nadir Pointing Configuration (B)

(Inertial Measurement Unit) and the shuttle state estimator unit are used for obtaining attitude and rate information, without additional instrumentation. Other options may be studied in the future if necessary.

B. IMAGING SPECTROMETER SYSTEM DESCRIPTION

In order to correlate the analysis reported here to the IS applications, it is desirable to understand the basic operating principle of the IS instrument. Figure 4 shows a sketch of the basic elements of the IS, except the memory banks, registers, and the processors. Some of the IS parameters that are relevant to the geometric error analysis, along with definitions of the IS terminologies, are also listed in Fig. 4. It is understood that the sketch and the parameter values used are for illustrative purposes only since the parameters may change as the development of the IS system is finalized.

Referring to Fig. 4, as the reflection from the ground objects passes through a narrow slit, it strikes the incident surface of the prism. The prism separates the incident light into spectral images projected onto an area array of light detectors. The area array consists of 384 linear arrays, corresponding to 384 spectral channels. Each linear array consists of 384 detector elements. Each detector element corresponds to an image area of 30m x 30m on the ground. Hence, each linear array corresponds to an image of a specific spectral channel of the same ground area of 30m (along-track) x 11520m (cross-track). This 11.52 km cross-track measure, referred to as the swath width, defines the IS coverage for each orbit pass. The 30m x 30m area is referred to as the pixel (picture element) which defines the resolution of the image, i.e., within this element no features can be resolved. The IS is operated based on a push broom principle. That is, a specific detector element on the instrument (moving with the spacecraft) collects photons from the 30m x 30m moving window for a specific period

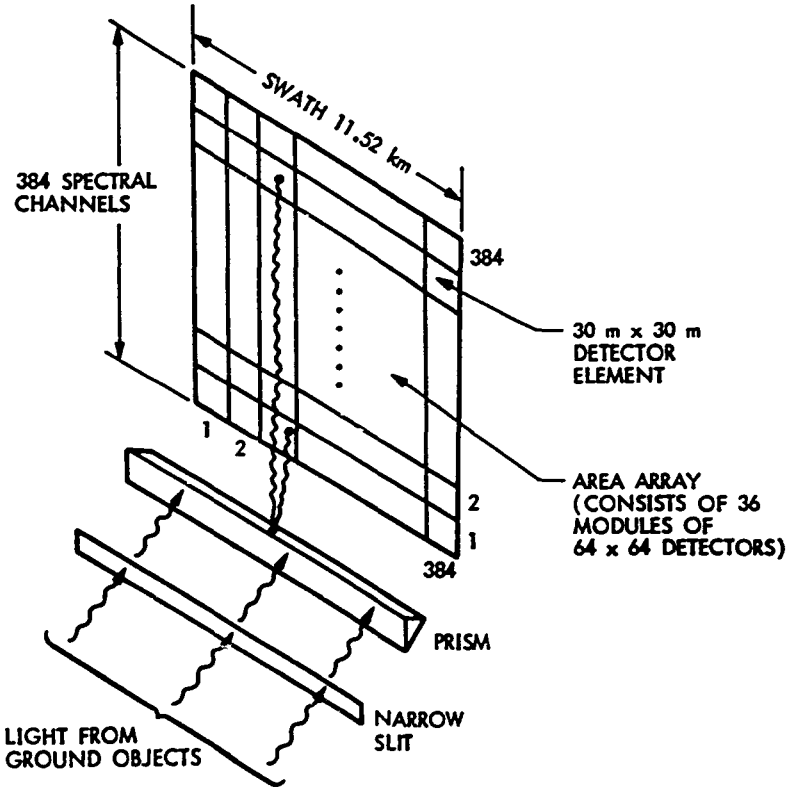

KEY PARAMETERS

- LINE TIME = 4 ms
- SPECTRUM:
  VISIBLE REGION 0.4 - 1.0 μm
  SHORT WAVELENGTH IR 1.0 - 2.5 μm
- FIELD OF VIEW: ± 0.825°
- SWATH WIDTH: 11.52 km
- POINTING ANGLES (RANGE):
  ± 45° (PITCH)
  ± 20° (ROLL)
- ORBIT: 400 km CIRCULAR

DEFINITIONS

GIFOV (GROUND INSTANTANEOUS FIELD OF VIEW): PROJECTION ON THE GROUND OF EACH SQUARE DETECTOR

LINE TIME: TIME TO MOVE ALONG THE GROUND A DISTANCE OF 1 GIFOV

DN: DATA NUMBER, THE "BRIGHTNESS" OF OF THE ASSOCIATED PIXEL

PIXEL: PICTURE ELEMENT (30 m x 30 m HERE, IT DEFINES THE RESOLUTION OF THE IMAGE)

SWIR: SHORT WAVE LENGTH IR

VIS: VISIBLE WAVE LENGTH

Figure 4. Imaging Spectrometer Basic Operating Principles

of time called the line time. The line time in this case is the time required to move 30m along-track,which is determined by the orbit. For a 400 km circular orbit, it is about 4 ms. At the end of each line time, the total number of photons collected by each detector is recorded and processed and the detector/ register is reset and a new 4 ms cycle is repeated. For digital processing, the amount of light collected by a collector is assigned a number called DN (data number), which is proportional to the number of photons accumulated. Therefore, the processor has to record and process 384 x 384,or approximately 1.475×10^5 DN's every 4 ms.

As the shuttle flies over an area, banks after banks of DN's are collected. By spacing the banks of DN's 30m apart, the features of the ground image emerge. The ratios of the DN's of various channels for the same area are of special interest, as these ratios are closely correlated to geological and ecological states of the earth including mineral deposits, forestry, crops,

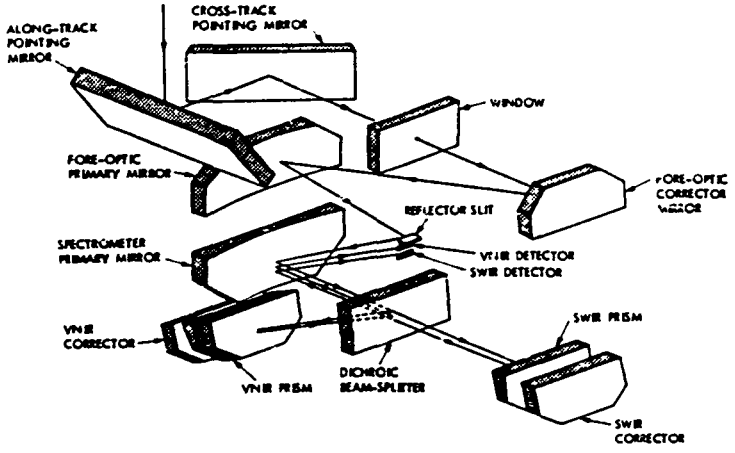

Figure 5. Shuttle Imaging Spectrometer Optical System Configuration

disease and insect infestations, land and soil erosion, precipitation in the form of snow and ice, air and water quality, etc.

The Imaging Spectrometer optical system configuration and the arrangement of lenses, mirrors, slit, prisms, focal plane detector, etc. are shown in Fig.5 [2]. Additional information on the instrument design and requirements can be found in Refs. 2 and 3.

III. ERROR SOURCES AND SHUTTLE ATTITUDE DYNAMICS

A. ERROR SOURCES

There are two types of errors that are important to the imaging spectrometer experiment — the direct errors and the derived errors. The direct errors are those pertaining to the spacecraft and instrument pointing, ephemeris, and instrument errors as shown in Fig. 6. The derived errors are the geometric errors and pattern distortions of ground objects which result from the direct errors and the effects of earth rotation, curvature, oblateness, and local vertical uncertainties. Fig. 1 shows relationships of the error sources and the system dynamics.

- ATTITUDE DEVIATIONS, RATE ERRORS AND STRUCTURAL VIBRATION
- MEASUREMENT NOISE AND DRIFT
- MISALIGNMENT OF SHUTTLE IMU AND ATTITUDE REFERENCE FRAME
- MISALIGNMENT BETWEEN SHUTTLE AND IS INSTRUMENT REFERENCES
- EPHEMERIS PREDICTION ERRORS
- EARTH ROTATION, CURVATURE, AND OBLATENESS
- IS INSTRUMENT ERRORS INCLUDING
  - OPTICAL JITTER
  - NONLINEARITIES
  - PROCESSING
  - REPEATABILITY

Figure 6. Error Sources

In this section, the steady state analysis is performed in the frequency domain. The PSD (power spectral density) for the pointing errors and the rate errors were obtained by considering the dynamics of the Space Shuttle Orbiter, the IMU (Inertial Measurement Unit), the attitude control state estimator, the measurement noise, the misalignment of reference frames, and the disturbances including gravity gradient, gyroscopic torques, and aerodynamic drag torques.

B. SHUTTLE MASS PROPERTY

The shuttle mass properties employed here were obtained from the Shuttle Operational Data Book [4] for OV-102/STS-3. The mass and the c.m. are, respectively:

Shuttle mass: 102,153.73 kg (224,738.21 lbs)

Shuttle c.m.: $X_o = 1105.5"$, $Y_o = 0$, $Z_o = 374.3"$

where the coordinates X_o, Y_o, and Z_o are the Orbiter Coordinates [5] defined in Figure 7. The moment of inertia matrix ($kg\text{-}m^2$) is, in the shuttle body frame (refer to Fig. 8),

$$I_B = \begin{bmatrix} 1.36 \times 10^6 & -4.69 \times 10^3 & -3.49 \times 10^5 \\ -4.69 \times 10^3 & 1.00 \times 10^7 & -3.32 \times 10^3 \\ -3.49 \times 10^5 & -3.32 \times 10^3 & 1.05 \times 10^7 \end{bmatrix}$$

$$\simeq \begin{bmatrix} 1.36 \times 10^6 & 0 & -3.49 \times 10^5 \\ 0 & 1.00 \times 10^7 & 0 \\ -3.49 \times 10^5 & 0 & 1.05 \times 10^7 \end{bmatrix} \qquad (1)$$

The magnitude of the off-diagonal terms of the inertia matrix I_B suggests strong couplings exist especially between the X_B- and the Z_B-axis. To simplify the dynamic equations, it is convenient to consider principal-axis

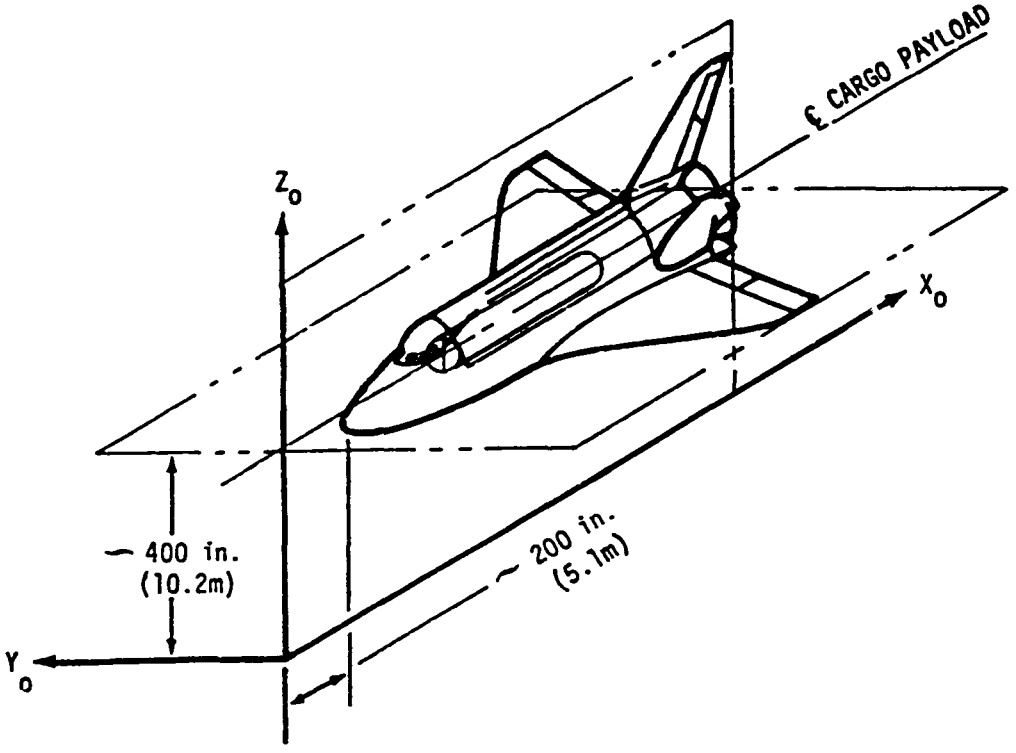

ORBITER COORDINATES

TYPE: Rotating, Orbiter referenced

ORIGIN: Approximately 200 inches (5.1m) ahead of the nose and approximately 400 inches (10.2m) below the centerline of the cargo bay

ORIENTATION AND LABELING:

The X-axis is parallel to the centerline of the cargo bay, negative in the direction of launch

The Z-axis is positive upward in landing attitude

The Y-axis completes the right-handed system

The standard subscript is 0

Figure 7. Orbiter Coordinate System

pointing instead of body-axis pointing, e.g., pointing $-Z_p$ rather than $-Z_B$ as illustrated in Figure 8.

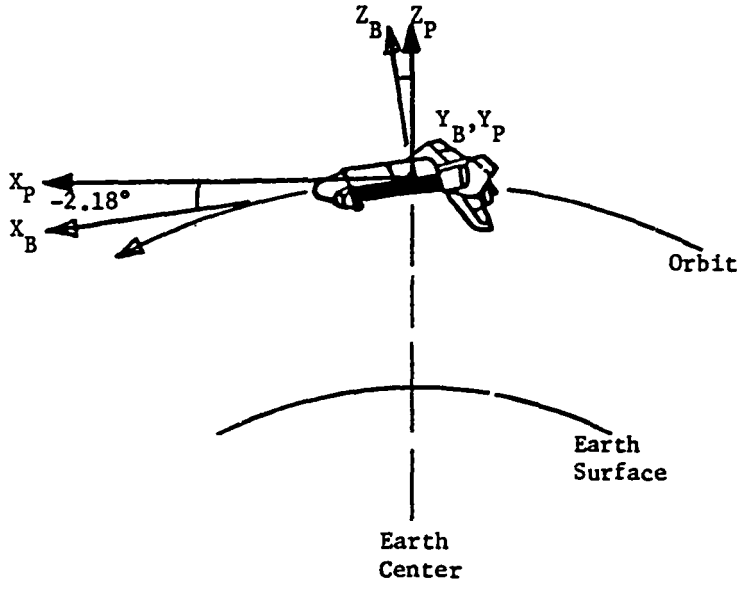

(X_B, Y_B, Z_B) -- Shuttle Body Coordinates

(X_P, Y_P, Z_P) -- Shuttle Principal Axes

Figure 8. Shuttle Body and Principal Coordinates (Payload-Bay Nadir Pointing Shown)

The orientations of the principal axes can be determined by rotating the body frame an angle α about the Y_B-axis, i.e., let B: $X_B \rightarrow X_p$, then

$$B = \begin{bmatrix} \cos\alpha & 0 & -\sin\alpha \\ 0 & 1 & 0 \\ \sin\alpha & 0 & \cos\alpha \end{bmatrix} \qquad (2)$$

and

$$I_P = B\, I_B\, B^T \qquad (3)$$

It can be shown that

$$\alpha = \frac{1}{2} \tan^{-1} \left(\frac{-2\, I_{BXZ}}{I_{BZZ} - I_{BXX}} \right) \qquad (4)$$

provided that $I_{BXY} = I_{BYZ} = 0$.

For $I_{BXX} = 1.36 \times 10^6$ kg-m^2, $I_{BZZ} = 1.05 \times 10^7$ kg-m^2, and $I_{BXZ} = 3.49 \times 10^5$ kg-m^2, the angle $\alpha = -2.18^\circ$. Therefore, in order to do principal-axis nadir pointing, the shuttle has to rotate 2.18° about the orbit normal (see Figure 8). The moments of inertia about the principal axes are

$$\tilde{I}_p = \text{diag}\ (1.38 \times 10^6,\ 1.00 \times 10^7,\ 1.05 \times 10^7),\ \text{kg-m}^2.$$

C. ASSESSMENT OF DISTURBANCES

The shuttle motion is characterized in part by the environmental disturbances, the major sources of which are the aerodynamic drag, gravity gradient, gyroscopic effect, solar radiation, and on-board causes such as astronaut activities, equipment vibrations, and venting. On-board activities may be partially eliminated or reduced through mission planning and their effects will be assessed in the future. In this subsection, the gyroscopic torques, the gravity gradient torques, and the aerodynamic drag torques are estimated. The solar pressure is at least one order of magnitude less than the aerodynamic drag forces and, hence, it is not included in this analysis.

C.1 The Aerodynamic Drag Torques

To estimate the aerodynamic drag torques, an approach referred to as the three-plate model [6] has been used. Referring to Figure 9, let $\bar{n}_1$, $\bar{n}_2$, and $\bar{n}_3$ be the unit normal vectors for the equivalent plates 1, 2, and 3. Where $\bar{n}_1$, $\bar{n}_2$, and $\bar{n}_3$ are in the direction of X_B-, Y_B-, and Z_B-axis, respectively. To express $\bar{n}_i$ in body frame,

$$\bar{n}_1 = \begin{bmatrix}1\\0\\0\end{bmatrix}, \bar{n}_2 = \begin{bmatrix}0\\1\\0\end{bmatrix}, \bar{n}_3 = \begin{bmatrix}0\\0\\1\end{bmatrix} \tag{5}$$

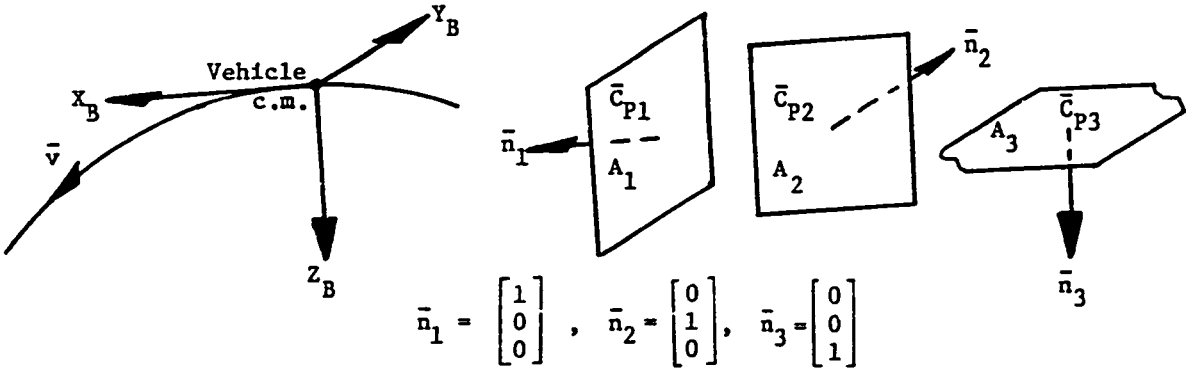

$$\bar{n}_1 = \begin{bmatrix}1\\0\\0\end{bmatrix}, \bar{n}_2 = \begin{bmatrix}0\\1\\0\end{bmatrix}, \bar{n}_3 = \begin{bmatrix}0\\0\\1\end{bmatrix}$$

Figure 9. The Three-Plate Aerodynamic Model in Body Frame

Let A_1, A_2, and A_3 be the corresponding areas on which the aerodynamic pressure applies, and $\bar{C}_{P1}$, $\bar{C}_{P2}$, and $\bar{C}_{P3}$ the three corresponding centers of pressure, respectively. The model assumes that the aerodynamic force applies to each area in the direction opposite to the vehicle velocity vector and assumes no shading among the plates. It is further assumed that the drag coefficient C_D is constant and the lift coefficient C_L is zero.

Let $\bar{v}_B = (v_{B1}, v_{B2}, v_{B3})^T$ be the inertial velocity vector in the body frame, with magnitude v. The force and torque applied on A_i are

$$\bar{F}_{Bi} = -\left(\tfrac{1}{2} C_D \rho v^2 A_i\right) \left|(\bar{n}_i, \bar{u}_B)\right| \bar{u}_B \tag{6}$$

$$\bar{T}_{Bi} = \bar{r}_{Bi} \times \bar{F}_{Bi} = -\left(\tfrac{1}{2} C_D \rho v^2 A_i\right) \left|(\bar{n}_i, \bar{u}_B)\right| \bar{r}_{Bi} \times \bar{u}_B \tag{7}$$

where ρ is the atmospheric density at the orbital altitude, $\bar{u}_B = \bar{v}_B/v$ the unit velocity vector, and r_{Bi} the vectors of the center of pressure of A_i relative to the vehicle center of mass.

The total aerodynamic forces and torques on the vehicle are

$$\bar{F}_B = \sum_{i=1}^{3} -\left(\tfrac{1}{2} C_D \rho v^2 A_i\right) \left| \left(\bar{n}_i, \bar{u}_B\right) \right| \bar{u}_B \tag{8}$$

$$\bar{T}_B = \sum_{i=1}^{3} -\left(\tfrac{1}{2} C_D \rho v^2 A_i\right) \left| \left(\bar{n}_i, \bar{u}_B\right) \right| \bar{r}_{Bi} \times \bar{u}_B \tag{9}$$

The value of C_D depends on the shape of the vehicle. In Ref. 7, the values of 2.5 to 3.0 were suggested. The value of $C_D = 2.0$ is used here as it was used in Ref. 6 for Space Shuttle Simulation.

The atmospheric mass density ρ can be found in a JPL internal memorandum. For 1985 mission time, the peak density is expected to occur in April for the 400 km orbit; the densities are

2.64×10^{-12} kg/m^3 (predicted)

and

3.77×10^{-12} kg/m^3 (97.7 percentile)

The orbital velocity v for a 400 km circular orbit is computed as $v = 7669.60$ m/sec or $v^2 = 5.882 \times 10^7$ (m/sec)^2.

The plate areas, according to the attachment (SSFS On-Orbit Aero Data, 7/24/80) to Ref. 6, with Cargo Bay doors open, are

$$\begin{aligned} A_1 &= 119.45 \text{ m}^2 \\ A_2 &= 229.92 \text{ m}^2 \\ A_3 &= 454.46 \text{ m}^2 \end{aligned} \tag{10}$$

However, a different set of values are given in Ref. 8.

$$\begin{aligned} A_1 &= 64.1 \text{ m}^2 \\ A_2 &= 212.7 \text{ m}^2 \\ A_3 &= 367.0 \text{ m}^2 \end{aligned} \tag{11}$$

The values in (10) were used in this work.

The position vectors $\bar{r}_{Bi}$ may be obtained using data given in Ref. 4 and Ref. 6. The values are,

$$\bar{r}_{B1} = \begin{bmatrix} 3.797 \\ 0 \\ -.231 \end{bmatrix} \text{ m}$$

$$\bar{r}_{B2} = \begin{bmatrix} .927 \\ 0 \\ -.742 \end{bmatrix} \text{ m} \qquad (12)$$

$$\bar{r}_{B3} = \begin{bmatrix} 1.166 \\ 0 \\ -1.074 \end{bmatrix} \text{ m}$$

The torques $\bar{T}_{Bi}$ for the predicted density, are

$$\bar{T}_{B1} = -1.855 \times 10^{-2} |u_{B1}| \begin{bmatrix} -r_{B13}u_{B2} + r_{B12}u_{B3} \\ r_{B13}u_{B1} + r_{B11}u_{B3} \\ -r_{B12}u_{B1} + r_{B11}u_{B2} \end{bmatrix}$$

$$\bar{T}_{B2} = -3.570 \times 10^{-2} |u_{B2}| \begin{bmatrix} -r_{B23}u_{B2} + r_{B22}u_{B3} \\ r_{B23}u_{B1} - r_{B21}u_{B3} \\ -r_{B22}u_{B1} + r_{B21}u_{B2} \end{bmatrix} \qquad (13)$$

$$\bar{T}_{B3} = -7.057 \times 10^{-2} |u_{B3}| \begin{bmatrix} -r_{B33}u_{B2} + r_{B32}u_{B3} \\ r_{B33}u_{31} - r_{B31}u_{B3} \\ -r_{B32}u_{Bi} + r_{B31}u_{B2} \end{bmatrix}$$

In Eq. (13), the torques are known once the unit velocity vector $\bar{u}_B$ is specified; $\bar{u}_B$ varies with the pointing configuration and spacecraft attitude.

C.1.1. Drag Torques for Configuration A

Referring to Fig. 2, since this is "$-Z_P$" pointing, for nominal attitude, the vehicle moves in the X_P direction. Let $\bar{u}_P$ be the unit velocity vector in the P-frame and let A_α be the rotation matrix due to α, then

$$\bar{u}_B = A_\alpha^T \bar{u}_P = \begin{bmatrix} \cos\alpha & 0 & \sin\alpha \\ 0 & 1 & 0 \\ -\sin\alpha & 0 & \cos\alpha \end{bmatrix} \begin{bmatrix} 1 \\ 0 \\ 0 \end{bmatrix}$$

$$= \begin{bmatrix} \cos\alpha \\ 0 \\ -\sin\alpha \end{bmatrix} \qquad (14)$$

Since $\alpha (= -2.18^\circ = -.038 \text{ rad})$ is small,

$$\bar{u}_B \doteq \begin{bmatrix} 1 \\ 0 \\ -\alpha \end{bmatrix} \qquad (15)$$

Using Eqs. (12), (13), and (15), and

$$\bar{T}_P = \sum_{i=1}^{3} A_\alpha \bar{T}_{Bi} \qquad (16)$$

the torques in the P-Frame, for nominal attitude, are

$$\bar{T}_P = \begin{bmatrix} 0 \\ 9.84 \times 10^{-3} \\ 0 \end{bmatrix} \quad \text{N-m} \qquad (17)$$

For small attitude errors, ϕ, θ, and ψ, from the rotating orbital frame,

$$\bar{u}_P = A \begin{bmatrix} 1 \\ 0 \\ 0 \end{bmatrix} \qquad (18)$$

where,

$$\tilde{A} = \begin{bmatrix} 1 & \psi & -\theta \\ -\psi & 1 & \phi \\ \theta & -\phi & 1 \end{bmatrix}$$

and

$$\bar{u}_B = A_\alpha^T \, A \begin{bmatrix} 1 \\ 0 \\ 0 \end{bmatrix} \tag{20}$$

Using Eqs. (12), (13), and (20), the predicted aerodynamic torques become, by retaining only the first order terms, in N-m,

$$\bar{T}_p = \sum_{i=1}^{3} A_\alpha \, \bar{T}_{Bi} \tag{21}$$

$$= \begin{bmatrix} 4.29 \times 10^{-3} \psi \\ 4.29 \times 10^{-3} + 7.04 \times 10^{-2} \, (\theta-\alpha) + 7.58 \times 10^{-2} |\theta-\alpha| + 2.65 \times 10^{-2} |\psi| \\ 7.04 \times 10^{-2} \, \psi \end{bmatrix}$$

C.1.2. Drag Torques for Configuration B

Referring to Figure 3, under this configuration, X_p is in the Nadir direction and Y_p is in the direction of motion for nominal attitude. In this case,

$$\bar{u}_p = \begin{bmatrix} 0 \\ 1 \\ 0 \end{bmatrix} \tag{22}$$

$$\bar{u}_B = A_\alpha^T \, \bar{u}_p = \begin{bmatrix} 0 \\ 1 \\ 0 \end{bmatrix} \tag{23}$$

and from Eqs. (12), (13), and (23),

$$\bar{T}_p = \sum_{i=1}^{3} A_\alpha \bar{T}_{Bi}$$

$$= \begin{bmatrix} -3.96 \times 10^{-2} \\ 0 \\ -4.53 \times 10^{-2} \end{bmatrix} \quad \text{N-m} \tag{24}$$

In the presence of small attitude errors, ϕ, θ, and ψ, the aerodynamic drag torques are

$$\bar{T}_P = \begin{bmatrix} -2.45 \times 10^{-2} - 7.58 \times 10^{-2}|\phi| - 4.29 \times 10^{-3}|\phi| + 3.31 \times 10^{-2}\alpha \\ -3.31 \times 10^{-2}\phi + 2.65 \times 10^{-2}\psi \\ -(3.31 \times 10^{-2} + 8.23 \times 10^{-2}|\phi| + 7.04 \times 10^{-2}|\psi| + 2.65 \times 10^{-2}\alpha) \end{bmatrix} \tag{25}$$

C.1.3. Estimation of Disturbance PSD

Before the PSD's are estimated, the uncertainty part of the disturbance torques has to be determined. The torques of Eqs. (21) and (25) consist of static parts and the dynamic parts. The dynamic parts are functions of the attitude errors ϕ, θ, and ψ. The attitude errors are assumed to be random and time-varying with standard deviation of 1° (.01745 rad.) per axis. Therefore, the estimated values of the random disturbance torques are, for Configuration A

$$\bar{\sigma}_{T_{PA}} = \begin{bmatrix} 7.48 \times 10^{-5} \\ 1.86 \times 10^{-3} \\ 1.23 \times 10^{-3} \end{bmatrix} \quad \text{N-m} \tag{26}$$

and that for Configuration B are,

$$\bar{\sigma}_{T_{PB}} = \begin{bmatrix} 1.33 \times 10^{-3} \\ 7.40 \times 10^{-4} \\ 1.89 \times 10^{-3} \end{bmatrix} \quad \text{N-m} \tag{27}$$

and the corresponding PSD's are obtained by the following approximation with the correlation time of T = 180 seconds,

$$Q_{T_{PA}} = 2T \left(\bar{\sigma}^2_{T_{PA}}\right)$$

$$= \begin{bmatrix} 2.01 \times 10^{-6} \\ 1.25 \times 10^{-3} \\ 5.44 \times 10^{-4} \end{bmatrix} \quad (N\text{-}m)^2 - sec \tag{28}$$

$$\bar{Q}_{T_{PB}} = 2T\,(\bar{\sigma}^2_{T_{PB}})$$

$$= \begin{bmatrix} 6.32 \times 10^{-4} \\ 1.97 \times 10^{-4} \\ 1.29 \times 10^{-3} \end{bmatrix} \quad (N\text{-}m)^2 - sec \tag{29}$$

C.2 The Gravity Gradient Torques and Gyroscopic Torques

The gravity gradient torques and the gyroscopic torques can be estimated using the following equations, respectively:

$$\bar{T}_{gP} = 3\omega_o^2\, \tilde{u}_{RP}\, I_P\, \bar{u}_{RP} \tag{30}$$

and

$$\bar{T}_{GRP} = \bar{\omega}_{oP} \times \bar{H}_P = \tilde{\omega}_{oP}\, I_P\, \bar{\omega}_{oP} \tag{31}$$

Where $\bar{u}_{RP}$ and $\bar{\omega}_{oP}$ are the unit earth vector and the spin velocity vector, respectively, in principal frame, and $\tilde{u}_{RP}$ is the skew symmetric matrix of the vector $\bar{u}_{RP}$. For Configuration A,

$$\bar{u}_{RP} = A \begin{bmatrix} 0 \\ 0 \\ 1 \end{bmatrix} \tag{32a}$$

$$\bar{\omega}_{oP} = \begin{bmatrix} 0 \\ 1 \\ 0 \end{bmatrix} \omega_o \tag{32b}$$

and for Configuration B,

$$\bar{u}_{RP} = A \begin{bmatrix} -1 \\ 0 \\ 0 \end{bmatrix} \tag{33a}$$

$$\bar{\omega}_{oP} = A \begin{bmatrix} 0 \\ 0 \\ -1 \end{bmatrix} \omega_o \tag{33b}$$

the corresponding torques, to include only the first order effect, are, for Configuration A

$$\bar{T}_{gP} = 3\,\omega_o^2 \begin{bmatrix} (I_{PZZ} - I_{PYY})\phi \\ (I_{PZZ} - I_{PXX})\theta \\ 0 \end{bmatrix} = \begin{bmatrix} 1.92\,\phi \\ 33.11\,\theta \\ 0 \end{bmatrix} \text{ N-m} \tag{34a}$$

$$\bar{T}_{GRP} = \omega_o^2 \begin{bmatrix} -(I_{PZZ} - I_{PYY})\phi \\ 0 \\ (I_{PYY} - I_{PXX})\psi \end{bmatrix} = \begin{bmatrix} -.64\,\theta \\ 0 \\ 11.04\,\psi \end{bmatrix} \tag{34b}$$

and for Configuration B

$$\bar{T}_{gP} = -\,3\,\omega_o^2 \begin{bmatrix} 0 \\ (I_{PZZ} - I_{PXX})\theta \\ (I_{PXX} - I_{PYY})\psi \end{bmatrix} = \begin{bmatrix} 0 \\ -\,35.03\,\theta \\ 43.71\,\psi \end{bmatrix} \tag{35a}$$

$$\bar{T}_{GRP} = \omega_o^2 \begin{bmatrix} -(I_{PZZ} - I_{PYY})^{\circ} \\ (I_{PZZ} - I_{PXX})\theta \\ 0 \end{bmatrix} = \begin{bmatrix} -.64\,\phi \\ 11.68\,\theta \\ 0 \end{bmatrix} \tag{35b}$$

Since the gravity gradient torques and gyroscopic torques are proportional to the attitude errors, they may be included in the equations of motion

as part of the vehicle dynamics rather than disturbances to the plant.

D. THE MISALIGNMENT AND MEASUREMENT NOISE

In this subsection, the errors that will contribute to pointing uncertainties are estimated. These error sources include the misalignment errors of the IMU and the IS instrument, and the sensor noise.

D.1 The Misalignment Errors

Let b_{MS} be the misalignment between the IMU and the shuttle reference frame; let b_{SI} be the misalignment between the shuttle and the imaging spectrometer reference frame.

Based on the space shuttle performance requirement [5], the IMU 3σ misaligument uncertainty is $\pm$ .133°/axis, hence,

$$\sigma_{bMS} = .044^{o}/\text{axis} = 159.6 \quad \text{arc-sec/axis} \tag{36a}$$

However, based on a JPL internal memorandum, the shuttle flight test performance is much better,

$$\sigma_{bMS} = 82 \text{ arc-sec/axis} \tag{36b}$$

The performance data Eq. (36b) was used in this report.

The misalignment data for the IS instrument is not directly available. Based on Ref. 9, the estimated LANDSAT D initial alignment bias between the sensor optical axis and the vehicle pointing vector was $\pm$ 200 arc-sec. The alignment bias can be measured before launch and can be removed from the image data. The variation part that cannot be removed without ground control points was estimated as $\pm$ 30 arc-sec. This latter number was used in this work,

$$\sigma_{b_{SI}} = 30 \text{ arc-sec} \tag{37}$$

Therefore, the total misalignment error becomes

$$\sigma_{b_o} = (\sigma_{b_{MS}}^2 + \sigma_{b_{SI}}^2)^{1/2}$$

$$= 87.32 \text{ arc-sec.} \tag{38}$$

D.2 The IMU Model

The sensor dynamics for the shuttle IMU was modeled approximately by the first order low pass filter as shown in Figure 10.

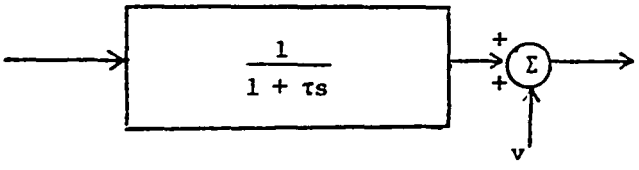

Figure 10. Simplified IMU Model

Where τ is the time constant and v the white gaussian noise. The time constant was estimated from a DRIRU II Model,

$$\tau = \frac{1}{\omega_s} = \frac{1}{14\pi} = .023 \text{ sec} \tag{39}$$

That is, this measurement is assumed to have a 7 Hz bandwidth.

To determine v, from Ref. 5, the 3σ IMU readout error is $\pm$ .073°/axis. Assume that the measurement noise is the readout error, then

$$\sigma_v = .0243^\circ/\text{axis} = 87.6 \text{ arc-sec/axis} \tag{40}$$

However, the actual performance of the shuttle IMU was much better; it has a 1σ gyro resolution error (σ_{RESO}) of 20 arc-sec/axis. If we assume the random noise has the same amplitude as that of the resolution noise, then

$$\sigma_v = \sqrt{2}\,\sigma_{RESO} \tag{41}$$

The corresponding measurement noise PSD, R, is estimated as,

$$R \simeq 2\left(\frac{1}{14\pi}\right)\sigma_v^2$$

$$= 8.55 \times 10^{-10} \text{ (rad)}^2\text{-sec} \tag{42}$$

E. SHUTTLE DYNAMICS AND INSTRUMENT POINTING ERRORS

E.1 The Equations of Motion

Consider Configuration A. For simplicity, the subscript P for principal axes is dropped from all equations. Again, let ϕ, θ, and ψ be the small roll, pitch, and yaw angles, respectively. Let $\bar{\omega} = (\omega_X, \omega_Y, \omega_Z)^T$ be the angular velocity vector of the shuttle, then for small attitude errors,

$$\begin{aligned} \omega_X &= \dot{\phi} + \psi\,\omega_o \\ \omega_Y &= \dot{\theta} + \omega_o \\ \omega_Z &= \dot{\psi} - \phi\,\omega_o \end{aligned} \tag{43}$$

and

$$\begin{aligned} \dot{\omega}_X &= \ddot{\phi} + \dot{\psi}\,\omega_o \\ \dot{\omega}_Y &= \ddot{\theta} \\ \dot{\omega}_Z &= \ddot{\psi} - \dot{\phi}\,\omega_o \end{aligned} \tag{44}$$

With this simplified relation between the inertial rates and the attitude error rates, one can show that the equations of motion may be summarized as follows, accounting only for first order effects:

$$\begin{bmatrix} I_X\ddot{\phi} + (I_X - I_Y + I_Z)\,\omega_o\dot{\psi} + 4\,(I_Y - I_Z)\,\omega_o^2\phi \\ I_Y\ddot{\theta} + 3\,(I_X - I_Z)\,\omega_o^2\theta \\ I_Z\ddot{\psi} - (I_X - I_Y + I_Z)\,\omega_o\dot{\phi} - (I_X - I_Y)\,\omega_o^2\psi \end{bmatrix} = \bar{T}_d + \bar{T}_c \tag{45}$$

The left-hand side of Eq. (45) accounts for the body dynamics and the gravity gradient and the gyroscopic torques; and on the right-hand side of Eq. (45) $\bar{T}_d$ and $\bar{T}_c$ are the disturbance torques and the control torques, respectively.

E.2 The Space Shuttle State Estimator

The Shuttle State Estimator consists of two parallel Kalman-type filters, one for acceleration estimation and one for rate estimation [10]. The attitude estimate is the extrapolation of the measured attitude and the rate estimate may be approximated by using a second order filter with parameters

determined by the filter gains. With the current baseline filter data, the equivalent damping coefficient and the corner frequency for the rate filter are .8 and .04 Hz (for vernier rate filter), respectively [11].

E.3 The System Pointing Errors

E.3.1. The Pitch Loop (Configuration A)

From Eq. (45) and ignoring the initial conditions, one has the following output function,

$$\theta(S) = \frac{1}{I_Y S^2 + 3\omega_o^2 (I_X - I_Z)} (T_{dY} + T_{cY}) \tag{46}$$

Figure 11 shows the open-loop block diagram for the dynamics of the instrument pointing error excited by the random disturbances. Included in the diagram are the dynamics of the vehicle, the IMU, and the rate filter. Measurement error and the misalignment error are also included.

E.3.2. The Roll and Yaw Loops (Configuration A)

The output equations for the coupled roll and yaw dynamics are, from Eq. (45)

$$\begin{bmatrix} \phi(S) \\ \psi(S) \end{bmatrix} = \frac{1}{D(S)} \begin{bmatrix} I_Z S^2 + \omega_o^2 (I_Y - I_X) & -\omega_o (I_X - I_Y + I_Z) S \\ \omega_o (I_X - I_Y + I_Z) S & I_X S^2 + 4\omega_o^2 (I_Y - I_Z) \end{bmatrix} \begin{bmatrix} T_X \\ T_Z \end{bmatrix} \tag{47}$$

where

$$D(S) = I_X I_Z S^4 + \omega_o^2 (I_X I_Z + I_Y^2 + 3I_Y I_Z - 3I_Z^2) S^2 + 4\omega_o^4 (I_Y - I_X)(I_Y - I_Z) \tag{48}$$

and

$$T_X = T_{cX} + T_{dX} \tag{49a}$$

$$T_Z = T_{cZ} + T_{dZ} \tag{49b}$$

Figure 12 shows the block diagram for the roll and yaw instrument error dynamics. The block diagrams for the pitch and the roll-yaw loops are similar except for

the coupling terms for the roll and yaw axes.

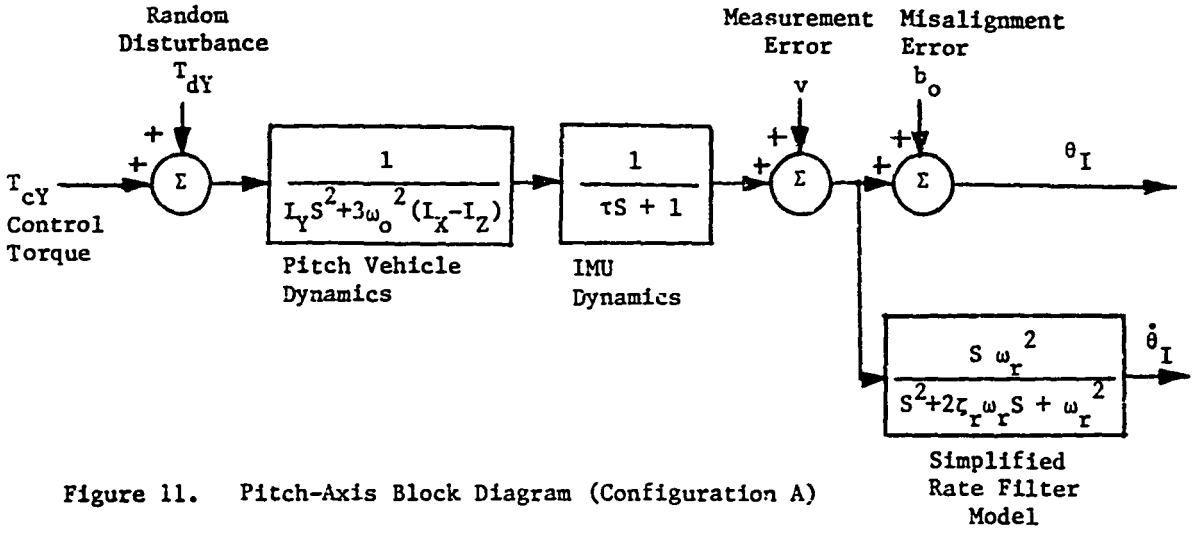

Figure 11. Pitch-Axis Block Diagram (Configuration A)

E.4 The Instrument Pointing Error PSD

E.4.1 The Pitch Error PSD (Configuration A)

The PSD's for the pitch-axis instrument pointing error and the rate error are,

$$P_\theta(\omega) = F_\theta^*(\omega)\, F_\theta(\omega) Q_Y + R + \sigma_{bo}^2\, \delta(\omega) \qquad (50)$$

$$P_{\dot\theta}(\omega) = (F_\theta^*(\omega)\, F_\theta(\omega) Q_Y + R)\, H_r^*(\omega)\, H_r(\omega) \qquad (51)$$

where $Q_Y = Q_{T_{PA}Y}$ and $Q_{T_{PA}Y}$ is the second component of Eq. (28), and where R, and σ_{bo} are defined in preceding sections, and $\delta(\omega)$ is the Dirac delta function; and where,

$$F_\theta(\omega) = G_\theta(\omega)\, H(\omega) \qquad (52a)$$

$$G_\theta(\omega) = \left[\frac{1}{I_Y S^2 + 3\,\omega_o^2(I_X-I_Z)}\right]_{S=j\omega} \qquad (52b)$$

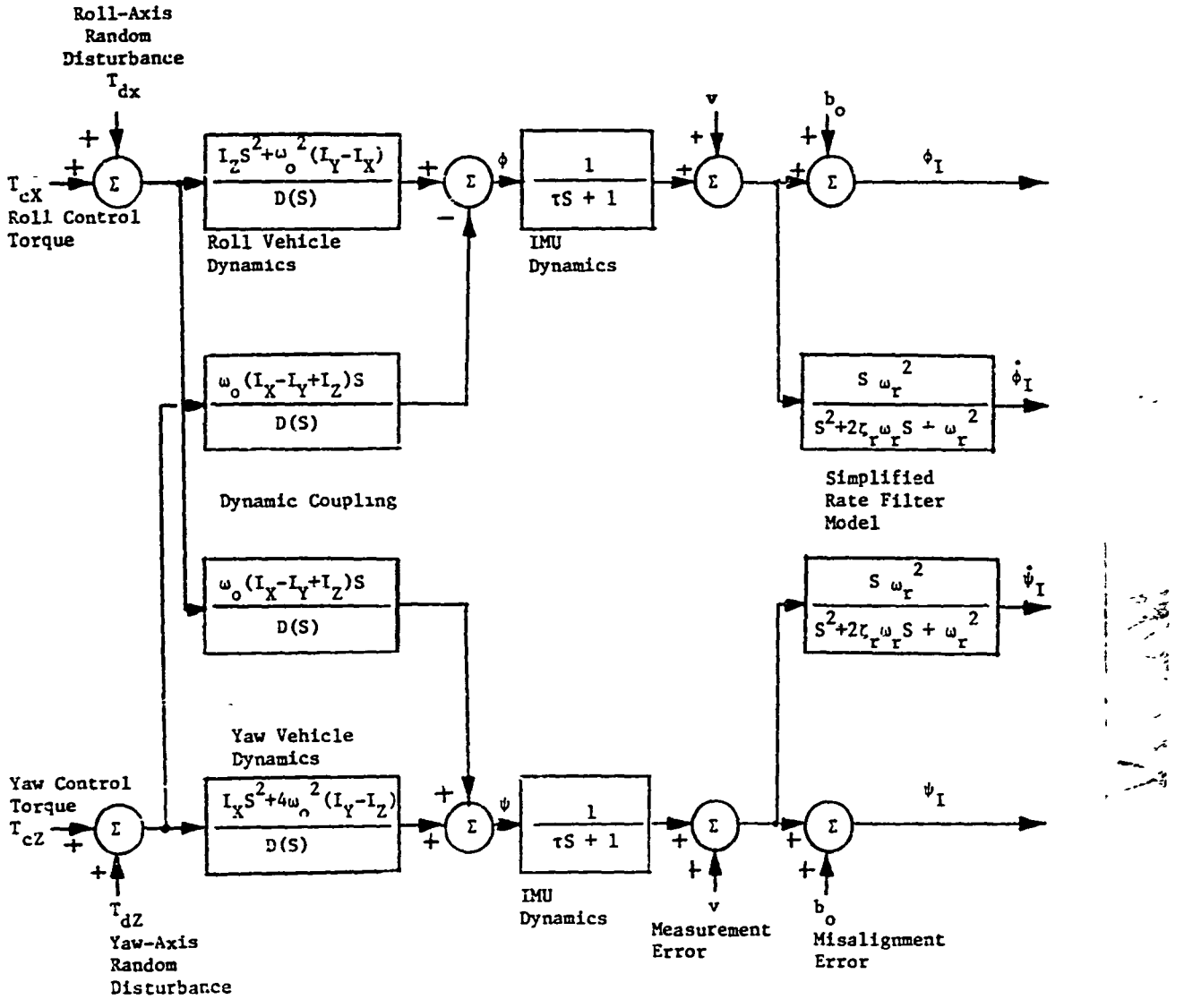

Figure 12. Roll and Yaw Axes Block Diagram. (Configuration A)

$$H(\omega) = \left[\frac{1}{\tau S + 1}\right]_{S=j\omega} \tag{52c}$$

$$F_\theta^*(\omega) = F_\theta\ (-\omega) \tag{52d}$$

$$H_r(\omega) = \left[\frac{S\,\omega_r^2}{S^2 + 2\zeta_r\omega_r S + \omega_r^2}\right]_{S=j\omega} \tag{52e}$$

The output power spectral density for the system is closely related to the frequency response of the system, which characterizes the steady state dynamics of the system, and, hence, it is meaningful only if the system is stable. Unfortunately, in Eq. (52b), $I_x < I_z$ which implies that the system is unstable. The destabilizing term comes from the gravity gradient because the nadir pointing axis is not the axis of minimum inertia. To proceed, one has to consider the gravity gradient as external disturbance rather than a part of the dynamics. Figure 13 shows the instrument pointing error PSD in $(\text{rad})^2$-sec as a function of frequency in Hz. Figure 14 shows the rate error PSD in $(\text{rad/sec})^2$-sec as a function of frequency.

E.4.2. The Roll and Yaw Error PSD (Configuration A)

The instrument pointing error PSD's for the roll and yaw axes are,

$$P_\phi(\omega) = F_\phi^*(\omega)\ F_\phi(\omega)\ Q_x + F_{\phi\psi}^*(\omega)\ F_{\phi\psi}(\omega)\ Q_z + R + \sigma_{bo}^2\ \delta(\omega) \tag{53a}$$

$$P_\psi(\omega) = F_\psi^*(\omega)\ F_\psi(\omega)\ Q_z + F_{\phi\psi}^*(\omega)\ F_{\phi\psi}(\omega)\ Q_x + R + \sigma_{bo}\ \delta(\omega) \tag{53b}$$

and the instrument pointing rate error PSD's for the roll and yaw axes are,

$$P_{\dot\phi}(\omega) = \left[F_\phi^*(\omega)\ F_\phi(\omega)\ Q_x + F_{\phi\psi}^*(\omega)\ F_{\phi\psi}(\omega)\ Q_z + R\right] H_r^*(\omega)\ H_r(\omega) \tag{54a}$$

$$P_{\psi}(\omega) = [F^{*}_{\psi}(\omega)\, F_{\psi}(\omega)\, Q_z + F^{*}_{\phi\psi}(\omega)\, F_{\phi\psi}(\omega)\, Q_x + R]\, H^{*}_{r}(\omega)\, H_{r}(\omega) \quad (54b)$$

where

$$F_{\phi}(\omega) = G_{\phi}(\omega)\, H(\omega) \quad (55a)$$

$$G_{\phi}(\omega) = \left[\frac{I_z S^2 + \omega_o^2 (I_y - I_x)}{D(S)}\right]_{S=j\omega} \quad (55b)$$

$$F_{\phi\psi}(\omega) = G_{\phi\psi}(\omega)\, H(\omega) \quad (56a)$$

$$G_{\phi\psi}(\omega) = \left[\frac{\omega_o (I_x - I_y + I_z)}{D(S)}\right]_{S=j\omega} \quad (56b)$$

$$F_{\psi}(\omega) = G_{\psi}(\omega)\, H(\omega) \quad (57a)$$

$$G_{\psi}(\omega) = \left[\frac{I_x S^2 + 4\omega_o^2 (I_y - I_z)}{D(S)}\right]_{S=j\omega} \quad (57b)$$

and Q_x and Q_z are the first and the third components of $\bar{Q}_{T_{PA}}$ in Eq. (28).

For the same reason discussed earlier, the roll and yaw dynamics are also unstable (referring to Eq. (48), D(s) has roots in the right-half complex plane). The PSD's for this case are obtained again by treating gravity gradient and gyroscopic torques as disturbances. Figures 13 and 14 show the roll and yaw power spectral densities.

E.4.3. The Error PSD's for Configuration B

The stability problem may be resolved by reorienting the shuttle from payload-bay nadir (Configuration A) to nose-down nadir (Configuration B). The advantage of this new configuration is that it is a gravity gradient stabilized system. However, there are drawbacks for this configuration. First, it will require a larger support-tower for the IS instrument, and the second drawback is that the aerodynamic forces and torques have increased significantly over the payload-bay nadir case.

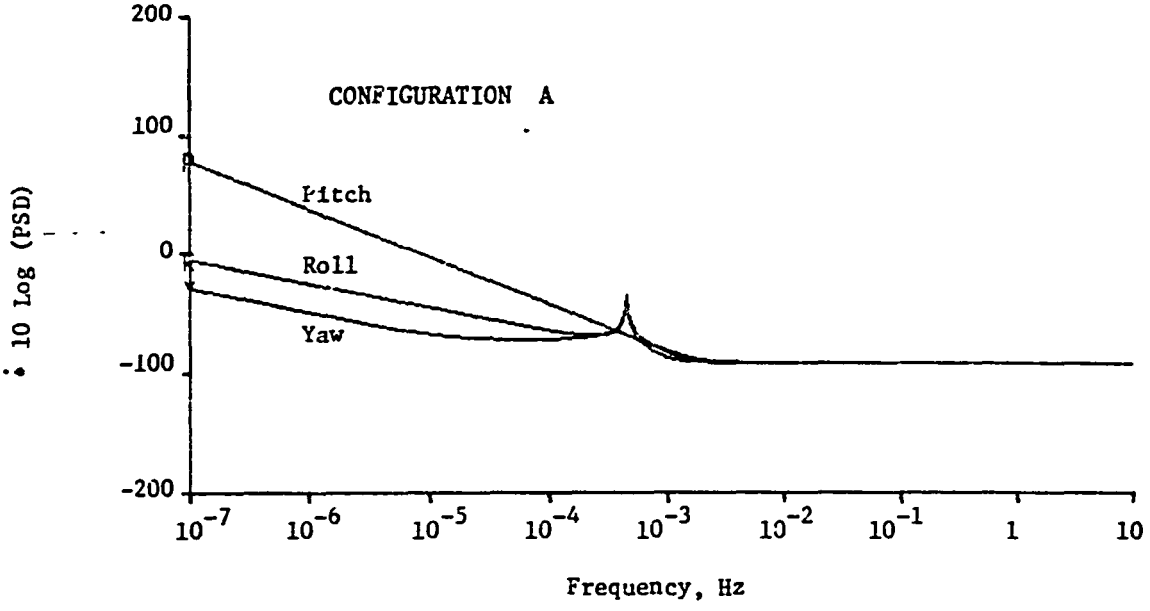

Figure 13. Instrument Pointing Error PSD, $(rad)^2$-sec

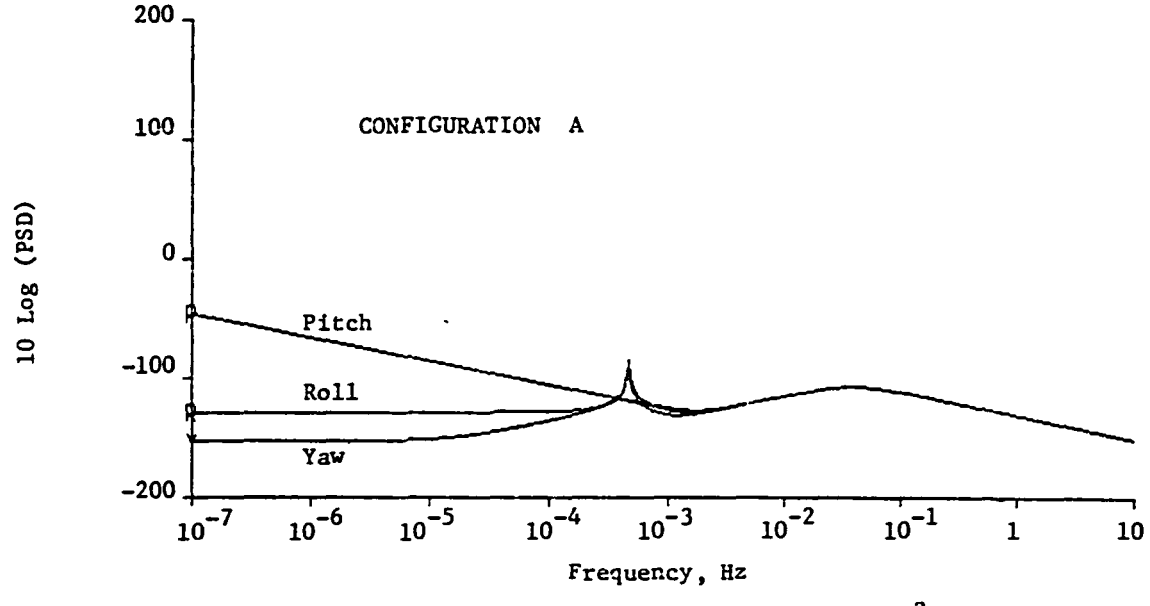

Figure 14. Instrument Pointing Rate Error, $(rad/sec)^2$-sec

To obtain the error power spectral density for Configuration B, it is only necessary to replace $\begin{bmatrix} X \\ Y \\ Z \end{bmatrix}_A$ and the corresponding notations of the equations in this section by $\begin{bmatrix} Y \\ -Z \\ -X \end{bmatrix}_B$. That is, for instance, Eq. (52b) becomes,

$$G_\theta(\omega) = \left[\frac{1}{I_Z S^2 + 3\,\omega_o^2 (I_Y - I_X)} \right]_{S=j\omega} \tag{58}$$

where $G_\theta(\cdot)$ here still represents the pitch dynamics. Since $I_Y > I_X$, Eq. (58) is stable.

The instrument pointing error PSD's are shown in Figure 15 and the rate error PSD's are illustrated in Figure 16.

The computer programs that are used for generating these results are included in Appendices C and D.

F. SUMMARY OF MAJOR FINDINGS

F.1 The Major Environmental Disturbances

The major disturbance sources that are modeled are the aerodynamic drag torques, the gravity gradient torques, and the gyroscopic torques. The unmodeled disturbances are the solar pressure torques, the on-board equipment vibrations, crew motions, and venting. Table 2 shows the static disturbance torques in N-m and the stochastic torque PSD's in $(N\text{-}m)^2$-sec for both Configurations A and B with a circular orbit of 400 km altitude.

F.2 The Measurement Uncertainties

The modeled measurement uncertainties are summarized in Table 3.

F.3 Ground Track Errors and Navigation Uncertainties

The power spectral densities for the ground track errors and the rate errors due to instrument pointing uncertainties for Configurations A and B are shown in Figure 17. It is important to note that strong resonances occur within

the frequency band of 10^{-5} Hz to 10^{-3} Hz. The ground track errors at higher frequencies, .01 Hz and above, are dominated by the measurement noise. Recall that the 1σ measurement noise is 28.28 arc-sec/axis. The corresponding ground track error is 54.84 m/axis or 77.56 m/lateral motion.

The 3σ ground track errors due to navigational uncertainties are about one order of magnitude greater than the attitude errors with the aid of TDRSS; and the error is greater with STDN as indicated in Table 4 [12]. Note that the values tabulated in Table 3 are the 3σ rms values.

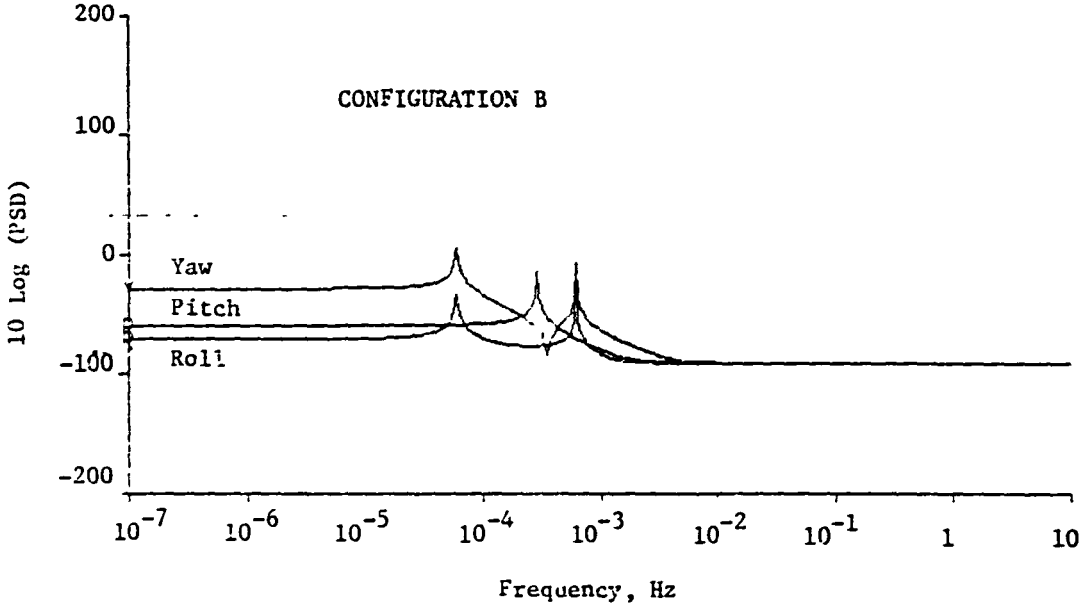

Figure 15. Instrument Pointing Error PSD, $(rad)^2$-sec

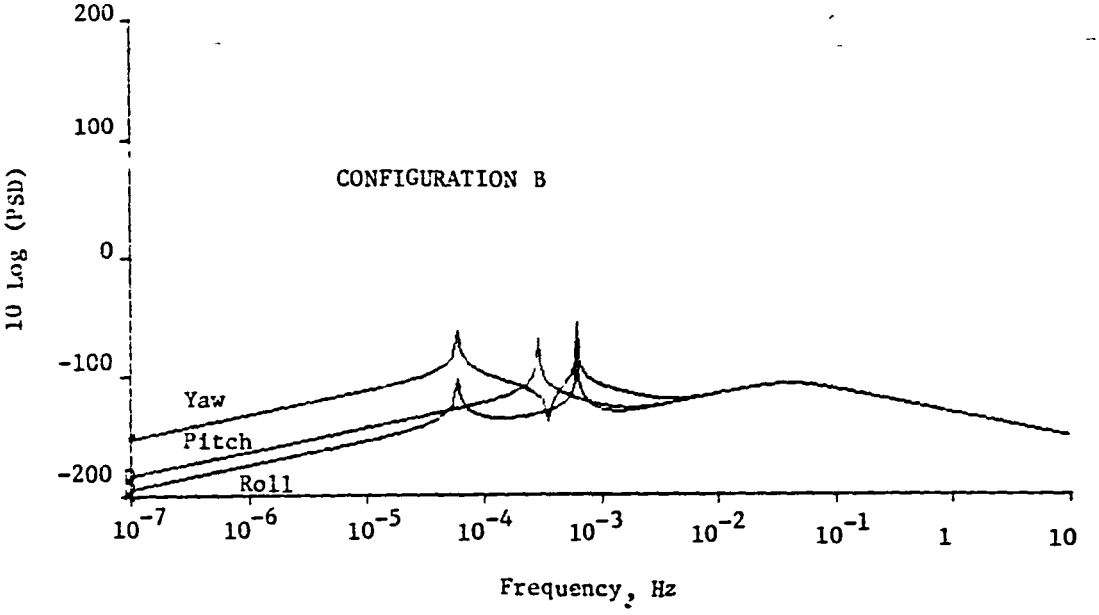

Figure 16. Instrument Pointing Rate Error, $(rad/sec)^2$-sec

Table 2. Modeled Environmental Disturbances

Sources		Static, N-m			Stochastic -- PSD, $(N-m)^2$-sec		
		X_P	Y_P	Z_P	X_P	Y_P	Z_P
Aerodynamic Drag Torques	Config. A	0	$-.68\times10^{-2}$	0	2×10^{-6}	1.2×10^{-3}	5.4×10^{-4}
	Config. B	-2.78×10^{-2}	0	-3.21×10^{-2}	6.3×10^{-4}	1.9×10^{-4}	1.2×10^{-3}
Gravity Gradient and Gyroscopic Torques		0	0	0	Proportional to attitude errors		

Table 3. Modeled Measurement Uncertainties

Sources	Performance (1σ)	Requirement (1σ)
IMU/Shuttle Misalignment	82 arc-sec	160 arc-sec
IMU Resolution	20 arc-sec	20 arc-sec
IMU Noise	(20) arc-sec	-
IMU Derived Rate	See filter dynamic model	
Rate Gyro	-	60 arc-sec/sec
Shuttle/IS Misalignment (1σ)	30 arc-sec	

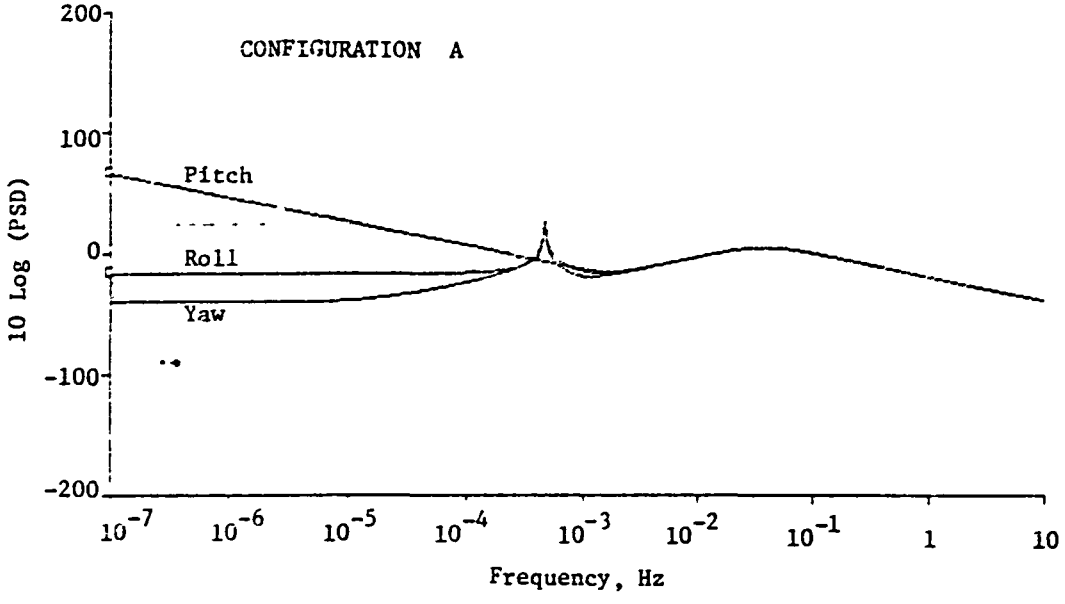

(a) IS Ground Track Error PSD, m^2-sec

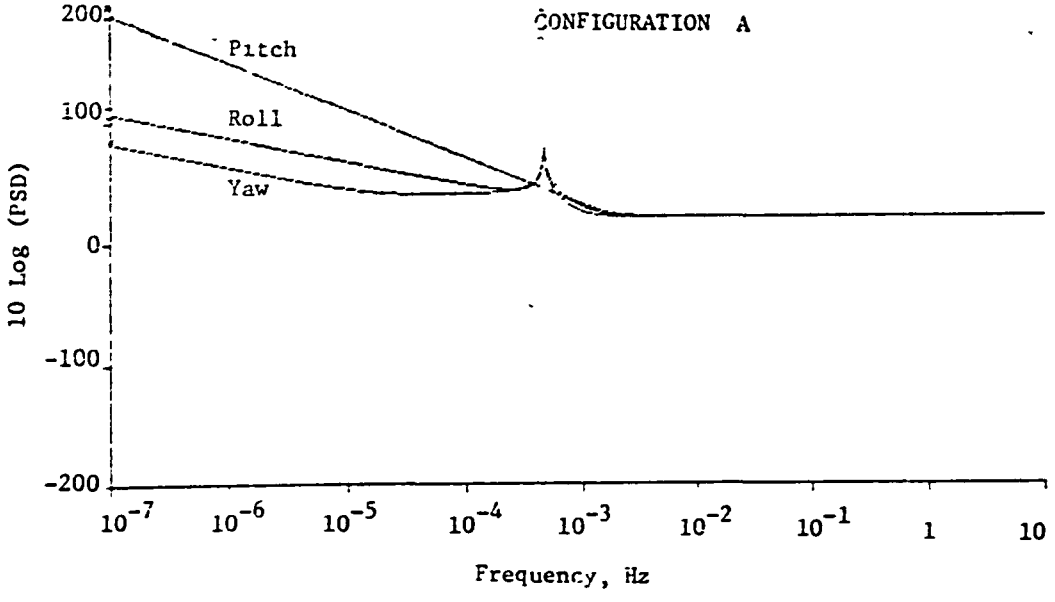

(b) IS Ground Track Rate Error PSD, $(m/sec)^2$-sec

Figure 17. IS Ground Track Error and Rate Error PSD

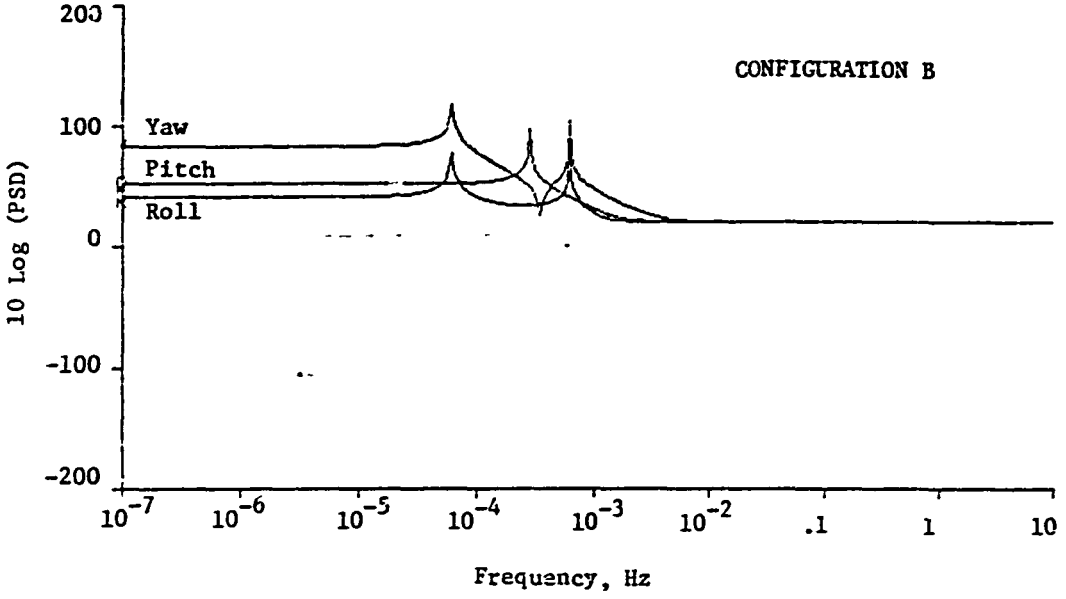

(c) IS Ground Track Error PSD, m^2-sec

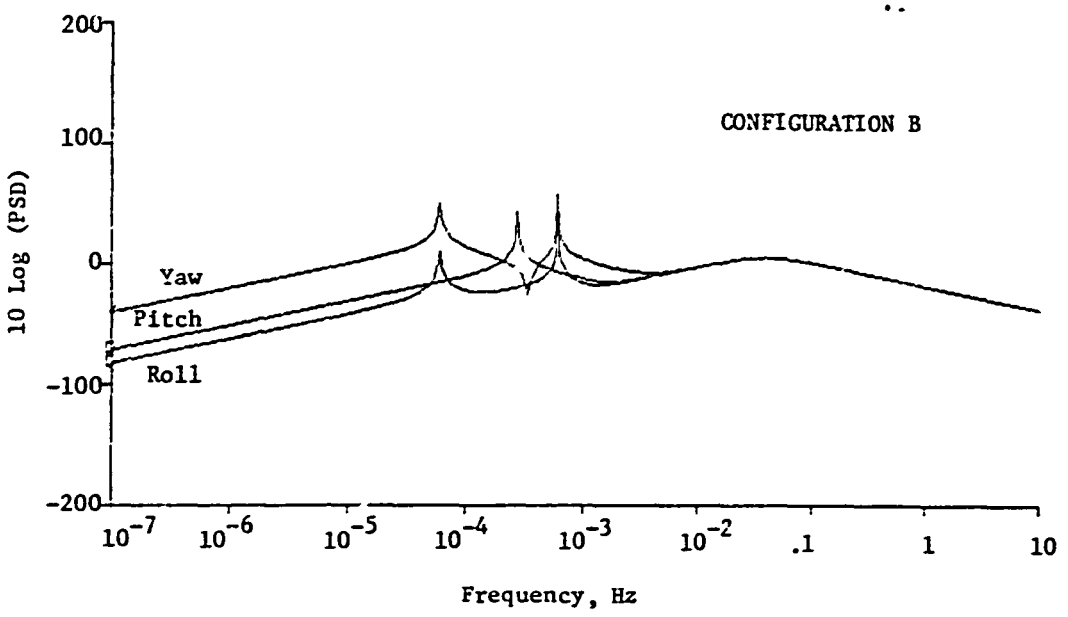

(d) IS Ground Track Rate Error PSD, $(m/sec)^2$-sec

Figure 17. (Continued)

Table 4. Expected On-Orbit Navigation Accuracies (3σ)

CASE	DESCRIPTION: NAVIGATION TRACKING SYSTEM	DESCRIPTION: UNMODELED PERTURBATION	DESCRIPTION: MINIMUM PERIGEE n.mi.	POSITION, FEET: RADIAL	POSITION, FEET: DOWNTRACK	POSITION, FEET: CROSSTRACK	VELOCITY, FPS: RADIAL	VELOCITY, FPS: DOWNTRACK	VELOCITY, FPS: CROSSTRACK
1	STDN*	NOMINAL	105	5,000	34,500	5,000	38.4	5.9	9.8
	TDRSS**		105	3,600	18,500	4,000	22.1	3.3	4.0
2	STDN	SMALL	105	3,000	22,000	1,500	24.6	3.3	2.0
			150	1,200	5,500	1,000	5.8	1.3	1.8
	TDRSS		105	1,800	10,000	2,000	11.0	1.8	2.9
			150	800	2,000	1,500	2.2	0.9	2.1
3	STDN	LARGE	105	8,000	80,000	5,000	91.2	8.0	8.0
	TDRSS		105	6,000	50,000	5,000	56.0	6.2	7.8

NOTE:

The correlation between downtrack position and radial velocity is -0.95

The correlation between radial position and downtrack velocity is -0.80

* Spaceflight Tracking and Data Network

** Tracking Data Relay Satellite System

IV. PARAMETRIC ANALYSIS OF GEOMETRIC ERRORS

In section III, the steady state error dynamics of the Shuttle Imaging Spectrometer system has been analyzed with the major error sources and disturbance effects estimated. In this section, the emphasis is on the geometric error analysis. Geometric errors are consequences of the more direct errors including attitude and rate errors, ephemeris uncertainties, misalignment errors, earth rotation and curvature, etc. Figure 1 shows how the various errors propagate and how the geometric errors and the ground pattern distortions can be generated through dynamic analysis and simulation. The block that is considered in this section is II. Due to mounting and other practical considerations, only the payload-bay principal-axis nadir pointing configuration is considered (see Fig. 2).

The geometric error mapping functions due to the individual error sources as well as the aggregated errors are derived. The earth curvature effect is incorporated in all of the results. For the purpose of quick reference, the key mapping functions are tabulated in Appendix A. A list of the source code of the computer program that has been used for generating the geometric error characteristic curves is given in Appendix E.

A. COORDINATE CONFIGURATIONS

In Fig. 18, the coordinate frame (X_p, Y_p, Z_p) on the Shuttle c.m. consists of the principal body axes. For the purpose of geometric analysis, another set of coordinates is used, i.e., the (X,Y,Z) frame centered at the nadir point on the ground. This frame is the nadir projection of the orbital rotating frame centered at the Shuttle c.m. Specifically, the X-axis is in the direction of the projected motion on the ground, or the along-track direction, the Z-axis is in the nadir direction, and the Y-axis is in the cross-track direction, so that a right-hand coordinate system is formed.

For the purpose of this report, it is assumed that the Imaging Spectrometer is attached to the payload bay with its optical axis aligned with the body

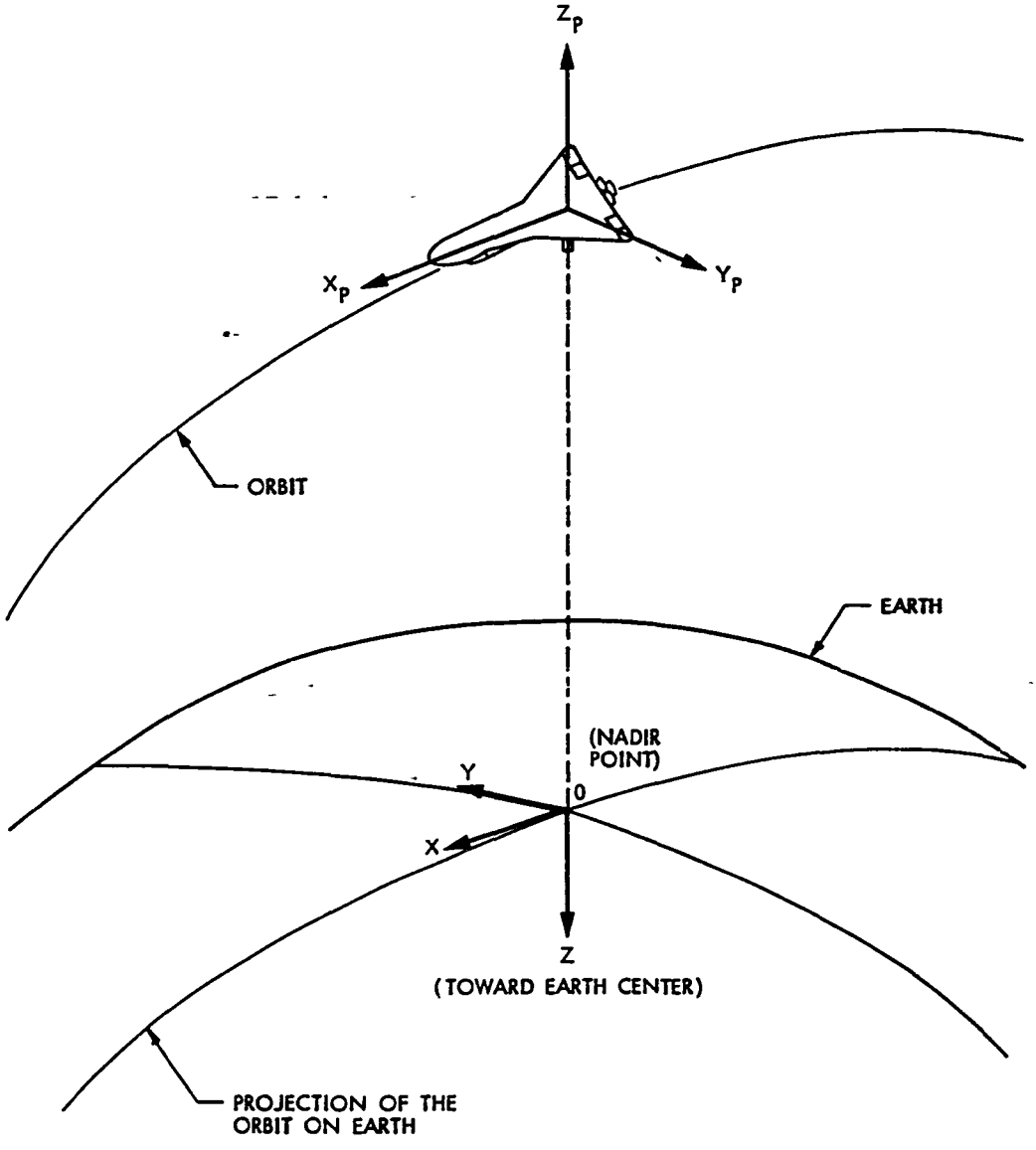

Figure 18. Payload-Bay Nadir Pointing Configuration and Coordinates

Z_p-axis. For normal IS operations, this is the desired configuration. However, for some IS experiments, such as those for assessing the atmospheric effects on the images, the IS instrument is required to point up to $\pm 45^\circ$ about the pitch axis (Y) from nadir (forward and backward looking) or up to $\pm 20^\circ$ about the roll axis (X) (side looking). For those cases, it is assumed that the instrument is gimbal mounted. However, since the analysis performed here is not primarily concerned with dynamics, no specific details are made at this time regarding mounting configurations.

B. GEOMETRIC ERRORS INDUCED BY EPHEMERIS UNCERTAINTIES

Ephemeris uncertainties include radial, along-track, and cross-track prediction errors. The geometric errors induced by ephemeris uncertainties are discussed in the following subsections.

B.1 Geometric Errors Due to Altitude Uncertainties

When the altitude of the shuttle varies, the ground point will shift in both the X and Y directions accordingly. This can be investigated in the following two ways.

B.1.1. With Fixed Viewing Angles

Referring to Figure 19, when the shuttle flies at nominal altitude h (position A), a ground point B with coordinates (Xo, Yo) corresponding to a view angle λ from the shuttle IS is located. After the shuttle elevates Δh to position A', point B' with coordinates (Xo', Yo') corresponding to the same view angle λ is located. The problem is to determine the shift of image due to the altitude change. Consider that when the altitude increases, the image of ground objects tends to move toward the nadir point, which causes reduction in image size and increase in field of view. Mathematically, the shift of image may be characterized by computing ΔX and ΔY, where

$$\Delta X = Xo - Xo'$$

$$\Delta Y = Y - Yo'$$

Starting by assuming (Xo, Yo) known, the task is to determine (Xo', Yo') by first computing the view angle λ. Figure 19b is generated by taking a side view from Fig. 19a in the direction perpendicular to Plane $A'AOC_eB'$. Apparently,

$$\sqrt{Xo^2 + Yo^2} = R \sin\beta$$

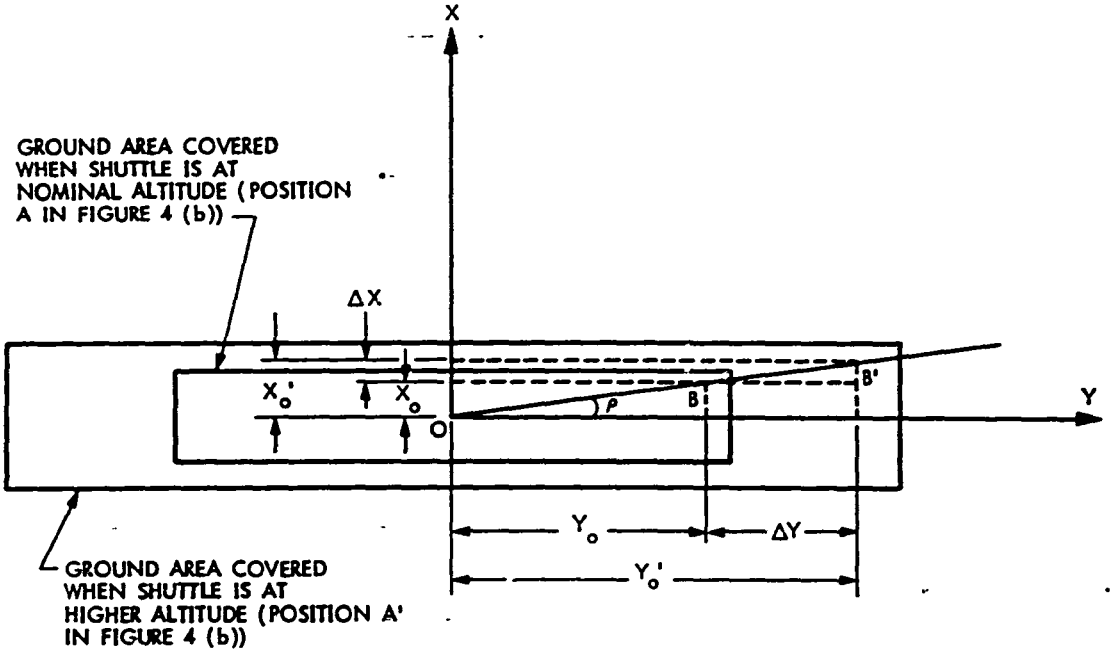

LEGEND:

B = A GROUND POINT CORRESPONDING TO VIEW ANGLE λ WHEN SHUTTLE IS AT NOMINAL ALTITUDE (POSITION A IN FIG. 4(b))

B' = THE GROUND POINT CORRESPONDING TO THE SAME VIEW ANGLE AFTER THE SHUTTLE ELEVATED Δh (POSITION A' IN FIG. 4(b))

(X_o, Y_o) = COORDINATES OF POINT B

(X_o', Y_o') = COORDINATES OF POINT B'

ΔX, ΔY = X AND Y COMPONENTS OF THE POSITION CHANGE

(a) TOP VIEW (LOOKING TOWARD NADIR)

Figure 19: Ground Point Shift in X and Y Direction due to Altitude Error

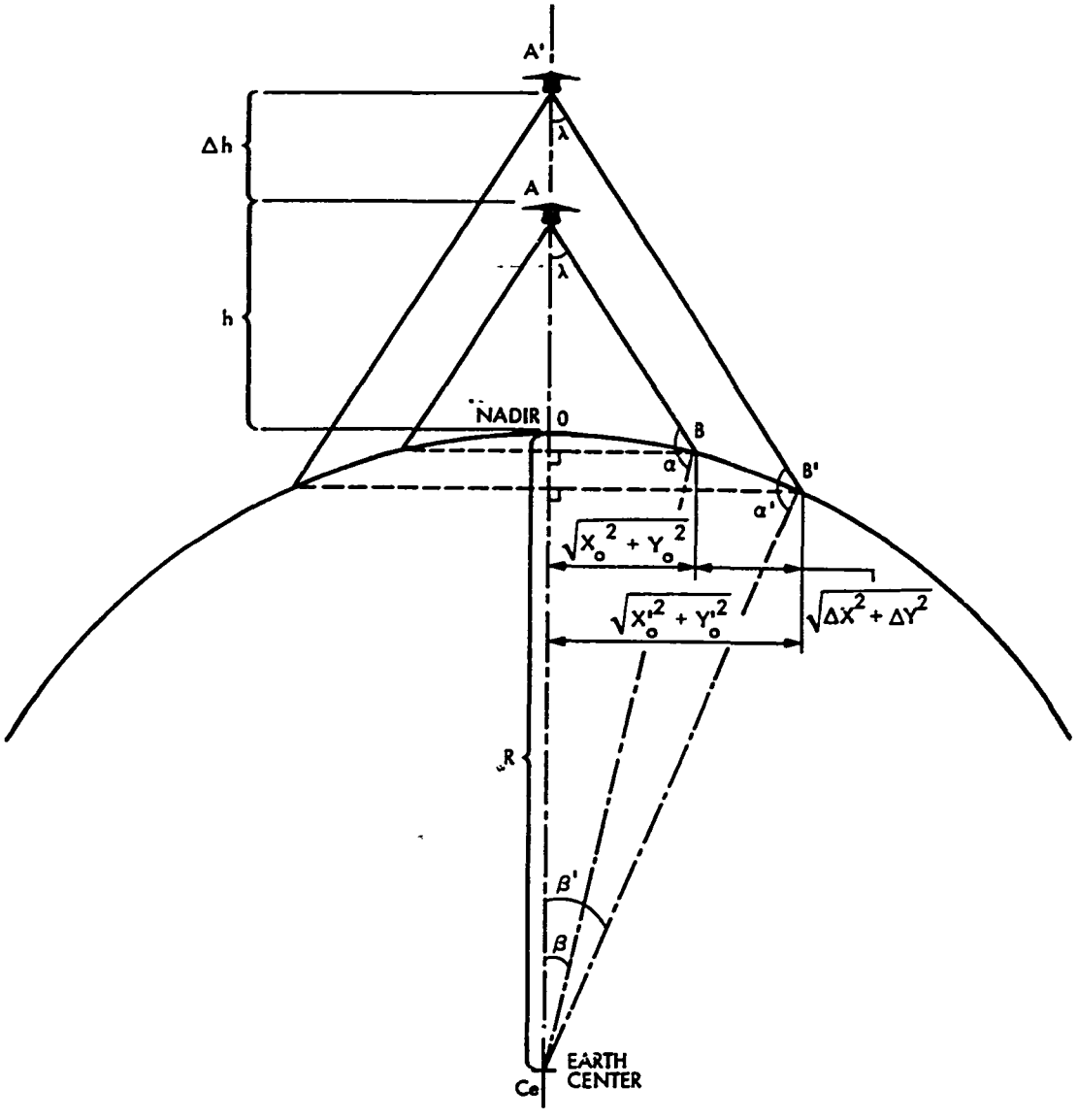

(b) SIDE VIEW

LEGEND:

h = NOMINAL ALTITUDE
Δh = ALTITUDE ERROR
λ = VIEW ANGLE
A = SHUTTLE'S POSITION AT NOMINAL ALTITUDE
A' = SHUTTLE'S POSITION AFTER BEING ELEVATED Δh

Figure 19. (Continued)

or

$$\beta = \sin^{-1}\left(\frac{\sqrt{Xo^2 + Yo^2}}{R}\right) \tag{59}$$

and

$$\alpha = 180° - \lambda - \beta \tag{60}$$

From triangle ABC_e, we have

$$\frac{R}{\sin \lambda} = \frac{R + h}{\sin \alpha} \tag{61}$$

Substituting Eqs. (59) and (60) into (61), it becomes

$$\frac{R}{\sin \lambda} = \frac{R + h}{\sin\left[180° - \lambda - \sin^{-1}\left(\frac{\sqrt{Xo^2 + Yo^2}}{R}\right)\right]}$$

which leads to

$$\tan \lambda = \frac{\sqrt{Xo^2 + Yo^2}}{R + h - \sqrt{R^2 - Xo^2 - Yo^2}}$$

hence,

$$\lambda = \tan^{-1}\left(\frac{\sqrt{Xo^2 + Yo^2}}{R + h - \sqrt{R^2 - Xo^2 - Yo^2}}\right) \tag{62}$$

To determine $\sqrt{Xo'^2 + Yo'^2}$, triangle $A'B'C_e$ is used,

$$\frac{R}{\sin \lambda} = \frac{R + h + \Delta h}{\sin \alpha'}$$

$$\therefore \alpha' = \sin^{-1}\left[\left(1 + \frac{h + \Delta h}{R}\right) \sin \lambda\right] \tag{63}$$

and

$$\sqrt{Xo'^2 + Yo'^2} = R \sin \beta'$$

$$= R \sin (\lambda + \alpha') \tag{64}$$

Substituting Eq. (63) into (64),

$$\sqrt{Xo'^2 + Yo'^2} = R \sin\left\{\lambda + \sin^{-1}\left[\left(1 + \frac{h + \Delta h}{R}\right) \sin \lambda\right]\right\} \tag{65}$$

Expanding the right hand side of Eq.(65), and adopting the "-" sign for $\cos\left\{\sin^{-1}\left[\left(1 + \frac{h + \Delta h}{R}\right) \sin \lambda\right]\right\}$, since $90° < \sin^{-1}\left[\left(1 + \frac{h + \Delta h}{R}\right) \sin \lambda\right] < 180°$, one has

$$\sqrt{Xo'^2 + Yo'^2} = R\left[\left(1 + \frac{h + \Delta h}{R}\right) \cos \lambda - \sqrt{1 - \left(1 + \frac{h + \Delta h}{R}\right)^2 \sin^2 \lambda}\right] \sin \lambda \tag{66}$$

Now, referring to Fig. 19(a), since B' is on the line OB, the angle ρ is determined by

$$\rho = \sin^{-1} \frac{Xo}{\sqrt{Xo^2 + Yo^2}} = \cos^{-1} \frac{Yo}{\sqrt{Xo^2 + Yo^2}} \tag{67}$$

Hence, from Eqs. (66) and (67),

$$Xo' = \sqrt{Xo'^2 + Yo'^2} \sin \rho = \frac{RXo \sin \lambda}{\sqrt{Xo^2 + Yo^2}} \left[\left(1 + \frac{h + \Delta h}{R}\right) \cos \lambda - \sqrt{1 - \left(1 + \frac{h + \Delta h}{R}\right)^2 \sin^2 \lambda}\right] \tag{68}$$

$$Yo' = \sqrt{Xo'^2 + Yo'^2} \cos \rho = \frac{RYo \sin \lambda}{\sqrt{Xo^2 + Yo^2}} \left[\left(1 + \frac{h + \Delta h}{R}\right) \cos \lambda - \sqrt{1 - \left(1 + \frac{h + \Delta h}{R}\right)^2 \sin^2 \lambda}\right] \tag{69}$$

where λ is obtained by Eq.(62).

Hence, from Eqs. (68), (69), and (62) the values for $\Delta X = Xo - Xo'$ and $\Delta Y = Yo - Yo'$ can be obtained.

When point A' is below point A, the negative value for Δh should be used in the above equations.

However, if one starts with given view angle λ and ρ, the values of Xo, Yo, Xo', and Yo' can be readily obtained using Eqs. (68) and (69) directly (set Δh to 0 for Xo and Yo).

B.1.2 With Fixed Ground Points

Referring to Fig.20, the view angle for the fixed ground point B will change as the shuttle altitude varies. Follow the same approach of paragraph B.1.1, the view angles Ω and Ω' can be found,

$$\Omega = \tan^{-1}\left(\frac{\sqrt{Xo^2 + Yo^2}}{R + h - \sqrt{R^2 - Xo^2 - Yo^2}}\right) \tag{70}$$

and

$$\Omega' = \tan^{-1}\left(\frac{\sqrt{Xo^2 + Yo^2}}{R + h + \Delta h - \sqrt{R^2 - Xo^2 - Yo^2}}\right) \tag{71}$$

Using Eqs. (70) and (71), the value of $\Delta\Omega = \Omega' - \Omega$ can be obtained. Again if point A' is below point A, the negative value for Δh should be used in the above equations.

B.2. Geometric Errors Due to Intrack and Crosstrack Prediction Errors

The intrack (along X-direction or direction of orbit) and the crosstrack (along Y-direction or "-" orbit normal direction) prediction errors will cause the ground objects to shift along the X and Y directions, respectively, as shown in Fig.21. To determine the overall geometric errors associated with ephemeris uncertainties, the intrack error ΔX^* and the crosstrack error ΔY^* can be incorporated in ΔX and ΔY found in Section B.1.1, respectively.

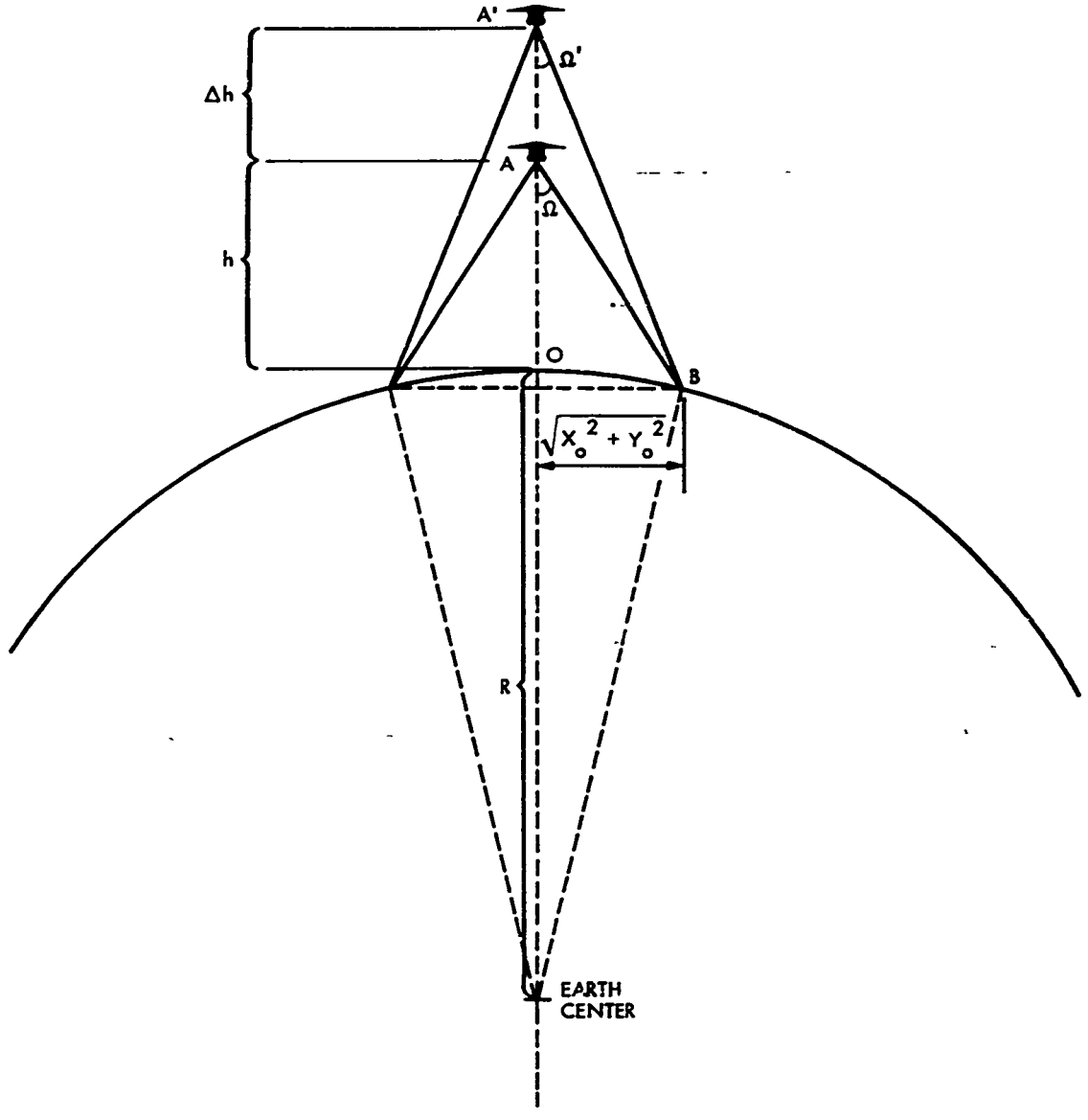

LEGEND:

Ω = VIEW ANGLE FROM SHUTTLE TO POINT B WHEN SHUTTLE IS AT NOMINAL ALTITUDE h

Ω' = VIEW ANGLE FROM SHUTTLE TO THE SAME POINT B AFTER SHUTTLE ELEVATES Δh

Figure 20. Change of View Angle of a Ground Point due to Altitude Error

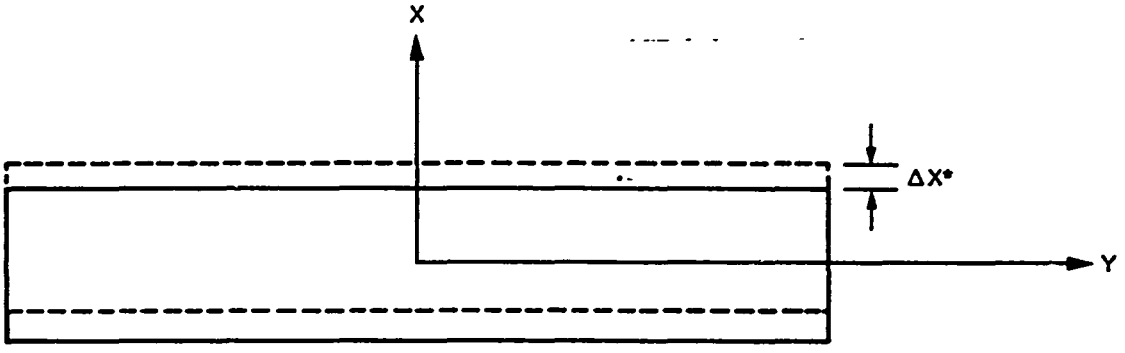

(a) INTRACK ERROR (Δ X*)

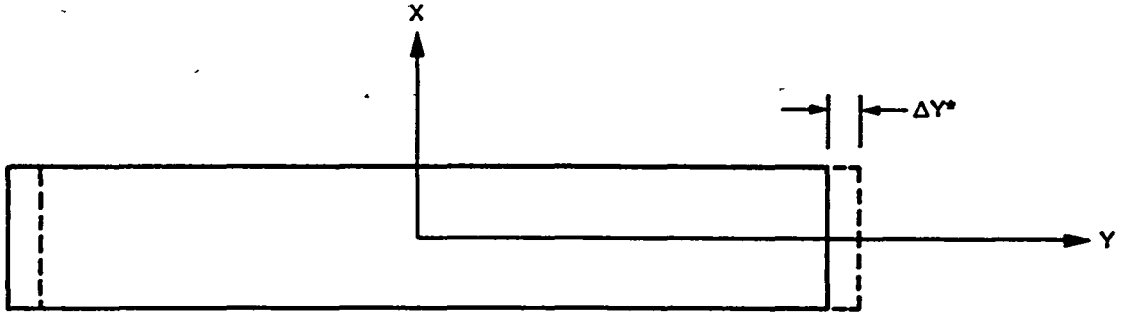

(b) CROSSTRACK ERROR (Δ Y*)

Figure 21. Geometric Errors Induced by Intrack and Crosstrack Prediction Errors

C. GEOMETRIC ERRORS INDUCED BY ATTITUDE UNCERTAINTIES

Attitude uncertainties refer to the angular errors with respect to the nominal roll (ϕ), pitch (θ), and yaw (ψ) axes. The effects of these errors to the images of ground objects are studied in this subsection first on the individual error basis and then on the aggregated basis. For convenience, in the subsequent discussions, the term nominal flight condition will be used to signify the condition of the shuttle flying in a 400 km circular orbit with the attitude of payload-bay nadir pointing.

C.1 Geometric Errors Induced by Roll Error

Referring to Fig. 22, consider the nominal flight condition with ϕ_o offset angle about the roll axis. The IS slit in this case is directed at the Y-axis on the ground. For a given view angle λ, the image point (or pixel) on the ground is P_o with coordinates (0,Y*). For the same roll offset and view angle the ground point P_o' is located after a roll error ϕ is introduced. The coordinates of P_o' are (0, Y*'). Equivalently, by rotating the optical instrument to the "left," the image recorded on the film appears to move to the "right." Therefore, the geometric error may be defined as the displacement of the object image after error is introduced relative to the image before the error is introduced. Mathematically, this is $\bar{P}_o - \bar{P}_o'$ or $\bar{P}_{\phi_o,\lambda} - \bar{P}_{\phi_o+\phi,\lambda}$. Since, in the case being considered, the image is on the Y-axis, one has

$$\Delta X = 0 \tag{72}$$

$$\Delta Y = Y^* - Y^{*\prime} \tag{73}$$

where Y* and Y*' are,

$$Y^* = -R \sin(\lambda + \phi_o)\left[\left(1 + \frac{h}{R}\right)\cos(\lambda + \phi_o) - \sqrt{1 - \left(1 + \frac{h}{R}\right)^2 \sin^2(\lambda + \phi_o)}\right] \tag{74}$$

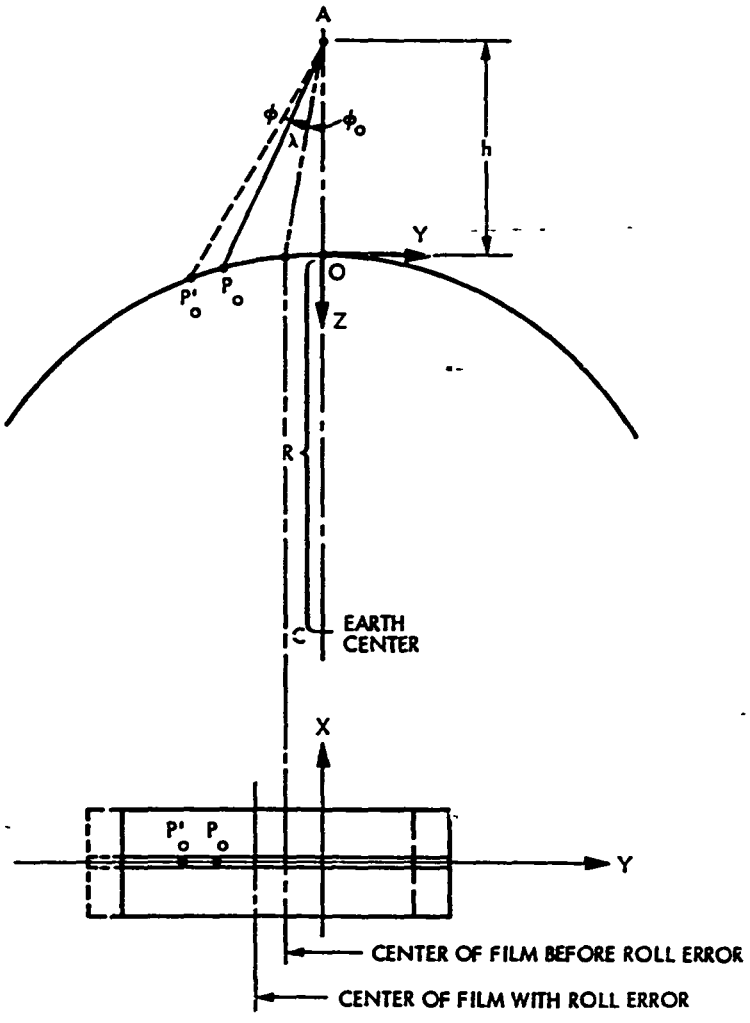

LEGEND:

λ = VIEW ANGLE

ϕ_o = ROLL OFFSET ANGLE

ϕ = ROLL ERROR

P_o = THE GROUND POINT CORRESPONDING TO VIEW ANGLE λ AND ROLL OFFSET ϕ_o

P'_o = THE GROUND POINT CORRESPONDING TO THE SAME λ AND ϕ_o AFTER ROLL ERROR ϕ IS INTRODUCED

Figure 22. Shift of Ground Point Induced by Roll Error

$$Y^{*'} = -R \sin(\lambda + \phi_o + \phi) \left[\left(1 + \frac{h}{R}\right) \cos(\lambda + \phi_o + \phi) - \sqrt{1 - \left(1 + \frac{h}{R}\right)^2 \sin^2(\lambda + \phi_o + \phi)} \right] \quad (75)$$

C.2 Geometric Errors Induced by Pitch Error

Consider the case of pitch attitude error. Let θ_o be the offset angle about the pitch axis (desired attitude), and θ be the pitch error. Referring to Fig.23, for a given view angle λ, projecting the slit onto the XY-plane forms two line segments: $\overline{BC}$, corresponding to null pitch error ($\theta = 0$), and $\overline{B'C'}$, corresponding to arbitrary pitch error θ. Projecting along the line of view $\overline{AC}$ onto the ground, P(X*,Y*) is obtained; similarly, P'(X*',Y*') is obtained, corresponding to line of view $\overline{AC'}$. The geometric error here is defined the same way as that for the roll case, i.e., $\overline{P}_{\theta_o,\lambda} - P_{\theta_o+\theta,\lambda}$, or

$$\Delta X = X^* - X^{*'} \quad (76)$$

$$\Delta Y = Y^* - Y^{*'} \quad (77)$$

The formulae for computing X*, Y*, X*', and Y*' are derived as follows. In Fig.23, assume that h, θ, θ_o, and λ are known. The lengths of the line segments $\overline{OB}$ and $\overline{OB'}$ are

$$\overline{OB} = h \tan \theta_o \quad (78a)$$

and

$$\overline{OB'} = h \tan(\theta_o + \theta) \quad (78b)$$

and that of $\overline{AB}$ and $\overline{AB'}$ are

$$\overline{AB} = \frac{h}{\cos \theta_o} \quad (79a)$$

$$\overline{AB'} = \frac{h}{\cos(\theta_o + \theta)} \quad (79b)$$

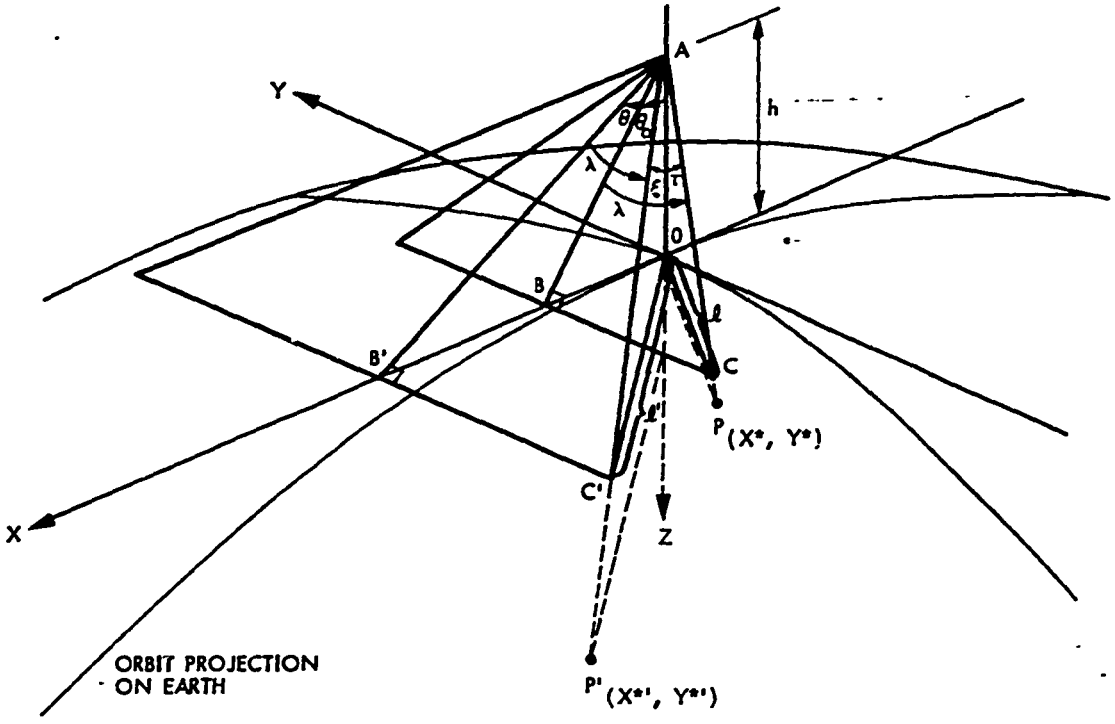

LEGEND:

- λ = VIEW ANGLE
- θ_o = PITCH OFFSET ANGLE
- θ = PITCH ERROR
- P = THE GROUND POINT CORRESPONDING TO VIEW ANGLE λ AND PITCH OFFSET θ_o
- P' = THE GROUND POINT CORRESPONDING TO THE SAME λ AND θ_o AFTER PITCH ERROR θ IS INTRODUCED

Figure 23. Shift of Ground Point Induced by Pitch Error

$\overline{BC}$ and $\overline{B'C'}$, with respect to Y-axis, can be obtained as

$$\overline{BC} = -\overline{AB} \tan \lambda = \frac{-h \tan \lambda}{\cos \theta_o} \tag{80a}$$

and

$$\overline{B'C'} = -\overline{AB'} \tan \lambda = \frac{-h \tan \lambda}{\cos(\theta_o+\theta)} \tag{80b}$$

implies that the signs of $\overline{BC}$ and $\overline{B'C'}$ are opposite to that of λ. ℓ and ℓ' are, referring to Fig. 23,

$$\ell = \sqrt{\overline{OB}^2 + \overline{BC}^2} = h \sec \theta_o \sqrt{\sin^2 \theta_o + \tan^2 \lambda} \tag{81a}$$

and

$$\ell' = \sqrt{\overline{OB'}^2 + \overline{B'C'}^2} = h \sec (\theta_o + \theta) \sqrt{\sin^2 (\theta_o + \theta) + \tan^2 \lambda} \tag{81b}$$

the angles τ and ξ (see Fig. 23) can then be determined,

$$\tau = \tan^{-1} \left(\frac{\ell}{h}\right) = \tan^{-1} \left(\sec \theta_o \sqrt{\sin^2 \theta_o + \tan^2 \lambda}\right) \tag{82a}$$

and

$$\xi = \tan^{-1} \left(\frac{\ell'}{h}\right) = \tan^{-1} \left[\sec (\theta_o + \theta) \sqrt{\sin^2 (\theta_o + \theta) + \tan^2 \lambda}\right] \tag{82b}$$

Finally,

$$X^* = \sqrt{X^{*2} + Y^{*2}} \frac{\overline{OB}}{\ell}$$

$$= R \left[\left(1 + \frac{h}{R}\right) \cos \tau - \sqrt{1 - \left(1 + \frac{h}{R}\right)^2 \sin^2 \tau}\right] \frac{\sin \tau \sin \theta_o}{\sqrt{\sin^2 \theta_o + \tan^2 \lambda}} \tag{83a}$$

$$Y^* = \sqrt{X^{*2} + Y^{*2}} \frac{\overline{BC}}{\ell}$$

$$= -R \left[\left(1 + \frac{h}{R}\right) \cos \tau - \sqrt{1 - \left(1 + \frac{h}{R}\right)^2 \sin^2 \tau}\right] \frac{\sin \tau \tan \lambda}{\sqrt{\sin^2 \theta_o + \tan^2 \lambda}} \tag{83b}$$

$$X^{*'} = \sqrt{X^{*'2} + Y'^2}\,\frac{\overline{OB'}}{\ell'}$$

$$= R\left[\left(1 + \frac{h}{R}\right)\cos\xi - \sqrt{1 - \left(1 + \frac{h}{R}\right)^2 \sin^2\xi}\right] \frac{\sin\xi \sin(\theta_o + \theta)}{\sqrt{\sin^2(\theta_o + \theta) + \tan^2\lambda}} \tag{83c}$$

$$Y^{*'} = \sqrt{X^{*'2} + Y^{*'2}}\,\frac{\overline{B'C'}}{\ell'}$$

$$= -R\left[\left(1 + \frac{h}{R}\right)\cos\xi - \sqrt{1 - \left(1 + \frac{h}{R}\right)^2 \sin^2\xi}\right] \frac{\sin\xi \tan\lambda}{\sqrt{\sin^2(\theta_o + \theta) + \tan^2\lambda}} \tag{83d}$$

However, if one starts with (X*, Y*) given, then λ and θ_o would have to be computed. In that case,

$$\lambda = -\tan^{-1}\left[\frac{Y^*}{\left(R + h - \sqrt{R^2 - X^{*2} - Y^{*2}}\right)\sqrt{1 + \left(\dfrac{X^*}{R + h - \sqrt{R^2 - X^{*2} - Y^{*2}}}\right)^2}}\right] \tag{84a}$$

and

$$\theta_o = \tan^{-1}\left(\frac{X^*}{R + h - \sqrt{R^2 - X^{*2} - Y^{*2}}}\right) \tag{84b}$$

Once λ and θ_o are determined, τ and ξ can be computed using (82), and X*' and Y*' are determined using (83).

C.3 Geometric Errors Induced by Yaw Error

For a given yaw offset angle, ψ_o, and the view angle, λ, the ground point P(X*, Y*) is located. A new point P'(X*', Y*') is found as yaw attitude error, ψ, is introduced (see Fig.24). The values for X*, Y*, X*', and Y*' can be computed as follows:

$$X^* = \left[\left(1 + \frac{h}{R}\right)\cos\lambda - \sqrt{1 - \left(1 + \frac{h}{R}\right)^2 \sin^2\lambda}\right] R \sin\lambda \sin\psi_o \tag{85a}$$

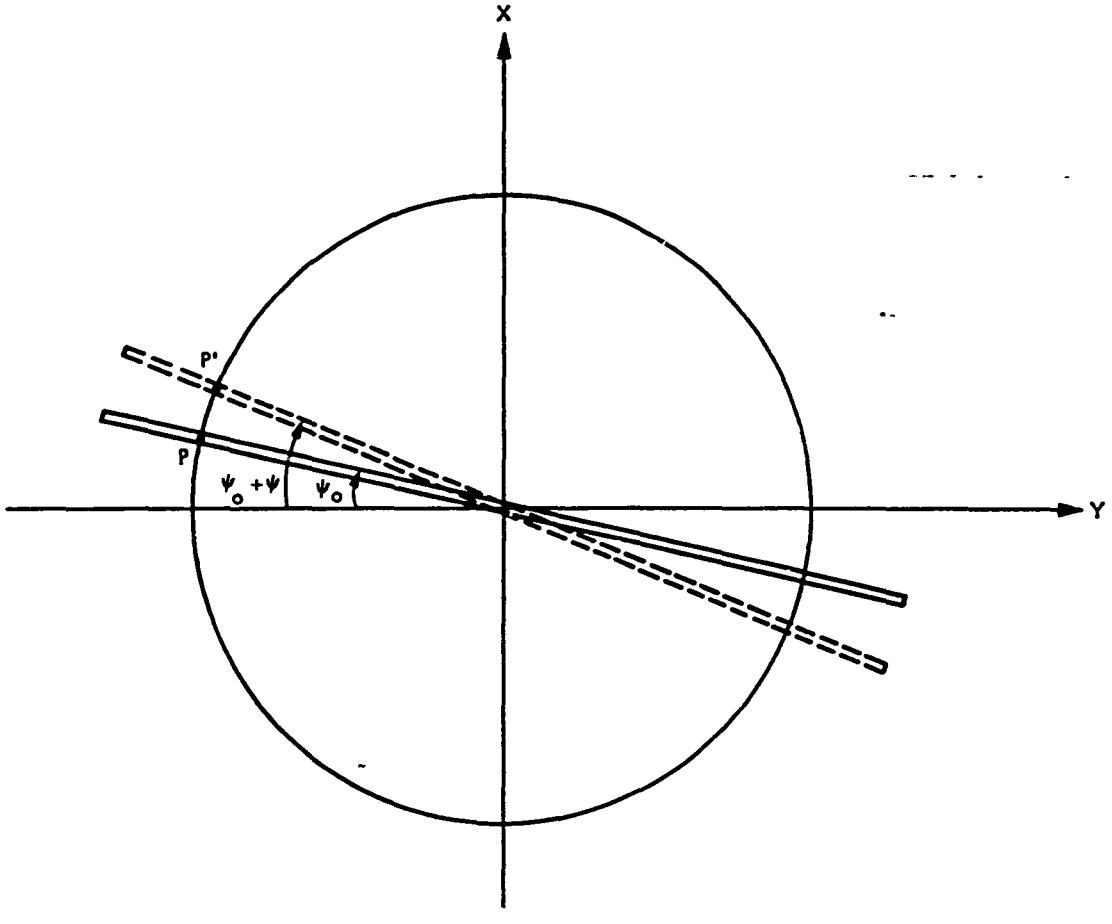

LEGEND:

ψ_o = YAW OFFSET ANGLE

ψ = YAW ERROR

P = THE GROUND POINT CORRESPONDING TO VIEW ANGLE λ AND YAW OFFSET ψ_o

P' = THE GROUND POINT CORRESPONDING TO THE SAME λ AND ψ_o AFTER YAW ERROR ψ IS INTRODUCED

Figure 24. Shift of Ground Point Induced by Yaw Error

$$Y^* = -\left[\left(1 + \frac{h}{R}\right)\cos\lambda - \sqrt{1 - \left(1 + \frac{h}{R}\right)^2 \sin^2\lambda}\right] R \sin\lambda \cos\psi_o \qquad (85b)$$

$$X^{*'} = \left[\left(1 + \frac{h}{R}\right)\cos\lambda - \sqrt{1 - \left(1 + \frac{h}{R}\right)^2 \sin^2\lambda}\right] R \sin\lambda \sin(\psi_o + \psi) \qquad (86a)$$

and

$$Y^{*'} = -\left[\left(1 + \frac{h}{R}\right)\cos\lambda - \sqrt{1 - \left(1 + \frac{h}{R}\right)^2 \sin^2\lambda}\right] R \sin\lambda \cos(\psi_o + \psi) \qquad (86b)$$

From Eqs. (85) and (86), we can obtain

$$\Delta X = X^* - X^{*'}$$

$$\Delta Y = Y^* - Y^{*'}$$

C.4 Geometric Errors Induced by Roll, Pitch, and Yaw Attitude Errors

C.4.1. The Shift of IS Line-of-Sight due to Attitude Error

Referring to Fig.25, the shuttle is flying at an arbitrary attitude (ϕ, θ, ψ). Consider the 3-2-1 sequence, i.e., the yaw, pitch, and roll rotation sequence. After yaw and pitch rotations, the Imaging Spectrometer line-of-sight will shift to $\overline{AB}$, where $B(X_1, Y_1)$ is its intersection with the XY-plane. The (X_1, Y_1) coordinates are determined as follows:

$$X_1 = X_o + h \tan\theta \cos\psi \qquad (87a)$$

$$Y_1 = Y_o + h \tan\theta \sin\psi \qquad (87b)$$

Through a roll angle rotation, point B will move to $C(X_2, Y_2)$ on the XY-plane, where

$$X_2 = X_o + h \tan\theta \cos\psi + \frac{h}{\cos\theta} \tan\phi \sin\psi \qquad (88a)$$

$$Y_2 = Y_o + h \tan\theta \sin\psi - \frac{h}{\cos\theta} \tan\phi \cos\psi \qquad (88b)$$

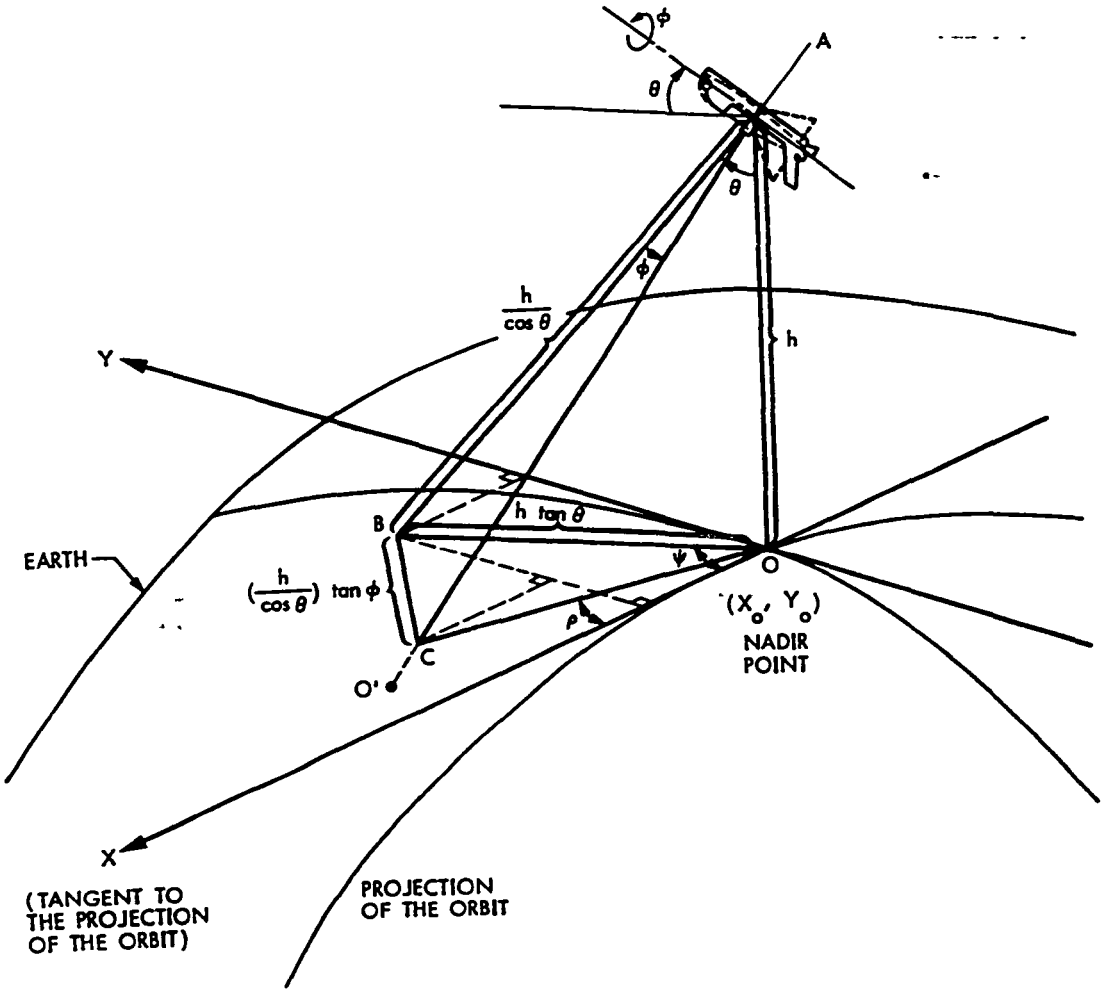

Figure 25. The Shift of Ground Projection of the IS Line-of-Sight due to Attitude Error

The interest here is to determine the coordinates of O'(X,Y) corresponding to the final line-of-sight projected onto the ground. By taking a view normal to the ACO-plane, Figure 26 is obtained. The quantities ε, ℓ, and ρ are obtained as follows,

$$\varepsilon = \tan^{-1}\left(\frac{\sqrt{X_2^2 + Y_2^2}}{h}\right) \tag{89a}$$

$$\ell = R \sin \varepsilon \left[\left(1 + \frac{h}{R}\right) \cos \varepsilon - \sqrt{1 - \left(1 + \frac{h}{R}\right)^2 \sin^2 \varepsilon}\right] \tag{89b}$$

and

$$\rho = \sin^{-1}\left(\frac{Y_2}{\sqrt{X_2^2 + Y_2^2}}\right) = \cos^{-1}\left(\frac{X_2}{\sqrt{X_2^2 + Y_2^2}}\right) \tag{89c}$$

Hence, the coordinates of X and Y are,

$$X = \ell \cos \rho = R \sin \varepsilon \left[\left(1 + \frac{h}{R}\right) \cos \varepsilon - \sqrt{1 - \left(1 + \frac{h}{R}\right)^2 \sin^2 \varepsilon}\right] \frac{X_2}{\sqrt{X_2^2 + Y_2^2}} \tag{90a}$$

$$Y = \ell \sin \rho = R \sin \varepsilon \left[\left(1 + \frac{h}{R}\right) \cos \varepsilon - \sqrt{1 - \left(1 + \frac{h}{R}\right)^2 \sin^2 \varepsilon}\right] \frac{Y_2}{\sqrt{X_2^2 + Y_2^2}} \tag{90b}$$

where X_2 and Y_2 are given in Eq. (88).

Note that this derivation is general enough so that the formulae are valid if one replaces the attitude errors with errors plus offsets, i.e., replacing ϕ, θ, and ψ by $\phi_o + \phi$, $\theta_o + \theta$, and $\psi_o + \psi$, respectively.

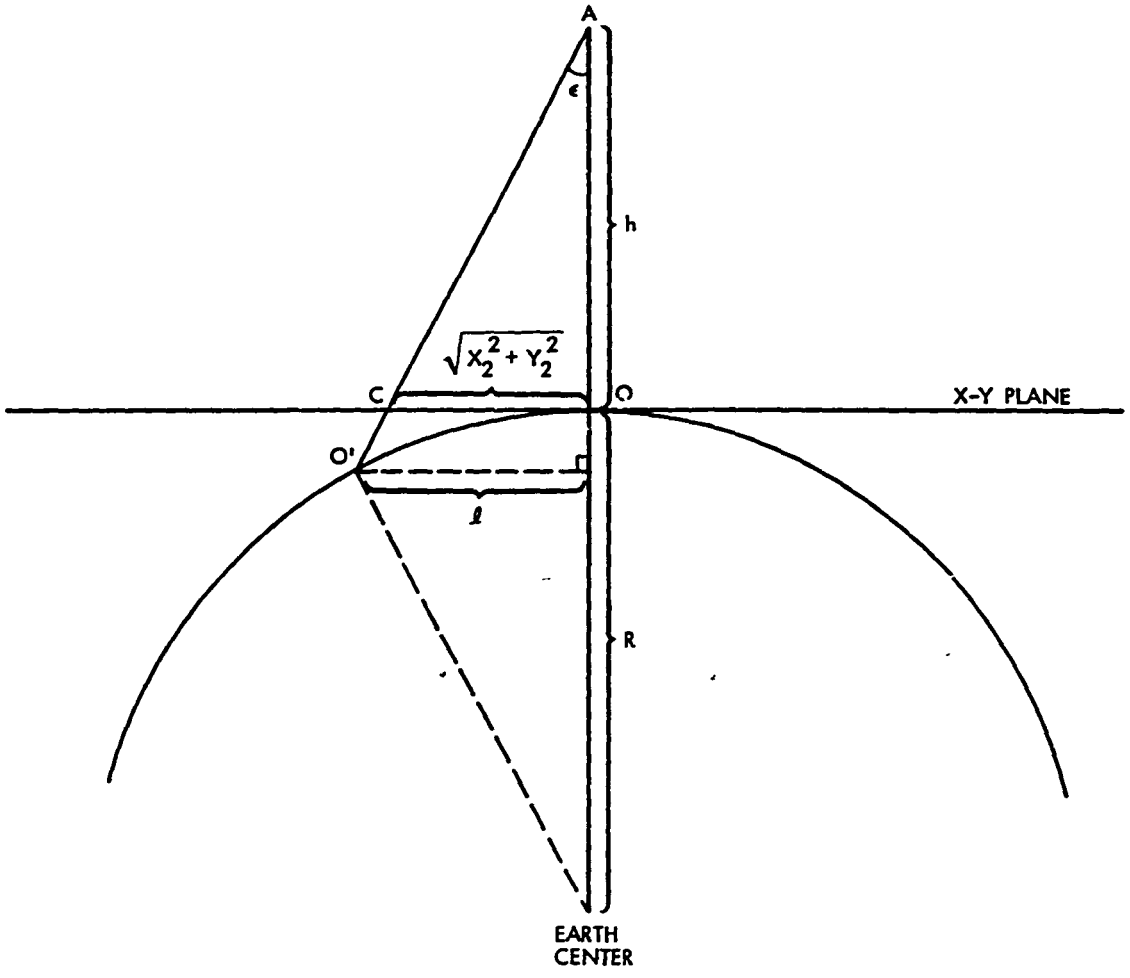

Figure 26. Side View of Figure 25

C.4.2. The Shift of Ground Image Due to Attitude Error

For simplicity, ϕ, θ, and ψ are used to represent the attitude angles as sums of attitude offsets and attitude errors. To fix the derivation, the yaw (ψ), pitch (θ), and roll (ϕ) Euler sequence is assumed.

In this subsection, the results of subsection C.4.1 are extended to cover the entire field of view of the IS slit. First consider the case of a nominal flight with zero attitude offset. Referring to Fig. 27 , let O be the nadir point which is the origin of the XY-Frame and the X'Y'-Frame. The X'Y'-Frame is formed by rotating the XY-Frame through an angle ψ about the yaw axis. Let P be a point corresponding to a view angle λ (negative value shown in Fig. 27) on the Y-axis before any rotation occurs. After a ψ rotation, for the same view angle, the IS is sighting point P_1. Similarly, after a pitch (θ) and then roll (ϕ) rotation, the points P_2 and then P_3 are sighted, respectively.

The coordinates of P_2 in the X'Y'-Frame are, from the results of subsections C.1 and C.2 and Fig. 23,

$$X'_2 = \frac{R \sin\theta \sin\xi_2 \left[\left(1 + \frac{h}{R}\right)\cos\xi_2 - \sqrt{1 - \left(1 + \frac{h}{R}\right)^2 \sin^2\xi_2}\right]}{\sqrt{\sin^2\theta + \tan^2\lambda}} \qquad (91a)$$

$$Y'_2 = -\frac{R \tan\lambda \sin\xi_2 \left[\left(1 + \frac{h}{R}\right)\cos\xi_2 - \sqrt{1 - \left(1 + \frac{h}{R}\right)^2 \sin^2\xi_2}\right]}{\sqrt{\sin^2\theta + \tan^2\lambda}} \qquad (91b)$$

where the angle ξ_2 is the angle ξ defined in Fig. 23 corresponding to point P_2 here, and

$$\xi_2 = \tan^{-1}\left(\sec\theta \sqrt{\sin^2\theta + \tan^2\lambda}\right) \qquad (91c)$$

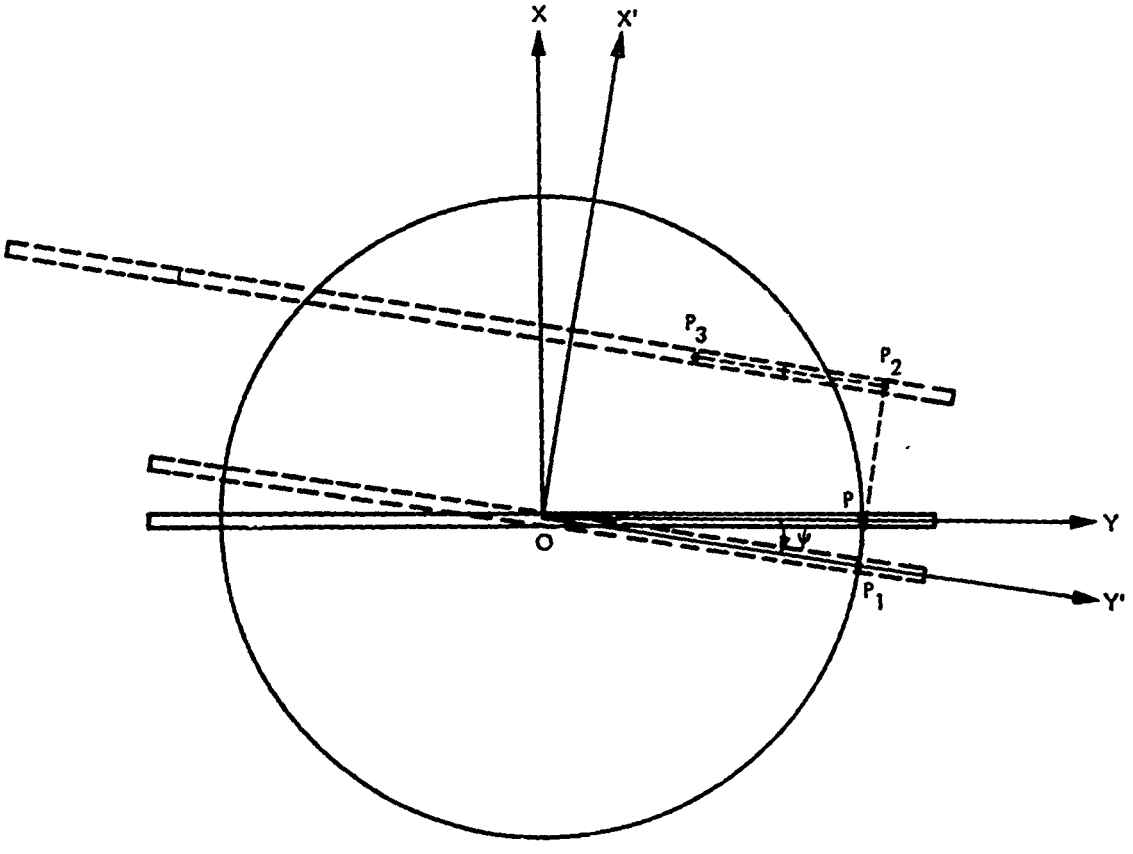

Figure 27. Shift of Ground Point Induced by Attitude Errors

The coordinates of P_3 in the X'Y'-Frame are

$$X_3' = \frac{R \sin\theta \sin\xi_3 \left[\left(1+\frac{h}{R}\right)\cos\xi_3 - \sqrt{1-\left(1+\frac{h}{R}\right)^2 \sin^2\xi_3}\right]}{\sqrt{\sin^2\theta + \tan^2(\lambda+\phi)}} \tag{92a}$$

$$Y_3' = -\frac{R \tan(\lambda+\phi) \sin\xi_3 \left[\left(1+\frac{h}{R}\right)\cos\xi_3 - \sqrt{1-\left(1+\frac{h}{R}\right)^2 \sin^2\xi_3}\right]}{\sqrt{\sin^2\theta + \tan^2(\lambda+\phi)}} \tag{92b}$$

where ξ_3 is similarly defined as ξ_2 and

$$\xi_3 = \tan^{-1}\left(\sec\theta \sqrt{\sin^2\theta + \tan^2(\lambda+\phi)}\right) \tag{92c}$$

or, finally, in the XY-Frame

$$X_3 = X_3' \cos\psi - Y_3' \sin\psi \tag{93a}$$

$$Y_3 = X_3' \sin\psi + Y_3' \cos\psi \tag{93b}$$

where X_3' and Y_3' are given in (92).

The geometric error caused by the attitude errors is therefore,

$$\Delta X = X - X_3 \tag{94a}$$

$$\Delta Y = Y - Y_3 \tag{94b}$$

where

$$X = 0$$

$$Y = -R \sin\lambda \left[\left(1+\frac{h}{R}\right)\cos\lambda - \sqrt{1-\left(1+\frac{h}{R}\right)^2 \sin^2\lambda}\right]$$

Now, consider the case of the shuttle (or the IS) flying at a nominal attitude $(\phi_o, \theta_o, \psi_o)$ with attitude uncertainties of (ϕ, θ, ψ). Let $P_o(X_o, Y_o)$ be a ground point that is sighted by the IS with a view angle λ and attitude $(\phi_o, \theta_o, \psi_o)$. After (ϕ, θ, ψ) attitude rotations from the nominal, the ground point $P_3(X_3, Y_3)$ is sighted with the same view angle. In this case, the geometric error is

$$\Delta X = X_o - X_3 \tag{95a}$$

$$\Delta Y = Y_o - Y_3 \tag{95b}$$

where

$$X_o = X_o' \cos \psi_o - Y_o' \sin \psi_o \tag{96a}$$

$$Y_o = X_o' \sin \psi_o + Y_o' \cos \psi_o \tag{96b}$$

$$X_3 = X_3' \cos (\psi_o + \psi) - Y_3' \sin (\psi_o + \psi) \tag{96c}$$

$$Y_3 = X_3' \sin (\psi_o + \psi) + Y_3' \cos (\psi_o + \psi) \tag{96d}$$

and

$$X_o' = \frac{R \sin \theta_o \sin \xi_o \left[\left(1 + \frac{h}{R}\right) \cos \xi_o - \sqrt{1 - \left(1 + \frac{h}{R}\right)^2 \sin^2 \xi_o}\right]}{\sqrt{\sin^2 \theta_o + \tan^2 (\lambda + \phi_o)}} \tag{97a}$$

$$Y_o' = - \frac{R \tan (\lambda + \phi_o) \sin \xi_o \left[\left(1 + \frac{h}{R}\right) \cos \xi_o - \sqrt{1 - \left(1 + \frac{h}{R}\right)^2 \sin^2 \xi_o}\right]}{\sqrt{\sin^2 \theta_o + \tan^2 (\lambda + \phi_o)}} \tag{97b}$$

where

$$\xi_o = \tan^{-1} \left(\sec \theta_o \sqrt{\sin^2 \theta_o + \tan^2 (\lambda + \phi_o)}\right) \tag{97c}$$

and

$$X_3' = \frac{R \sin (\theta_o + \theta) \sin \xi_3 \left[\left(1 + \frac{h}{R}\right) \cos \xi_3 - \sqrt{1 - \left(1 + \frac{h}{R}\right)^2 \sin^2 \xi_3}\right]}{\sqrt{\sin^2 (\theta_o + \theta) + \tan^2 (\lambda + \phi_o + \phi)}} \tag{98a}$$

$$Y_3' = - \frac{R \tan (\lambda + \phi_o + \phi) \sin \xi_3 \left[\left(1 + \frac{h}{R}\right) \cos \xi_3 - \sqrt{1 - \left(1 + \frac{h}{R}\right)^2 \sin^2 \xi_3}\right]}{\sqrt{\sin^2 (\theta_o + \theta) + \tan^2 (\lambda + \phi_o + \phi)}} \tag{98b}$$

and where

$$\xi_3 = \tan^{-1} \left[\sec (\theta_o + \theta) \sqrt{\sin^2 (\theta_o + \theta) + \tan^2 (\lambda + \phi_o + \phi)}\right] \tag{98c}$$

To include errors caused by altitude uncertainties, one can replace h by h_o in Eq. (97), and h by $h_o + \Delta h$ in Eq. (98), where h_o is the nominal or estimated altitude and $h_o + \Delta h$ is the actual altitude.

D. GEOMETRIC ERRORS INDUCED BY ATTITUDE RATE ERRORS

Attitude rates cause attitude angle changes which in turn cause geometric errors. To account for attitude rates, one integrates the rates to obtain the attitude angles, and then uses the formulae derived to obtain the corresponding time-varying geometric errors. The instantaneous attitude angles are:

$$\phi' = \phi_o + \int_{t_o}^{t} \dot{\phi} d\tau \tag{99a}$$

$$\theta' = \theta_o + \int_{t_o}^{t} \dot{\theta} d\tau \tag{99b}$$

$$\psi' = \psi_o + \int_{t_o}^{t} \dot{\psi} d\tau \tag{99c}$$

E. GEOMETRIC ERRORS INDUCED BY MISALIGNMENT ERRORS

The misalignment errors can be incorporated in the attitude errors. Let $(\phi_b, \theta_b, \psi_b)$ be the attitude bias or misalignment, then the effective IS attitude angles will be

$$\phi' = \phi_o + \phi_b + \phi \tag{100a}$$

$$\theta' = \theta_o + \theta_b + \theta \tag{100b}$$

$$\psi' = \psi_o + \psi_b + \psi \tag{100c}$$

The corresponding geometric errors can be determined using the formulae derived in subsection C.

F. GEOMETRIC ERRORS INDUCED BY EARTH ROTATION

The effect of earth rotation on images varies with the position of the Shuttle relative to the earth and the Shuttle orbital elements. In general, ground images become skewed as a result of earth rotation.

Referring to Fig. 28, Let O be the nadir point at which the latitude is ζ. Let ω_e be the spin rate of the earth, where $\omega_e = \frac{2\pi}{86400} = 7.2722 \times 10^{-5}$ rad/sec. Let V_e be the linear velocity of the earth at O,

$$V_e = \omega_e R \cos \zeta \tag{101}$$

Let Γ be the orbital inclination at the equator, and let Λ be the orbital inclination to the local meridian at O. From Fig. 29 and Appendix B, one has the following spherical geometrical relation,

$$\cos \Gamma = \cos \zeta \sin \Lambda$$

or

$$\sin \Lambda = \frac{\cos \Gamma}{\cos \zeta} \tag{102a}$$

and

$$\cos \Lambda = \sqrt{1 - \sin^2 \Lambda} = \sqrt{1 - \left(\frac{\cos \Gamma}{\cos \zeta}\right)^2} \tag{102b}$$

From Fig. 29 again, Λ is also the angle between the linear velocity vector V_e and the Y-axis. Hence, velocity components V_{eX} and V_{eY} are, using (102),

$$V_{eX} = V_e \sin \Lambda = \frac{V_e \cos \Gamma}{\cos \zeta} \tag{103a}$$

and

$$V_{eY} = V_e \cos \Lambda = V_e \sqrt{1 - \left(\frac{\cos \Gamma}{\cos \zeta}\right)^2} \tag{103b}$$

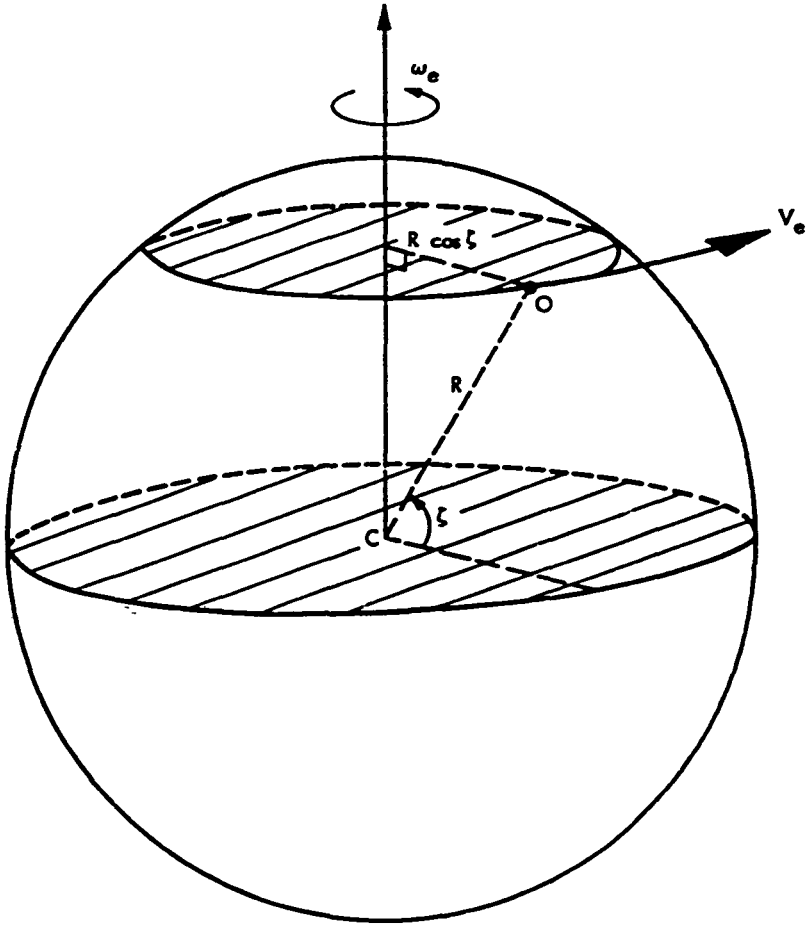

LEGEND:

ω_e = ANGULAR VELOCITY OF EARTH SPIN

ζ = LATITUDE AT POINT O

V_e = LINEAR VELOCITY OF THE EARTH AT POINT O

Figure 28. Linear Velocity of the Earth at the Nadir Point

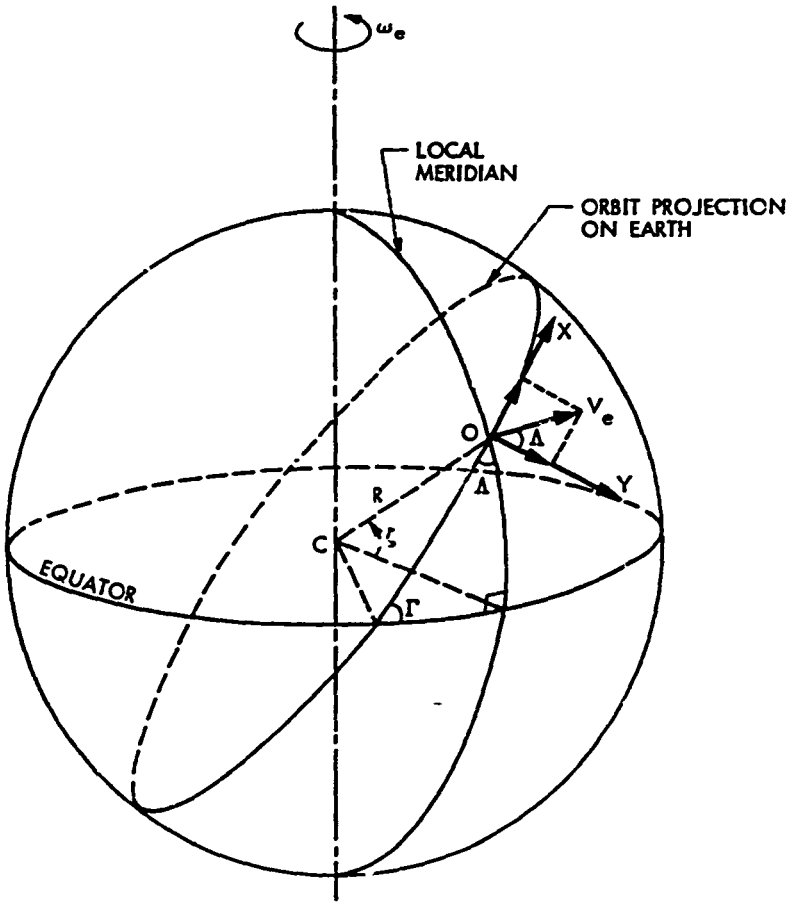

(a) INTRACK AND CROSSTRACK COMPONENTS OF EARTH LINEAR VELOCITY VECTOR AT THE NADIR POINT

(b) ORBIT INCLINATION TO THE LOCAL MERIDIAN (A), degrees

ORBITAL INCLINATION (degrees)	NORTH LATITUDE, degrees				
	0	20	40	60	80
0	90	–	–	–	–
18.5	71.5	–	–	–	–
40	50	54.61	90	–	–
60	30	32.15	40.75	90	–
85	5	5.32	6.53	10.04	30.13
90	0	0	0	0	0

Figure 29. Earth Sperical Geometry

During the time interval from t_1 to t_2, the ground point has moved from P(X, Y) to P'(X', Y'), the corresponding position changes are,

$$\Delta X = \int_{t_1}^{t_2} V_{eX} dt = \int_{t_1}^{t_2} \frac{Ve \cos \Gamma}{\cos \zeta} dt \tag{104a}$$

$$\Delta Y = \int_{t_1}^{t_2} V_{eY} dt = \int_{t_1}^{t_2} Ve \sqrt{1 - \left(\frac{\cos \Gamma}{\cos \zeta}\right)^2} dt \tag{104b}$$

Note that for small time intervals, ζ may be considered constant and (104) may be approximated as

$$\Delta X \cong \frac{\cos \Gamma}{\cos \zeta} V_e \ (t_2 - t_1) \tag{105a}$$

$$\Delta Y \cong \sqrt{1 - \left(\frac{\cos \Gamma}{\cos \zeta}\right)^2} \ V_e (t_2 - t_1) \tag{105b}$$

and

$$X' = X + \Delta X \tag{106a}$$

$$Y' = Y + \Delta Y \tag{106b}$$

G. NUMERICAL RESULTS: GEOMETRIC ERRORS AND ERROR SENSITIVITIES

Numerical results of error sensitivities and geometric errors due to various direct errors have been generated. These data are summarized in Tables 5-10 and discussed in the following subsections.

G.1 Geometric Errors Due to Altitude Uncertainties

Table 5 shows the geometric error for a 1 km altitude change and error sensitivity caused by altitude uncertainty. The nominal altitude of 400 km was used to generate these data. This result is also plotted in Fig. 30 as a function of view angles for altitude changes ranging from 1 km to 4 km. As indicated in this figure, the geometric errors are quite linear with the view angles and the altitude errors for the range shown.

For the Imaging Spectrometer illustrated in Fig. 4, the view angles are limited by the field of view of $\pm.825^{\circ}$. Using the various expected on-orbit navigation accuracies shown in Table 4, and the sensitivity data of Table 5, the corresponding geometric error can be determined. For instance, from Table 4, the 3σ altitude uncertainty, with TDRSS in the tracking system for the 150 nmi. orbit, if the small unmodeled perturbation is used, is 800 feet (or $\sim$244 m) and with the STDN system and large unmodeled perturbation and 105 nmi. orbit, the 3σ altitude uncertainty is 8000 feet (or $\sim$2440 m). From Table 5, the corresponding 3σ geometric errors for the largest view angle ($.825^{\circ}$) are 3.51 m and 35.1 m, respectively. Note that the nominal pixel size is 30 m.

G.2 Geometric Errors Due to Roll Uncertainties

The geometric errors for view angles ranging from -9° to $+9^{\circ}$ due to a roll error of 1° are tabulated in Table 6. The error sensitivity at the nominal attitude is also tabulated in Table 6. By comparing the errors for 1° and the sensitivity for the same view angle, it is found that the differences are .2% or less. That is, for small angles, the error sensitivity data can be used to compute errors. Fig. 31 shows the plots of geometric errors for roll errors of up to 5°. Unlike the errors corresponding to altitude uncertainties, these curves are relatively flat. The geometric error is about 7 km per 1° of roll error.

It is noted from Fig. 31, that for small roll errors, the geometric errors are nearly symmetrical with the view angles. For larger roll angles, the geometric errors are greater for view angles that have the same sign of ϕ. This is more visible from Fig. 32 which shows the plots of geometric errors corresponding to roll errors of 1° and 2° from a roll offset of 20°.

G.3 Geometric Errors Due to Pitch Uncertainties

Table 7 shows the error sensitivity and the geometric errors corresponding to the 1° pitch error for the view angles of up to $\pm 9^{\circ}$. The geometric errors caused by pitch errors are about the same in amplitude as those caused by roll errors. Fig. 33 shows that pitch curves are rather flat, unlike the corresponding roll curves. Figs. 34 and 35 show the 1° and 2° pitch uncertainty induced geometric error curves with 22.5° and 45° pitch offsets, respectively. These curves, especially those in Fig. 35, are more similar to the roll curves in shape.

G.4 Geometric Errors Due to Yaw Uncertainties

Geometric errors due to rotations about the yaw or the local vertical axis (assuming zero offsets) are tabulated in Table 8 for 1° and plotted in Fig. 36 for up to 5°. Linearity applies for both the view angles and the yaw angles for the ranges covered here. Unlike roll and pitch errors, yaw errors induce much smaller geometric errors.

G.5 Geometric Errors Due to Attitude Uncertainties

Table 9 shows the geometric errors due to 1° error in each of the roll, pitch, and yaw axes. The error magnitude for a given view angle is approximately the vector sum of the roll and pitch induced errors.

Fig. 37 shows the plots of geometric errors caused by up to 5° roll, pitch, and yaw errors. Fig. 38 shows two curves, one corresponding to 1° pitch error and the other, 1° yaw error, with the roll offset of 20°.

Comparing pitch curve with that of Fig. 33, the 20° roll offset has no noticeable effects on the geometric errors. On the other hand, the effects on the yaw curve are quite pronounced, as a large bias of approximately 2.5 km results due to the 20° roll.

Fig. 39 shows the 1° roll and 1° yaw curves for a pitch offset of 22.5°. Fig. 40 shows the same curves for 45° pitch offset.

With the large angular pitch offsets, the yaw curves appear quite different from those without pitch offset, as noted in Figs. 36, 39, and 40. With these offsets, yaw-induced error curves look quite similar to those induced by roll errors in shape. By offsetting the pitch angle to 45°, the yaw-induced geometric errors increase to about sevenfold from zero pitch offset, and more than twofold over the 22.5° pitch offset.

The roll-induced geometric errors were less drastically affected by pitch angular offsets. For instance, for 22.5° pitch offset, the error has increased about 7% from that with zero offset, and about 46% for 45° pitch offset.

G. 6 Ground Point Shift Due to Shuttle Motion and Earth Rotation

The earth rotation effect on the shift of the ground image varies with the latitude of the shuttle, and the combined effects of the earth rotation and shuttle motion vary with the orbital inclination in addition to the latitude. Table 10 shows the tabulation with latitude ranging from 0° to 80°. The largest earth rotation effect occurs at the equator, .46 km in one second, and diminishes to .08 km in one second at the latitude of 80° as shown in Fig. 41.

The combined effects are dominated by the motion of the shuttle since at 400 km altitude the projected ground speed is much greater than the earth rotation speed. In a one-second period, the image will shift more than 7 km for any latitude.

Table 5. Geometric Errors and Error Sensitivity Due to Altitude Uncertainties

- Nominal Earth Radius = 6356.785 km (Polar)
- Nominal Altitude = 400 km

View Angle, deg.	0	1	2	3	4	5	6	7	8	9
Geometric Error Induced by 1 km Altitude Error, km	0	0.01746	0.03492	0.05242	0.06995	0.08753	0.1052	0.1229	0.1407	0.1586
Geometric Error Sensitivity, km/km	0	0.01746	0.03492	0.05242	0.06995	0.08753	0.1052	0.1229	0.1407	0.1586

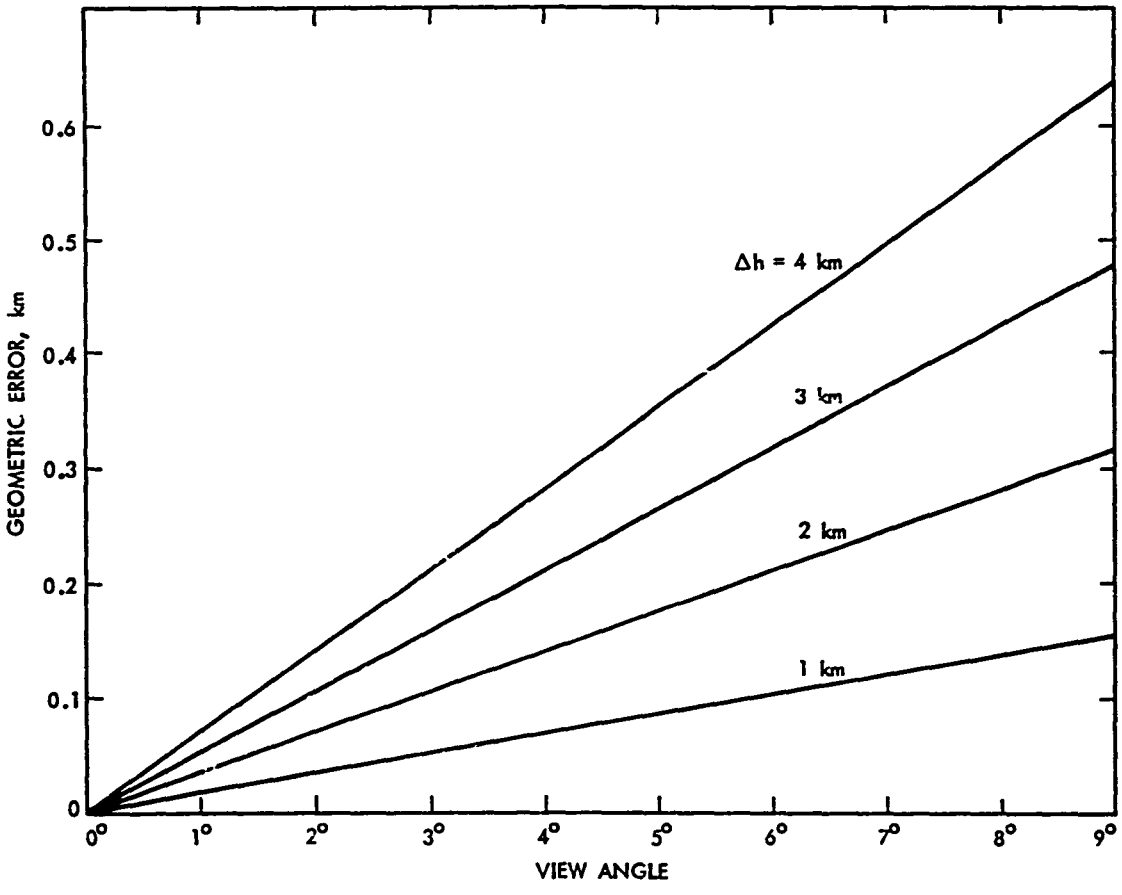

Figure 30. Geometric Error due to Altitude Uncertainties (Δh)

Table 6. Geometric Errors and Error Sensitivity Due to Roll Attitude Error

- Nominal Earth Radius = 6356.785 km (Polar)
- Nominal Altitude = 400 km

View Angle, deg.	-9	-8	-7	-6	-5	-4	-3	-2	-1	0
Geometric Error Induced by +1° Roll Error, km	7.153	7.114	7.081	7.052	7.029	7.010	6.996	6.987	6.982	6.982
Geometric Error Sensitivity, km/deg.	7.173	7.133	7.097	7.066	7.040	7.019	7.002	6.991	6.984	6.981
View Angle, deg.	1	2	3	4	5	6	7	8	9	
Geometric Error Induced by +1° Roll Error, km	6.987	6.996	7.010	7.029	7.052	7.081	7.114	7.153	7.196	
Geometric Error Sensitivity, km/deg.	6.984	6.991	7.002	7.019	7.040	7.066	7.097	7.133	7.173	

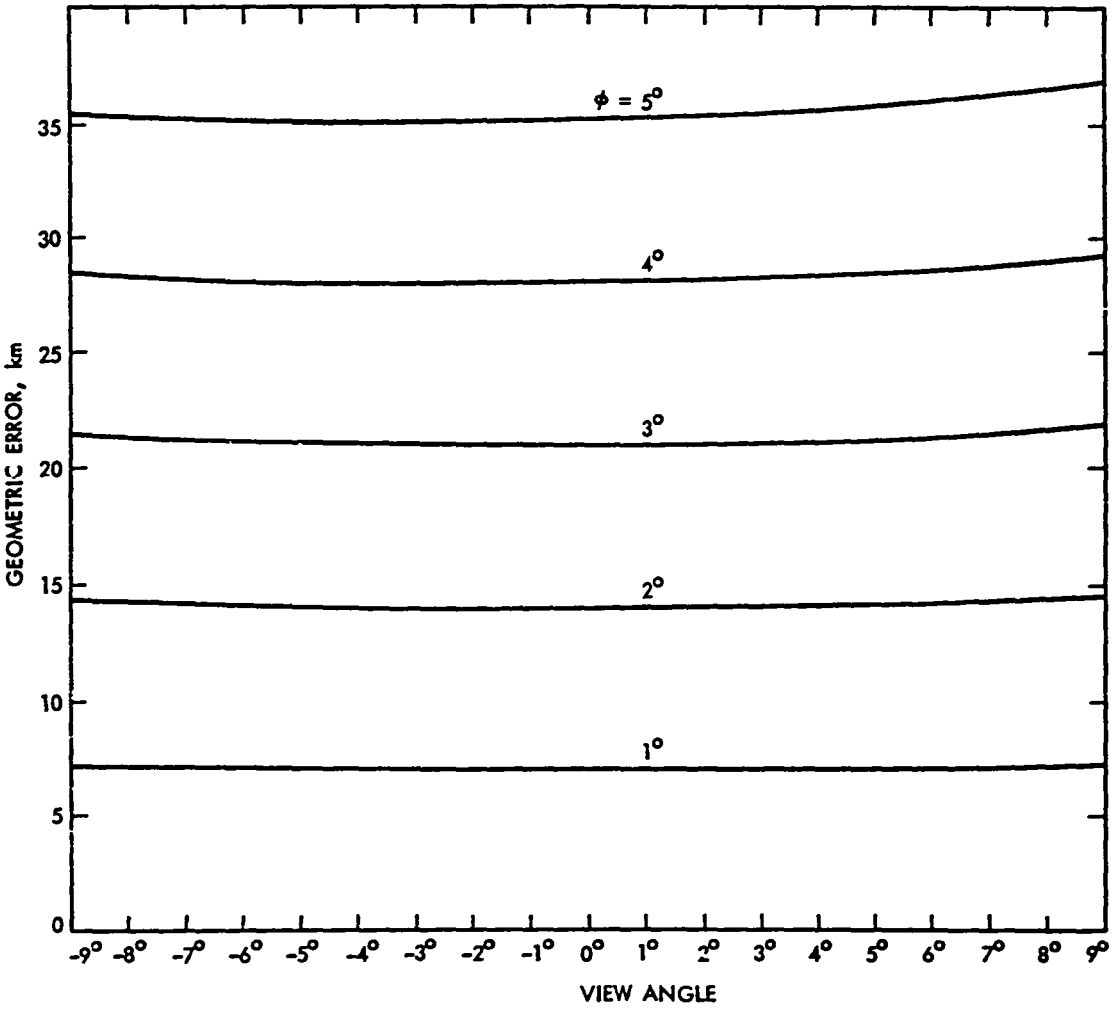

Figure 31. Geometric Error due to Roll Attitude Error (ϕ)

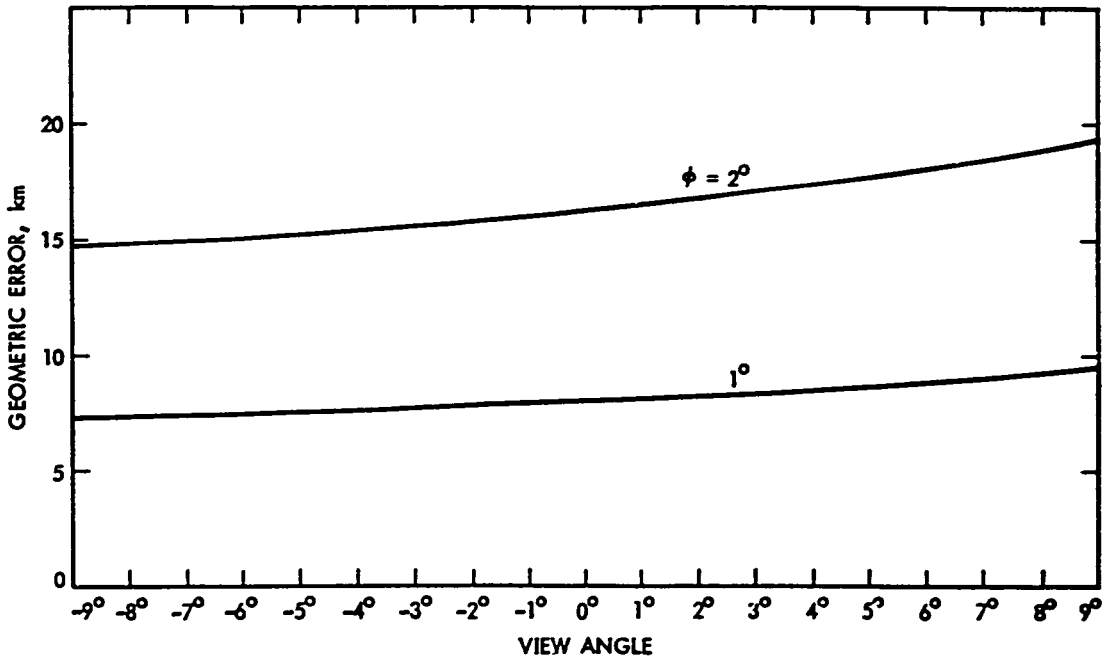

Figure 32. Geometric Error due to Roll Uncertainty (ϕ) About 20° Roll Offset

Table 7. Geometric Errors and Error Sensitivity Due to Pitch Attitude Error

- Nominal Earth Radius = 6356.785 km (Polar)
- Nominal Altitude = 400 km

View Angle, deg.	-9	-8	-7	-6	-5	-4	-3	-2	-1	0
Geometric Error Induced by 1° Pitch Error, km	6.988	6.986	6.985	6.985	6.984	6.983	6.983	6.982	6.982	6.982
Geometric Error Sensitivity, km/deg.	6.987	6.986	6.985	6.984	6.983	6.982	6.982	6.982	6.981	6.981

View Angle, deg.	1	2	3	4	5	6	7	8	9	
Geometric Error Induced by 1° Pitch Error, km	6.982	6.982	6.983	6.983	6.984	6.985	6.985	6.986	6.988	
Geometric Error Sensitivity, km/deg.	6.981	6.982	6.982	6.982	6.983	6.984	6.985	6.986	6.987	

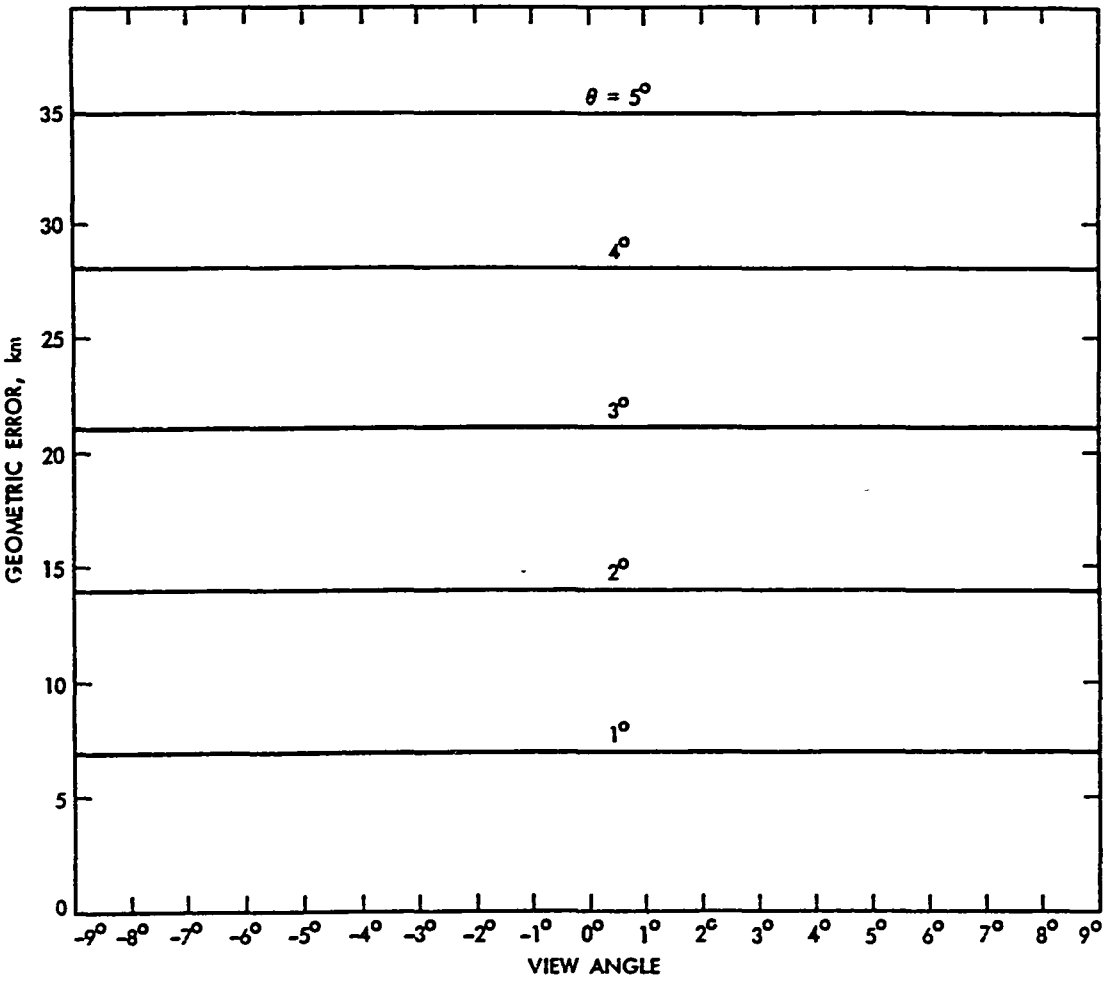

Figure 33. Geometric Error due to Pitch Attitude Error (θ)

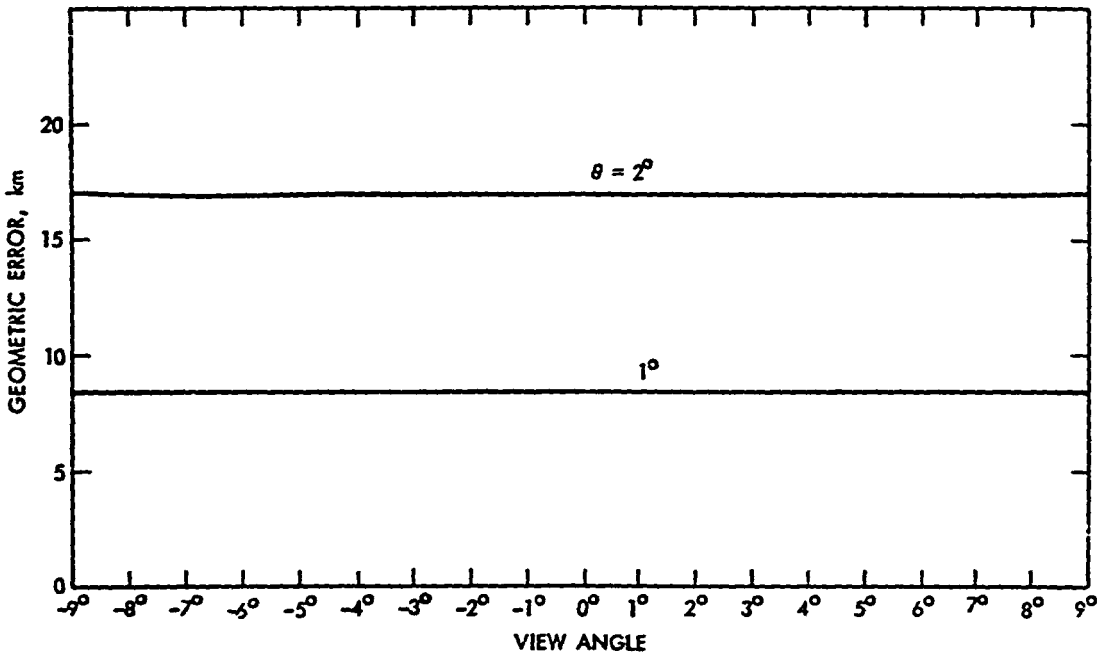

Figure 34. Geometric Error due to Pitch Uncertainty (θ) About 22.5° Pitch Offset

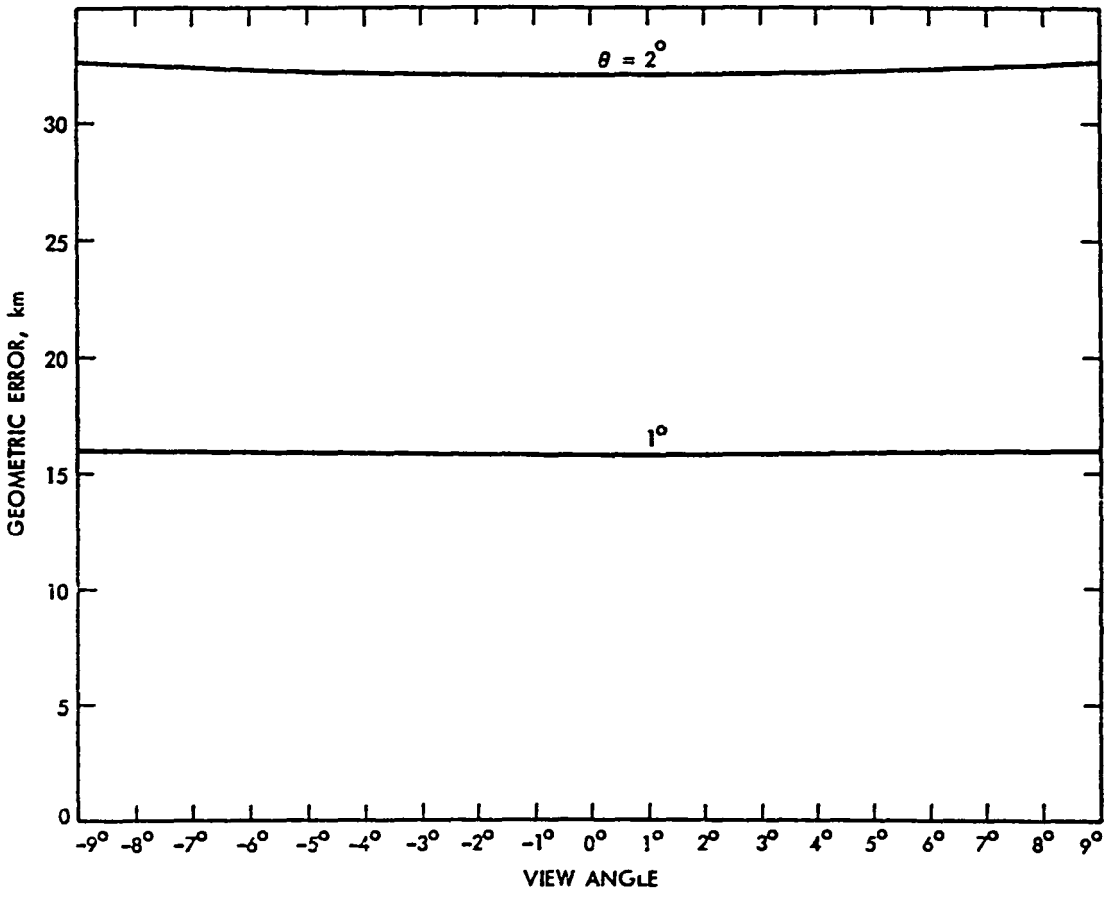

Figure 35. Geometric Error due to Pitch Uncertainty (θ) About 45° Pitch Offset

Table 8. Geometric Errors and Error Sensitivity Due to Yaw Attitude Error

- Nominal Earth Radius = 6356.785 km (Polar)
- Nominal Altitude = 400 km

View Angle, deg.	0	1	2	3	4	5	6	7	8	9
Geometric Error Induced by 1 Yaw Error, km	0	0.1219	0.2438	0.3659	0.4883	0.6109	0.7340	0.8576	0.9818	1.107
Geometric Error Sensitivity, km/deg.	0	0.1219	0.2438	0.3659	0.4883	0.6109	0.7340	0.8576	0.9818	1.107

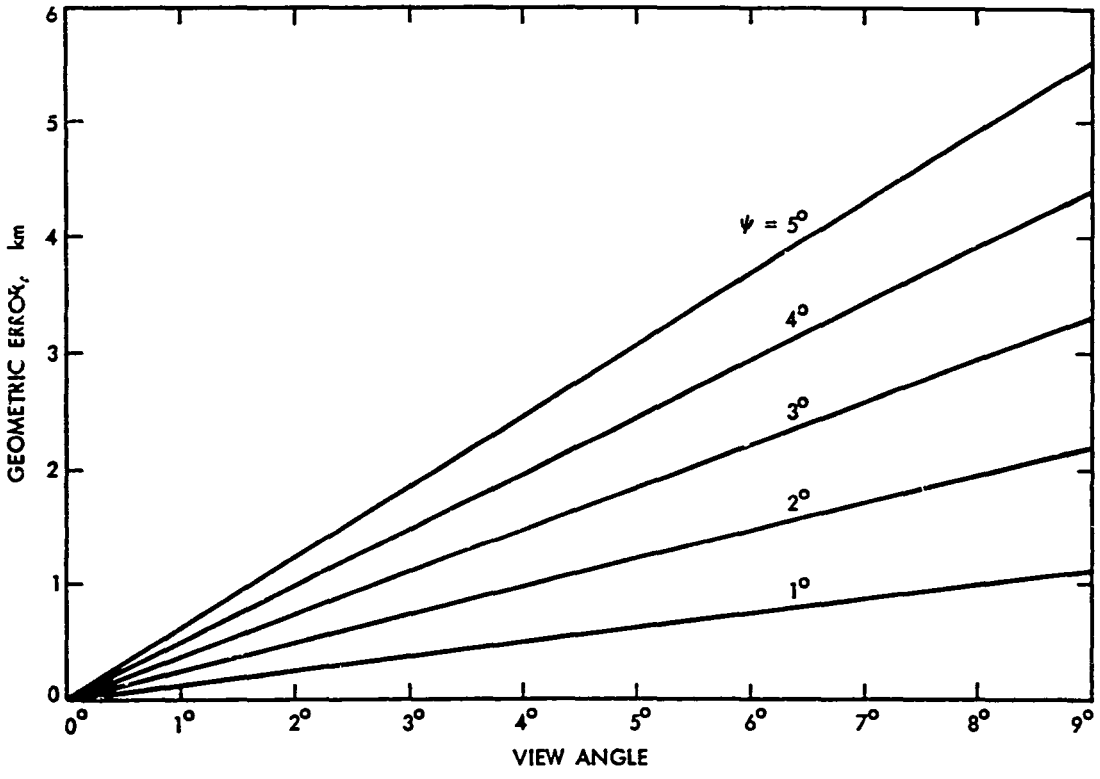

Figure 36. Geometric Error due to Yaw Attitude Error (ψ)

Table 9. Geometric Errors Induced by Yaw, Pitch, and Roll Errors

- Nominal Earth Radius = 6356.785 km (Polar)
- Nominal Altitude = 400 km
- Yaw Error = +1°
- Pitch Error = +1°
- Roll Error = +1°

View Angle, deg.	-9	-8	-7	-6	-5	-4	-3	-2	-1	0
Error, km	9.245	9.296	9.353	9.414	9.480	9.551	9.625	9.704	9.788	9.875
View Angle, deg.	1	2	3	4	5	6	7	8	9	
Error, km	9.966	10.06	10.16	10.27	10.37	10.48	10.60	10.72	10.85	

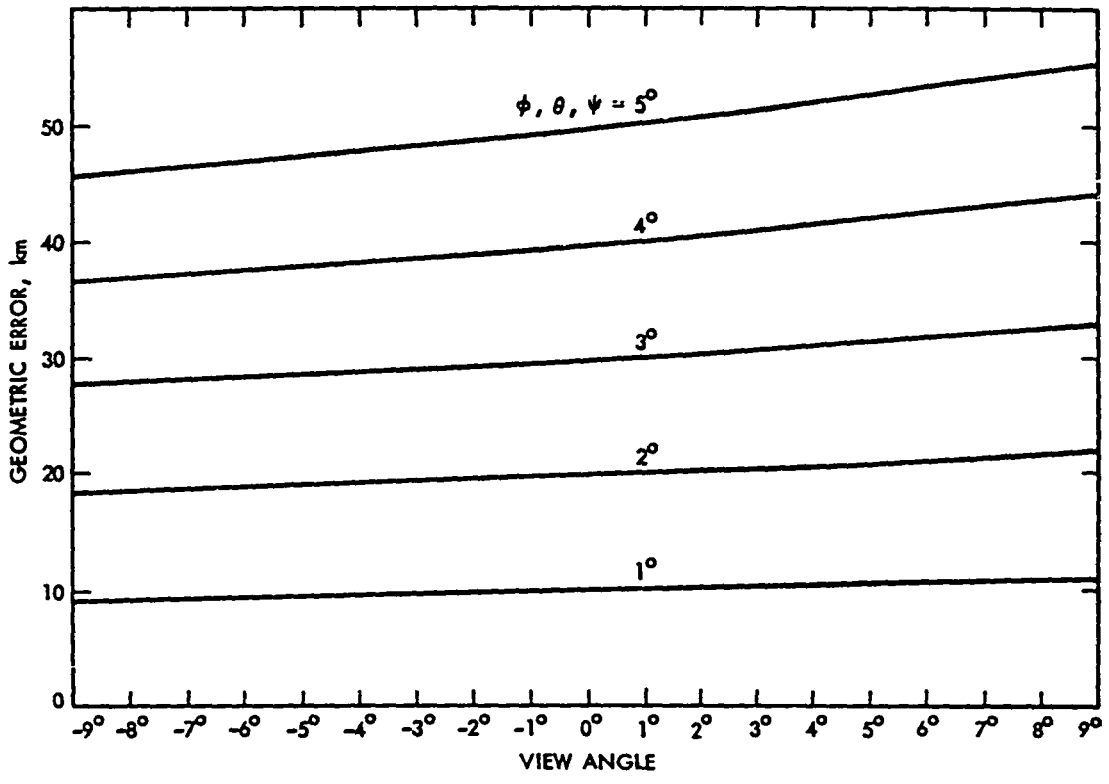

Figure 37. Geometric Error due to Roll (ϕ), Pitch (θ), and Yaw (ψ) Errors

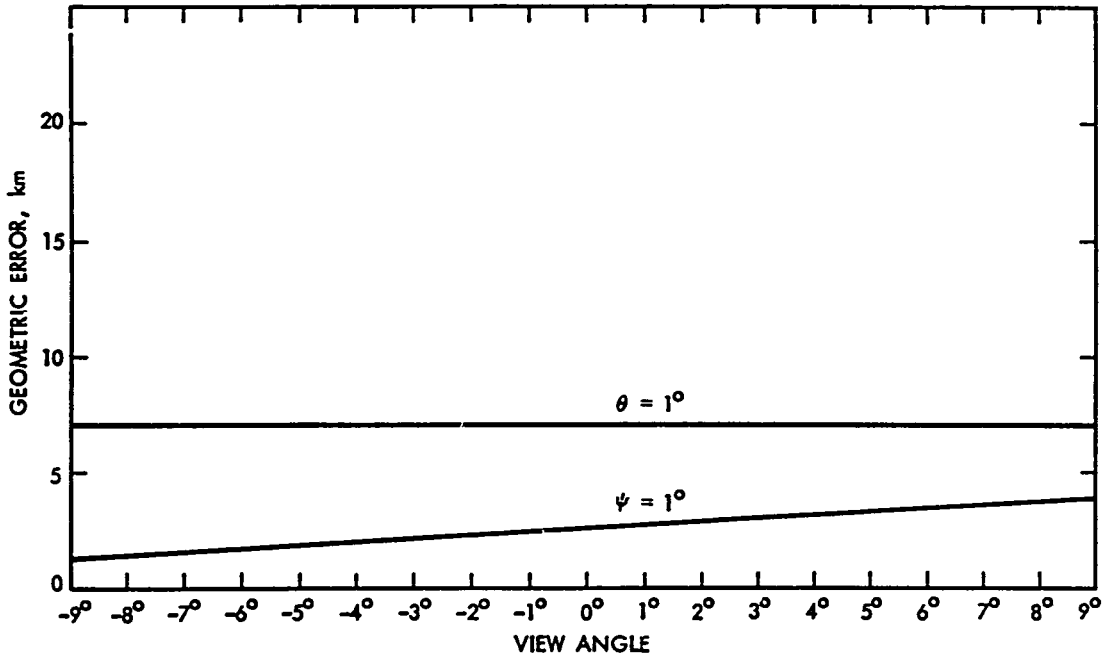

Figure 38. Geometric Error due to Pitch (θ) and Yaw (ψ) Uncertainties About 20° Roll Offset

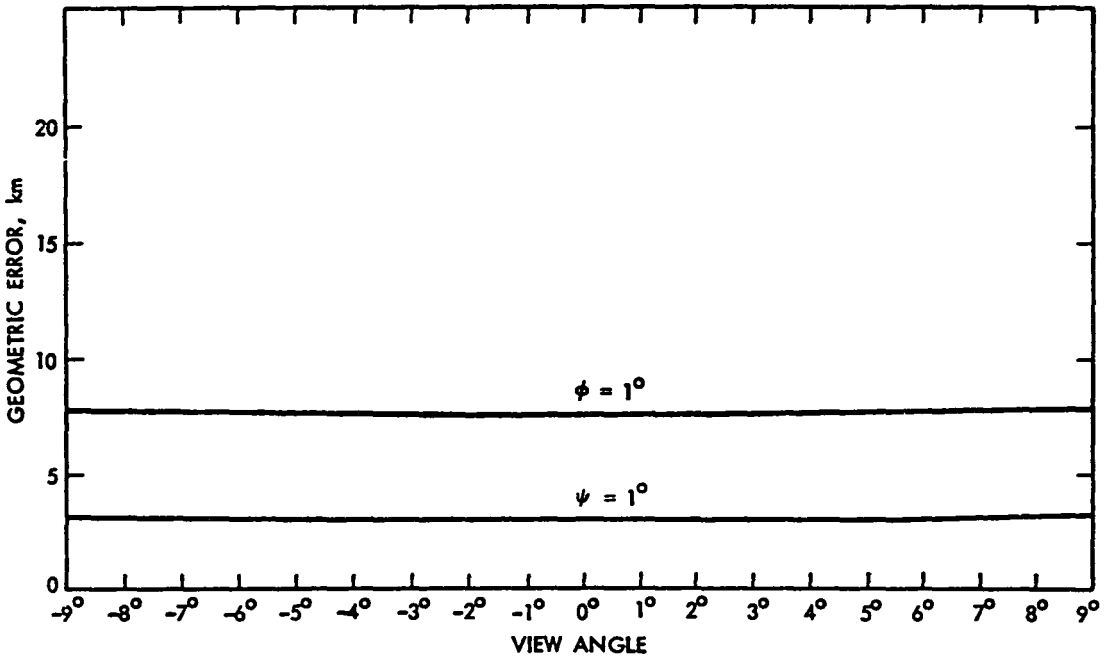

Figure 39. Geometric Error due to Roll (ϕ) and Yaw (ψ) Uncertainties About 22.5° Pitch Offset

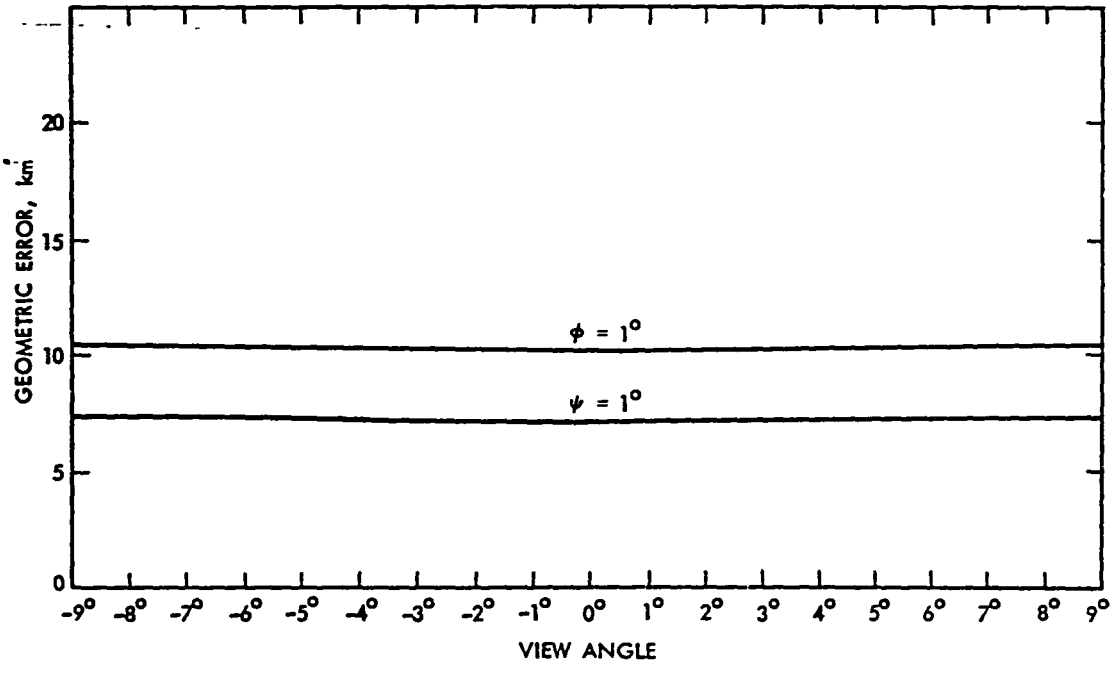

Figure 40. Geometric Error due to Roll (ϕ) and Yaw (ψ) Uncertainties About 45° Pitch Offset

Table 10. Ground Point Shift Induced by Shuttle Motion and Earth Rotation

- Nominal Earth Radius = 6356.785 km (Polar)
- Nominal Orbit Inclination = 85°
- Nominal Shuttle Ground Speed = 7.202 km/sec

Latitude, deg.	0	20	40	60	80
Ground Point Shift Velocity due to Earth Rotation, km/sec	0.4623	0.4344	0.3541	0.2311	0.08027
Ground Point Shift Velocity Relative to Nadir Point, km/sec	7.177	7.175	7.171	7.166	7.162
Angle of Velocity Vector with Y-axis, deg.	-86.32	-86.54	-87.19	-88.18	-89.44
Shift in 0.1 sec, km	0.7177	0.7175	0.7171	0.7166	0.7162

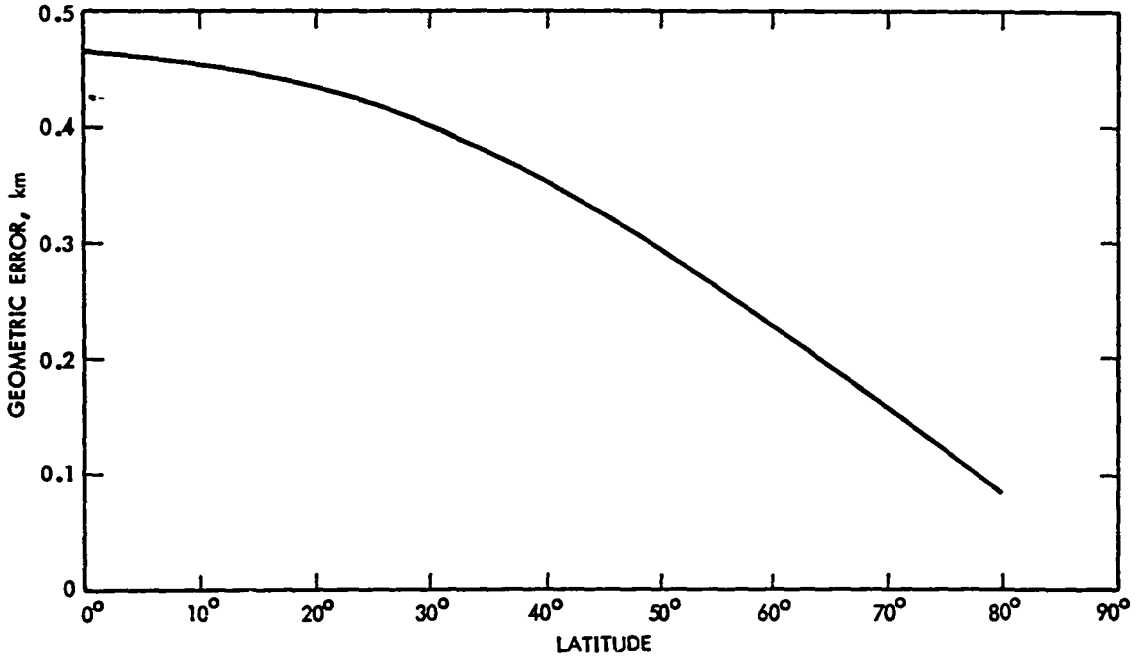

Figure 41. Geometric Error Caused by Earth Rotation for the Time Period of 1 Second

H. SUMMARY OF MAJOR FINDINGS

In this section geometric errors caused by the "direct error sources" are analyzed. Equations that map the direct errors onto the geometric errors are derived in Subsections B through G. Extensive illustrations of geometry are used to assist the derivations. Direct error effects included here are those of pointing errors and angular rates, ephemeris prediction errors including altitude, intrack, and crosstrack uncertainties, earth rotation and curvature, and shuttle and instrument misalignment. For quick reference the key error mapping functions are listed in Appendix A. A program list is given in Appendix E.

The numerical results for both the geometric errors and error sensitivities are tabulated in Tables 5 through 10 and also plotted in Figs. 30 through 41. To illustrate the effects of view angles and linearity, an extended range of $\pm 9^{\circ}$ is used. For the push broom imaging spectrometer studied here, the field of view is limited by $\pm .825^{\circ}$ (see Fig. 4). The following are the specific findings resulting from further analysis:

1. The effects of earth curvature are very small for the applications here. For instance, the linear displacement of a 10 km arc is 9.9999...km. Fig. 42 illustrates several cases of earth curvature effects.

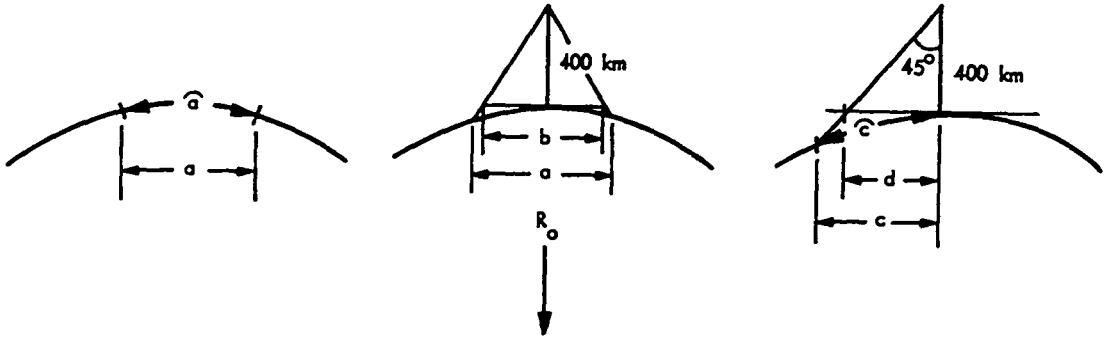

$\overset{\frown}{a}$ = 10 km
a = 9.99999 . . . km
b = 9.99994 . . . km
$\overset{\frown}{c}$ = 413.752 . . . km
c = 413.460 . . . km
a = 400 km

Figure 42. Effects of Earth Curvature

2. Altitude uncertainties cause only moderate geometric errors. Table 11 shows that the worst 1σ geometric error is 11.71 m and the corresponding rate is .133 m/sec. The worst case associates with the STDN system and large unmodeled perturbation and 200 km orbit. The least 1σ errors are .22 m and .0032 m/sec corresponding to the TDRSS system and small unmodeled perturbation and 300 km orbit. The effects of other navigation uncertainties such as downtrack and crosstrack position errors are not small, however. Table 12 shows the 3σ uncertainties in feet. Downtrack and crosstrack position errors are mapped directly to the geometric errors.

3. Geometric errors caused by altitude uncertainties are, within the range of interest here, proportional to the view angle and altitude error (see Table 5 and Fig. 30).

4. The effects of roll and pitch attitude errors are relatively large compared with those of altitude errors and yaw attitude errors. Table 13 shows that, for nominal flight conditions, the error sensitivity is approximately 1.94 m/arc sec, or ∿7000 m/degree. The yaw sensitivity is very small, from 0 for 0° view angle to .0279 m/arc sec for maximum IS view angle ±.825°.

The effects of attitude errors increase significantly for large attitude offsets. For instance, for 20° roll offset (side looking), the roll sensitivity increases to 2.28 m/arc sec from 1.94 and yaw sensitivity increases to .75 m/arc sec from .0279. The pitch sensitivity, in this case, is nearly unaffected. By offsetting the pitch angle to 45° (forward looking), the roll sensitivity increases to 2.83 m/arc sec, the pitch to 4.36 m/arc sec, and the yaw to 1.97 m/arc sec. Table 13 shows the error sensitivities and 1° geometric errors for many combinations of interest.

5. Without attitude offsets and within the IS field of view, the geometric errors are almost proportional to roll errors (Fig.31), pitch errors (Fig.33), and yaw errors (Fig.36), and are independent of the view angle except for the yaw cases (for which the error is proportional to the view angle). For the cases of large roll or pitch angular offset, most of the properties change only slightly (see Figs. 32, 34, 35, 38, 39, and 40).

6. The performance of the Imaging Spectrometer is limited by the shuttle Inertial Measuring Unit accuracy, the shuttle reference misalignment, and the misalignment between the shuttle and the Imaging Spectrometer, unless means of error reduction, such as using ground control points and a precision point mount between the shuttle and the IS instruments, are employed.

On top of these uncertainties, the shuttle deadband is another source of error that can cause gross geometric errors. This problem, of course, can be resolved by using a precision point mount.

Table 14 shows geometric errors caused by the IMU/shuttle misalignment, IMU resolution, IMU noise, rate gyro drift, and combined shuttle/IS misalignment, for nominal attitude and attitude offsets. Single axis geometric errors corresponding to the combined shuttle/IS misalignment are 169 m, 198 m, and 379 m, respectively, for nominal, 20° roll offset, and 45° pitch offset, for instance. Other cases are shown in detail in Table 14 .

7. Earth rotation causes images to shift toward the direction of rotation. The magnitude of this shift depends on the latitude of the object (see Fig. 41). For instance, at the equator, the object moves approximately 462 m in 1 second, while at 60° latitude, it moves only 231 m in one second.

Table 11. Geometric Errors Due to Expected On-orbit Navigation Uncertainty

Navigation Tracking System	Unmodeled Perturbation	Minimum Perigee, km	1σ Altitude Error, m	Max. Geom. Error in FOV, m	1σ Radial Velocity, m/s	Max. Geom. Error in FOV, m/s
STDN	Nominal	200	508	7.32	3.87	.056
TDRSS		200	366	5.27	2.25	.032
STDN	Small	200	305	4.39	2.50	.036
		300	122	1.76	.59	.0085
TDRSS		200	183	2.63	1.12	.016
		300	81	1.17	.22	.0032
STDN	Large	200	813	11.71	9.27	.133
TDRSS		200	610	8.78	5.69	.082

STDN — Spaceflight Tracking and Data Network
TDRSS — Tracking Data Relay Satellite System

Table 12. Expected On-Orbit Navigation Accuracies (Ref. 12)

Navigation Tracking System	Unmodeled Perturbation	Minimum Perigee, n.mi.	3σ Position, Feet			3σ Velocity, FPS		
			Radial	Down Track	Cross Track	Radial	Down Track	Cross Track
STDN	Nominal	105	5,000	34,500	5,000	38.4	5.9	9.8
TDRSS		105	3,600	18.500	4,000	22.1	3.3	4.0
STDN	Small	105	3,000	22,000	1,500	24.6	3.3	2.0
		150	1,200	5,500	1,000	5.8	1.3	1.8
TDRSS		105	1,800	10,000	2,000	11.0	1.8	2.9
		150	800	2,000	1,500	2.2	0.9	2.1
STDN	Large	105	8,000	80,000	5,000	91.2	8.0	8.0
TDRSS		105	6,000	50,000	5,000	56.0	6.2	7.8

NOTE:

The correlation between downtrack position and radial velocity is -0.95.
The correlation between radial position and downtrack velocity is -0.80.

STDN - Spaceflight Tracking and Data Network
TDRSS - Tracking Data Relay Satellite System

Table 13. Geometric Error Sensitivity

Nominal Orbit: 400 km Circular

Error Source	Attitude Offset	Error Sensitivity, m/arc sec		Geometric Error for 1° Angular Error, m
		For View Angle = 0°	For View Angle = ±.825°	
Roll angle	No offset	1.939	1.940	6,987
Pitch angle		1.939	1.939	6,982
Yaw angle		0	.0279	101
Roll angle	20° roll offset	2.25	2.28 2.22	8,200
Pitch angle		1.94	1.94	7,000
Yaw angle		.72	.75 .70	2,683
Roll angle	22.5° pitch offset	2.11	2.11	7,600
Pitch angle		2.31	2.31	8,300
Yaw angle		.83	.83	3,000
Roll angle	45° pitch offset	2.82	2.83	10,200
Pitch angle		4.33	4.36	15,700
Yaw angle		1.94	1.97	7,100
Altitude uncertainty		0	.0144 m/m	14.4 m per 1 km altitude change max in FOV

Table 14. Geometric Error Induced by Shuttle and Imaging Spectrometer Measurement Uncertainties

Nominal Orbit: 400 km Circular

Source	Attitude Offset	Per Axis, arc • sec	Per Axis Geometric Error, m	2 Axes,† Geometric Error, m
IMU/Shuttle Misalignment	No Offset	82	159	225
IMU Resolution*		20	39	55
IMU Noise		20	39	55
Rate Gyro		60 arc sec/sec	116 m/s	165 m/s
Combined Shuttle/IS Misalignment		87	169	239
IMU/Shuttle Misalignment	20° Roll Offset	82	187	245
IMU Resolution		20	46	60
IMU Noise		20	46	60
Rate Gyro		60 arc sec/sec	137 m/s	180 m/s
Combined Shuttle/IS Misalignment		87	198	260
IMU/Shuttle Misalignment	45° Pitch Offset	82	358	426
IMU Resolution		20	87	104
IMU Noise		20	87	104
Rate Gyro		60 arc sec/sec	262 m/s	312 m/s
Combined Shuttle/IS Misalignment		87	379	452

†Combined roll and pitch axes.

V. GROUND PATTERNS AND IMAGE DISTORTIONS

The extent that direct errors and earth geometric properties affect the performance of the Shuttle Imaging Spectrometer are analyzed and extensively illustrated with charts and tables in section IV. The advantages of tables and charts are that they carry precise and specific information which is invaluable for design and performance prediction. However, it is difficult to relate this information directly to images of ground objects by human brains. To compensate for this and to make direct observation of how errors in the system affect ground images, sclected ground patterns as seen through this optical system are studied here.

The patterns that are readily generated and, most importantly, suitable for exhibiting imaging distortions are square grid patterns.

To cover a large ground that is comparable to the field of view of the imaging spectrometer, a 10 km field is selected and the field is evenly divided into 10 segments of 1 km each. Since the imaging spectrometer employs a push broom principle, each field is then 10 km wide (cross track) and 30 m "long" (along track). However, to see a large ground area, a 10 km x 10 km field is employed with the along track grids tagged with time. Considering a perfectly spherical earth, an imaginary 10 x 10 grid is painted on the ground. As the satellite flies through this region, in the direction from the bottom to the top of the paper, a push broom camera should see a pattern just like that of Fig. 43(a). This pattern is referred to as the nominal ground pattern.

Fig. 43 shows how the ground pattern changes when simple attitude error occurs without considering the effect of Earth rotation. To show the effect of errors, the solid pattern (actual) is overlayed with the "+" pattern (the undistorted nominal pattern). Fig. 43(b) shows that when a 0.1^{o} roll attitude error occurs, the IS instrument points 0.1^{o} left of the object field and the image on

(a) NOMINAL GROUND PATTERN

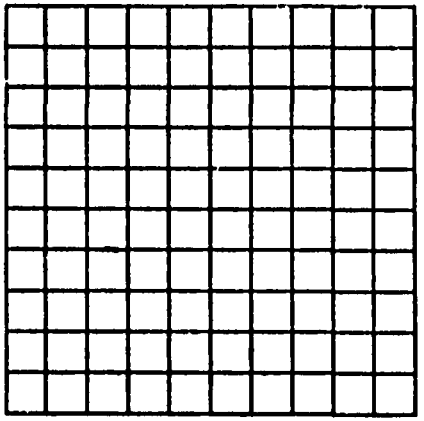

(b) WITH 0.1° ROLL ERROR

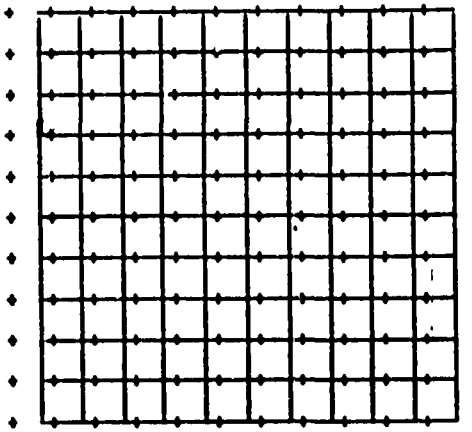

(c) WITH 5° YAW ERROR

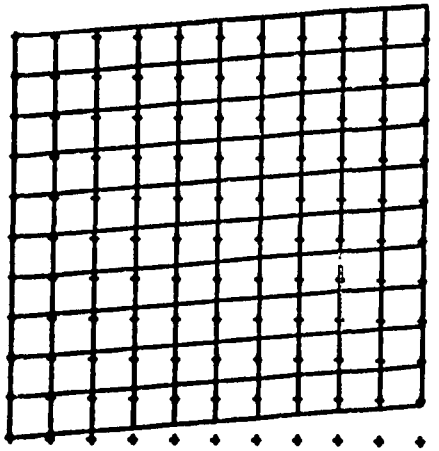

(d) WITH 0.1° PITCH ERROR

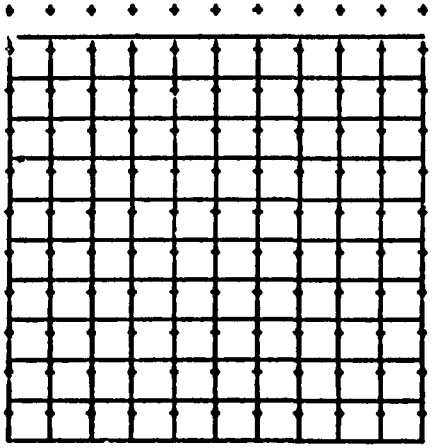

Fig. 43. Ground Pattern Distortions With No Earth Rotation Effect

the "film" has shifted to the right; therefore, the solid pattern has shifted to the right of the "+" pattern. The same explanation applies also to the 0.1^{o} pitch error as shown in Fig. 43(d), except that, for pitch, the pattern image has shifted to the "-along track" direction. A 5^{o} yaw error (clockwise rotation) will make the pattern appear skewed as shown in Fig. 43(c).

Fig. 44 shows the effects of simple attitude errors with 20^{o} roll offset. With the large roll angle, the nominal pattern itself has suffered cross track distortions, i.e., the pattern image appears shrunk cross-trackwise as shown in Fig. 44(a). In Fig. 44(b), (c), and (d), the "+" patterns represent the distorted nominal patterns due to roll offset alone and the solid patterns represent those due to attitude errors on top of roll offset. The distortions are similar to those found in Fig. 43 except that with the 20^{o} roll offset the images appear narrower.

The effects of simple attitude errors with 45^{o} pitch offset are shown in Fig. 45. The effect of pitch offset is similar to roll offset, i.e., the nominal pattern image has shrunk cross-trackwise. One might expect also along-track shrinkage. The reason that there is no along-track shrinkage is because of the push-broom effect. Shrinkage will occur for a frame camera, however. It is noted that the pattern images associated with the 45^{o} pitch offset are narrower than those of the 20^{o} roll offset. This is due to the fact that 20^{o} is a lot less than 45^{o}.

The effects of constant attitude rate errors are shown in Fig. 46. Rate errors cause accumulation of attitude errors, i.e., the attitude errors grow with time t. Take the 0.1 deg/sec rate error for the roll axis for instance, the roll error is 0.1 t; whereas, the 0.1^{o} roll error (Fig. 43(b)) at t = 0 is 0; therefore, the "+" pattern image coincides with the solid one at a very

(a) NOMINAL GROUND PATTERN

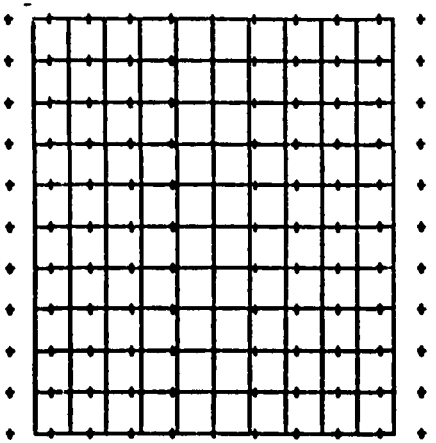

(b) WITH 0.05° ROLL ERROR

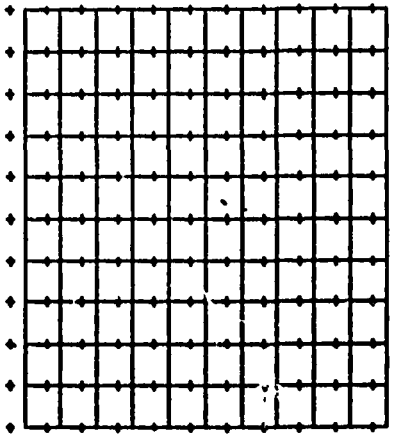

(c) WITH 5° YAW ERROR

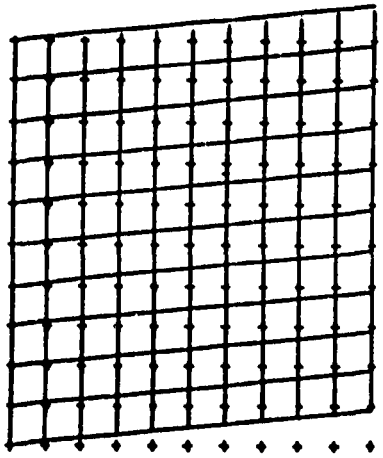

(d) WITH 0.1° PITCH ERROR

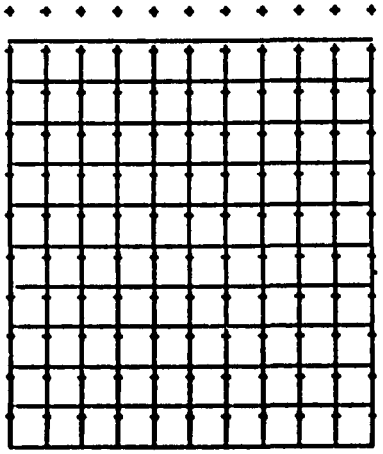

Fig. 44. Ground Pattern Distortions With 20° Roll Offset and No Earth Rotation Effect

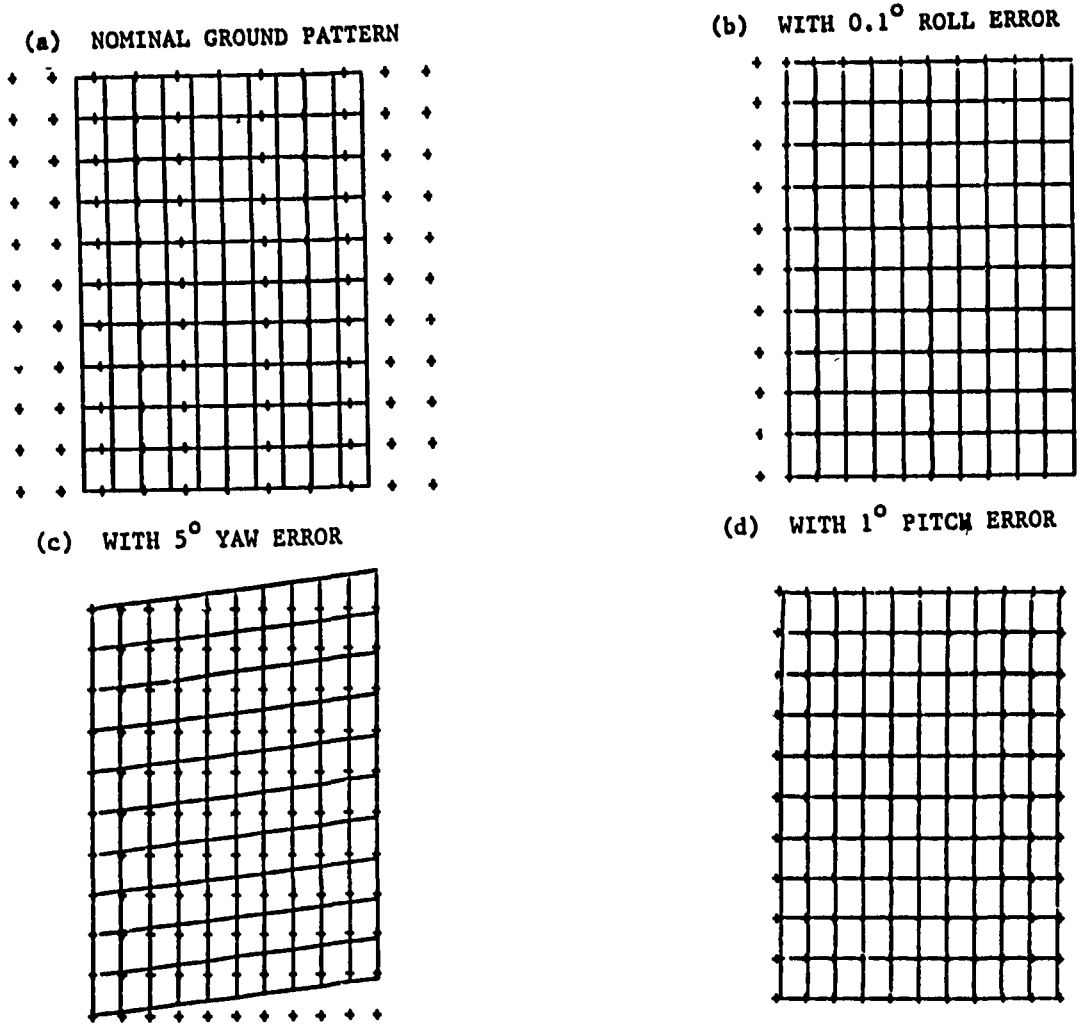

Fig. 45. Ground Pattern Distortions With 45° Pitch Offset and No Earth Rotation Effect

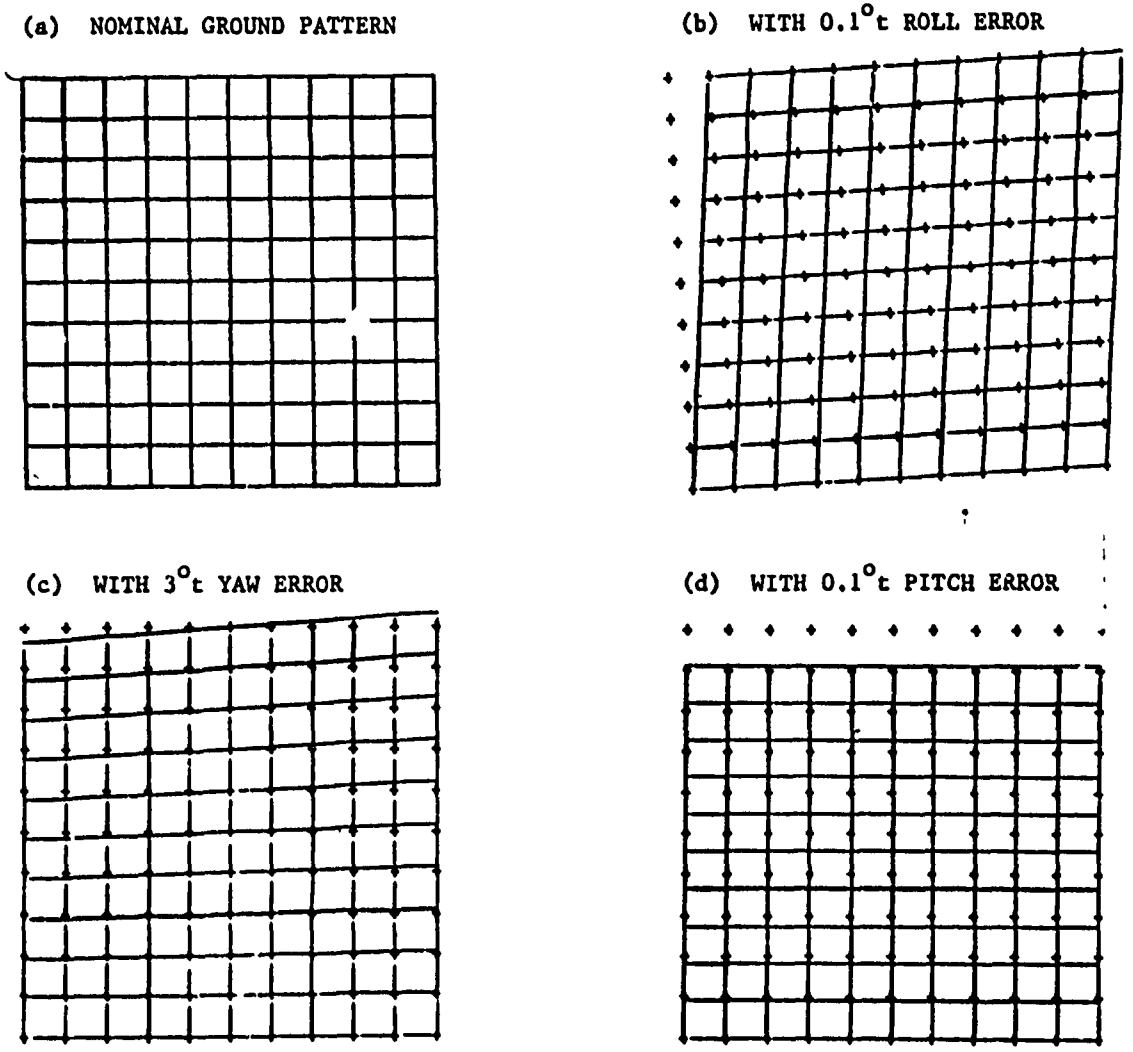

Fig. 46. Ground Pattern Distortions With Constant Rotation Rate and No Earth Rotation Effect

small t. Shown in Fig. 46(b) is the solid pattern shift to the right at a constant slope with time, which is quite different from Fig. 43(b). Similar comment applies to Fig. 46(c) and (d).

The effects of sinusoidal attitude rates on the pattern images are shown in Fig. 47. For instance, the sinusoidal rate causing a 0.2 sin (4.51378t) degree roll error will make the image appear as the shape "S", as shown in Fig. 47(b). The same function applied to the pitch axis will cause along-track distortions with densely packed grid lines followed by loosely packed ones, etc., as illustrated in Fig. 47(d).

Altitude change causes images to vary in size. Again, it affects the cross-track much more than the along-track due to the push-broom principle. As shown in Fig. 48, the solid image has shrunk cross-trackwise but expanded along-trackwise. The former is due to the altitude increase of 40 km which has no amplification effect on push-broom camera; the latter is due to the fact that, at higher altitude, the orbital rate is decreased, i.e., it will take a longer period of time to fly through the same ground area.

Finally, the effects of earth rotation are shown in Fig. 49. Earth rotation will cause the image to skew toward the direction of earth rotation. As discussed in section IV, the effect of the image shift is most pronounced when the satellite flies through the equator, and reduces as the latitude increases. Earth rotation will not cause along-track distortions.

Computer programs that are used to generate these patterns and distortions are listed in Appendix F.

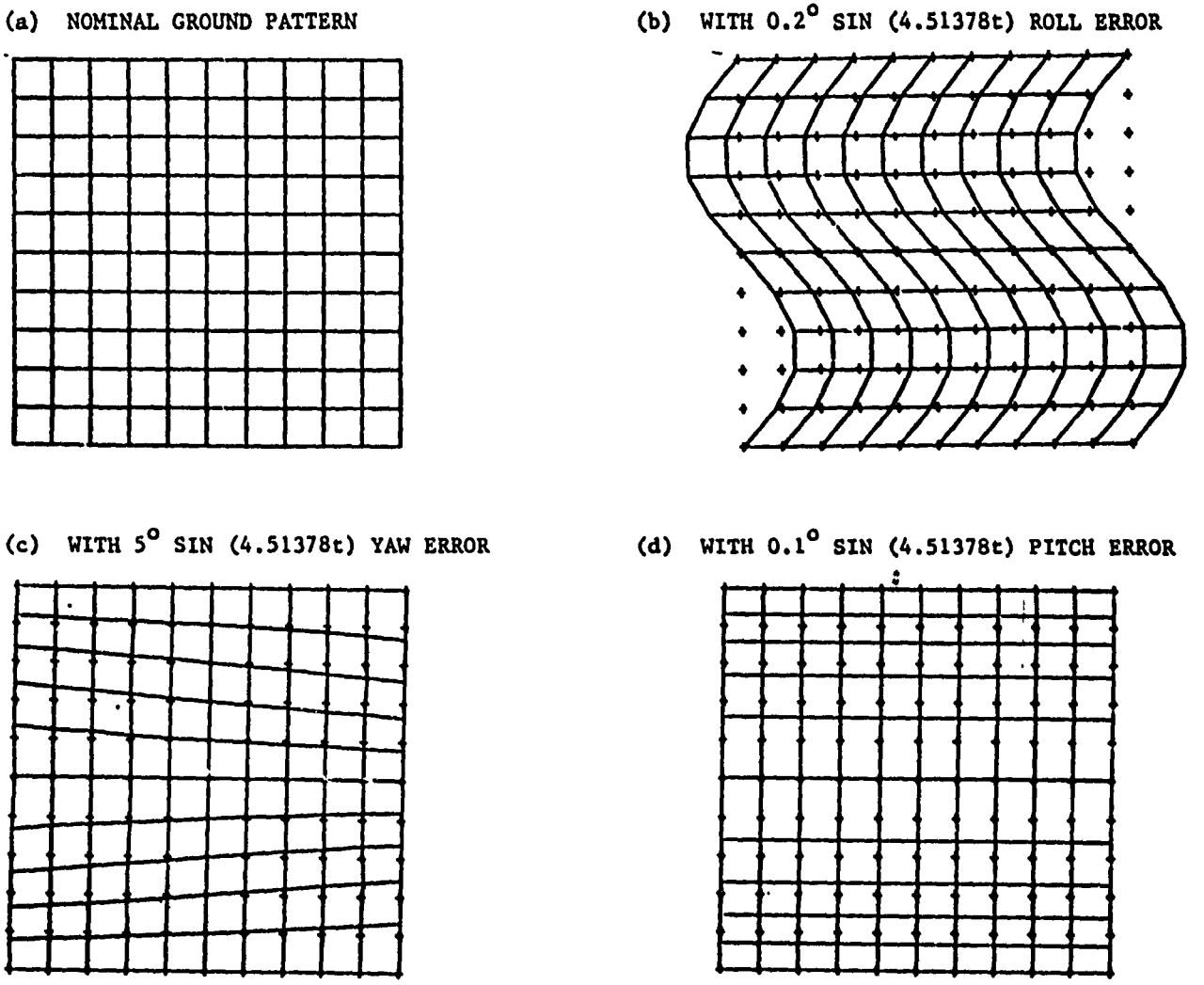

Fig. 47. Ground Pattern Distortions With Sinusoidal Rotation Rate and No Earth Rotation Effect

(a) NOMINAL GROUND PATTERN WITH 20° ROLL OFFSET

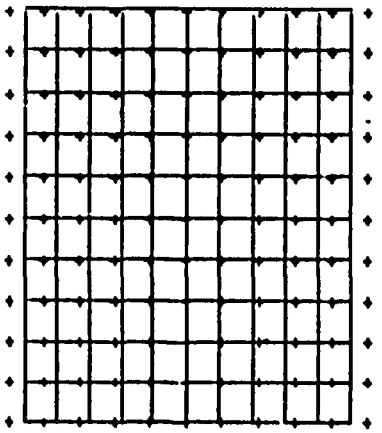

(b) NOMINAL GROUND PATTERN WITH NO OFFSETS

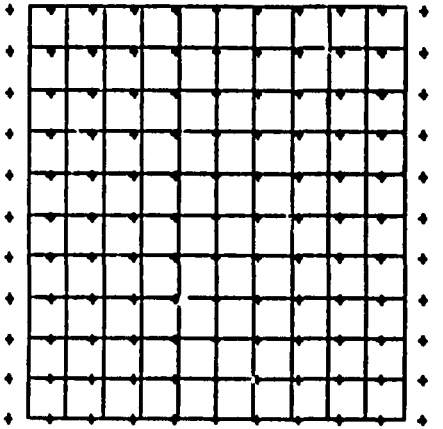

(c) NOMINAL GROUND PATTERN WITH 45° PITCH OFFSET

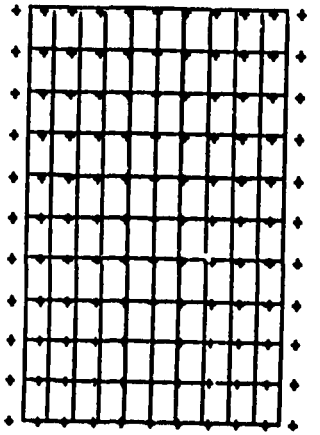

Fig. 48. Ground Pattern Distortions With Effect of Altitude Change (increase) of 40 km and No Earth Rotation Effect

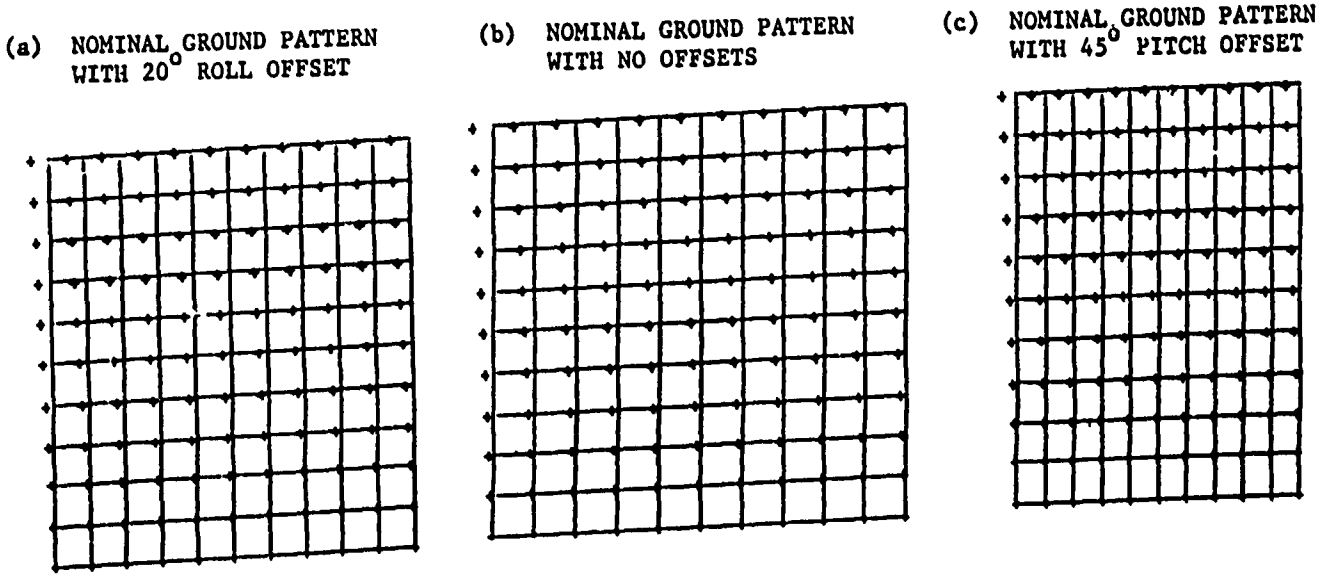

Fig. 49. Ground Pattern Distortions With Effect of Earth Rotation for 40° Latitude and Orbit Inclination of 85°

VI. CONCLUSIONS

1. The effects of earth curvature are very small for the application here (see Fig. 42).
2. Altitude uncertainties cause only moderate geometric errors. The worst 1σ geometric errors are 11.71 m in position and 0.133 m/sec in rate with STDN and large unmodeled perturbations at 200 km orbit. The performance improves with TDRSS. For the 300 km orbit and with small unmodeled perturbations, the 1σ geometric errors will reduce to 0.22 m and 0.0032 m/sec (see Table 11).
3. The effects of other navigation errors are significantly greater. The 1σ downtrack errors range from 203 m (300 km orbit) to 8128 m (200 km orbit); and those for the cross track are 152 m to 508 m (see Table 12).
4. The effects of roll and pitch attitude errors are relatively large compared with, for instance, those caused by yaw errors and altitude uncertainties. The error sensitivity is 1.94 m/arc sec or approximately 7000 m/degree. The yaw sensitivity is 0 for a 0° view angle and 0.028 m/arc sec for the maximum view angle of $\pm 0.825^{\circ}$ (see Table 12).
5. The error sensitivities of attitude errors increase significantly for large attitude offsets. For 20° side looking, the sensitivity increases to 2.28 m/arc sec for roll errors and to 0.75 m/arc sec for yaw errors, and the pitch error sensitivity is almost unaffected. For the 45° forward looking case, the sensitivities for the pitch, roll, and yaw errors increase to 2.83, 4.36, and 1.97 m/arc sec, respectively (see Table 13).
6. The performance of the Shuttle Imaging Spectrometer is limited by the Shuttle IMU (Inertial Measuring Unit) accuracy, instrument misalignment, Shuttle RCS (Reaction Control Subsystem) deadband, etc. unless some means of error reduc-

tion are employed. For instance, ground control points may be used to reduce navigation prediction errors; and precision point mounts, such as AGS (ASPS[+] Gimbal System) and IPS (Instrument Pointing System), may be used to reduce the attitude errors. The single axis geometric errors due-to-the combined Shuttle/IS misalignment, for instance, for normal nadir pointing, 20° side looking, and 45° forward looking are 169 m, 198 m, and 379 m, respectively (refer to Table 14).

7. Earth rotation causes shifts of images toward the direction of rotation. The magnitude of these shifts depends on the latitude of the object. For instance, at the equator the object moves approximately 462 m in one second (for 400 km orbit), and at 60° latitude it moves only 231 m in one second.

8. Distorted images for selected ground patterns provide revealing information of the effects of system errors to the images of ground objects.

[+] Annular Suspension Pointing System

REFERENCES

1. "LANDSAT D Position Determination and Correction Study," Final Report prepared for NASA Goddard Space Flight Center by General Electric-Space Division, GE DOC #76SDS4277, NASA CR-144829, 22 Nov. 1976.

2. "Shuttle Imaging Spectrometer Experiment, Vol. I: Investigation and Technical Plan," Proposal submitted to NASA, JPL internal document D-755, July 18, 1983.

3. Wellman, J.B., Breckinridge, J.B., Kupferman, P.N., and Salazar, R., "Imaging Spectrometer: An Advanced Multispectral Imaging Concept," Vol. I, Digest of 1982 International Geoscience and Remote Sensing Symposium, Munich, West Germany, June 1-4, 1982.

4. Shuttle Operational Data Book, JSC-08934, Vol. II, Rev. B, August 1980; Amendment 46, January 6, 1982.

5. Space Shuttle System Payload Accomodations, JSC-07700, Vol. XIV, Rev. G, September 26, 1980, Change No. 35, August 21, 1981.

6. "Three-Plate On-Orbit Aerodynamic Torque Model," SSFS Doc. Series AER037, JSC-12604 (LEC-10294) Johnson Space Center, Houston, TX, March 1977.

7. "General Consideration of Control Disturbances for Large Space Structures," Final Report for JPL, contract #955345, prepared by Lockheed Missiles and Space Co., Sunnyvale, CA, January 18, 1980.

8. Space Transportation System User Handbook, N77-82346, NASA, Washington, D.C., June 1977.

9. "LANDSAT D Position Determination and Correction Study," Final Report prepared for NASA Goddard Space Flight Center by General Electric-Space Division, CR-144829, November 22, 1978.

10. Space Shuttle Orbiter Flight Test, Level C, Functional Subsystem Software Requirements, Guidance, Navigation, and Control, Part C, Flight Control, Part 2, SD 76-SH-0009 Book 2B, September 15, 1980.

11. Sackett, L.L., and Kirchway, C.B., "Dynamic Interaction of the Shuttle On-Orbit Flight Control System with Deployed Flexible Payload," Paper #82-1535, AIAA Guidance and Control Conference, San Diego, CA, August 9-11, 1982.

12. Osborne, D., Update of JSC-07700, Vol. XIV, July 1982.

13. Wertz, J.R., Spacecraft Attitude Determination and Control, D. Reidel Publishing Co., Dordrecht, Holland, pp. 730-731, 1978.

APPENDICES

APPENDIX A

GEOMETRIC ERROR MAPPING FUNCTION TABLE

Part A: Given the attitude offsets and a view angle, find the coordinates of the corresponding ground points before and after the errors are introduced.

Error Sources	Geometric Error Mapping Function	Comments
Altitude Error, Δh	At nominal altitude h, a view angle λ is given which sights a ground point $P(0, Y_o)$. After elevating Δh, the same view angle will sight another ground point $P'(0, Y'_o)$. The following equations are for obtaining Y_o and Y'_o: $$Y_o = -R \sin \lambda \left[\left(1 + \frac{h}{R}\right) \cos \lambda - \sqrt{1 - \left(1 + \frac{h}{R}\right)^2 \sin^2 \lambda}\right]$$ $$Y'_o = -R \sin \lambda \left[\left(1 + \frac{h + \Delta h}{R}\right) \cos \lambda - \sqrt{1 - \left(1 + \frac{h + \Delta h}{R}\right)^2 \sin^2 \lambda}\right]$$	R = Earth Radius
Yaw Error, ψ	Given: a yaw offset ψ_o and a view angle λ which sights a ground point $P(X^*, Y^*)$. The same view angle will sight another ground point $P'(X^{*'}, Y^{*'})$ after yaw error ψ is introduced. The following equations are for obtaining X^*, Y^*, $X^{*'}$, and $Y^{*'}$: $$X^* = \left[\left(1 + \frac{h}{R}\right) \cos \lambda - \sqrt{1 - \left(1 + \frac{h}{R}\right)^2 \sin^2 \lambda}\right] R \sin \lambda \sin \psi_o$$ $$Y^* = -\left[\left(1 + \frac{h}{R}\right) \cos \lambda - \sqrt{1 - \left(1 + \frac{h}{R}\right)^2 \sin^2 \lambda}\right] R \sin \lambda \cos \psi_o$$	R = Earth Radius h = Nominal Altitude

Error Sources	Geometric Error Mapping Function	Comments
	$X^{*'} = \left[\left(1 + \frac{h}{R}\right) \cos \lambda - \sqrt{1 - \left(1 + \frac{h}{R}\right)^2 \sin^2 \lambda}\right] R \sin \lambda \sin (\psi_o + \psi)$ $Y^{*'} = -\left[\left(1 + \frac{h}{R}\right) \cos \lambda - \sqrt{1 - \left(1 + \frac{h}{R}\right)^2 \sin^2 \lambda}\right] R \sin \lambda \cos (\psi_o + \psi)$	
Roll Error, ϕ	Given: a roll offset ϕ_o and a view angle λ which sights a ground point P(0, Y*). The same view angle will sight another ground point P'(0, Y*') after roll error ϕ is introduced. The following equations are for obtaining Y* and Y*': $Y^* = -R \sin (\lambda + \phi_o) \left[\left(1 + \frac{h}{R}\right) \cos (\lambda + \phi_o) - \sqrt{1 - \left(1 + \frac{h}{R}\right)^2 \sin^2 (\lambda + \phi_o)}\right]$ $Y^{*'} = -R \sin (\lambda + \phi_o + \phi) \left[\left(1 + \frac{h}{R}\right) \cos (\lambda + \phi_o + \phi) - \sqrt{1 - \left(1 + \frac{h}{R}\right)^2 \sin^2 (\lambda + \phi_o + \phi)}\right]$	R = Earth Radius h = Nominal Altitude
Pitch Error, θ	Given: a pitch offset θ_o and a view angle λ which sights a ground point P(X*, Y*). The same view angle will sight another ground point P'(X*', Y*') after pitch error θ is introduced. The following equations are for obtaining X*, Y*, X*', and Y*': $X^* = R \left[\left(1 + \frac{h}{R}\right) \cos \tau - \sqrt{1 - \left(1 + \frac{h}{R}\right)^2 \sin^2 \tau}\right] \frac{\sin \tau \sin \theta_o}{\sqrt{\sin^2 \theta_o + \tan^2 \lambda}}$ $Y^* = -R \left[\left(1 + \frac{h}{R}\right) \cos \tau - \sqrt{1 - \left(1 + \frac{h}{R}\right)^2 \sin^2 \tau}\right] \frac{\sin \tau \tan \lambda}{\sqrt{\sin^2 \theta_o + \tan^2 \lambda}}$	R = Earth Radius h = Nominal Altitude For τ and ξ, refer to Fig. 23.

Error Sources	Geometric Error Mapping Function	Comments
	$X^{*'} = R\left[\left(1+\frac{h}{R}\right)\cos\xi - \sqrt{1-\left(1+\frac{h}{R}\right)^2\sin^2\xi}\right]\frac{\sin\xi\sin(\theta_o+\theta)}{\sqrt{\sin^2(\theta_o+\theta)+\tan^2\lambda}}$ $Y^{*'} = -R\left[\left(1+\frac{h}{R}\right)\cos\xi - \sqrt{1-\left(1+\frac{h}{R}\right)^2\sin^2\xi}\right]\frac{\sin\xi\tan\lambda}{\sqrt{\sin^2(\theta_o+\theta)+\tan^2\lambda}}$ $\tau = \tan^{-1}\left(\sec\theta_o\sqrt{\sin^2\theta_o+\tan^2\lambda}\right)$ $\xi = \tan^{-1}\left[\sec(\theta_o+\theta)\sqrt{\sin^2(\theta_o+\theta)+\tan^2\lambda}\right]$	
Yaw Error ψ, Followed by pitch error θ, then roll error ϕ	Given a yaw offset ψ_o, followed by a pitch offset θ_o, then a roll offset ϕ_o. A view angle λ is also given which sights a ground point $P_o(X_o,Y_o)$. After the errors ψ, θ, and ϕ are introduced, the same view angle will sight another ground point $P_3(X_3, Y_3)$. The following equations are for obtaining X_o, Y_o, X_3, and Y_3: $X_o' = \frac{R\sin\theta_o\sin\xi_o\left[\left(1+\frac{h}{R}\right)\cos\xi_o - \sqrt{1-\left(1+\frac{h}{R}\right)^2\sin^2\xi_o}\right]}{\sqrt{\sin^2\theta_o+\tan^2(\lambda+\phi_o)}}$ $Y_o' = -\frac{R\tan(\lambda+\phi_o)\sin\xi_o\left[\left(1+\frac{h}{R}\right)\cos\xi_o - \sqrt{1-\left(1+\frac{h}{R}\right)^2\sin^2\xi_o}\right]}{\sqrt{\sin^2\theta_o+\tan^2(\lambda+\phi_o)}}$	R = Earth Radius h = Nominal Altitude For ξ_o and ξ_3, refer to Fig. 23.

Error Sources	Geometric Error Mapping Function	Comments
	$X_3' = \dfrac{R \sin(\theta_o + \theta) \sin \xi_3 \left[\left(1 + \frac{h}{R}\right) \cos \xi_3 - \sqrt{1 - \left(1 + \frac{h}{R}\right)^2 \sin^2 \xi_3}\right]}{\sqrt{\sin^2(\theta_o + \theta) + \tan^2(\lambda + \phi_o + \phi)}}$	
	$Y_3' = -\dfrac{R \tan(\lambda + \phi_o + \phi) \sin \xi_3 \left[\left(1 + \frac{h}{R}\right) \cos \xi_3 - \sqrt{1 - \left(1 + \frac{h}{R}\right)^2 \sin^2 \xi_3}\right]}{\sqrt{\sin^2(\theta_o + \theta) + \tan^2(\lambda + \phi_o + \phi)}}$	
	$\xi_o = \tan^{-1}\left(\sec \theta_o \sqrt{\sin^2 \theta_o + \tan^2(\lambda + \phi_o)}\right)$	
	$\xi_3 = \tan^{-1}\left[\sec(\theta_o + \theta) \sqrt{\sin^2(\theta_o + \theta) + \tan^2(\lambda + \phi_o + \phi)}\right]$	
	$X_o = X_o' \cos \psi_o - Y_o' \sin \psi_o$	
	$Y_o = X_o' \sin \psi_o + Y_o' \cos \psi_o$	
	$X_3 = X_3' \cos(\psi_o + \psi) - Y_3' \sin(\psi_o + \psi)$	
	$Y_3 = X_3' \sin(\psi_o + \psi) + Y_3' \cos(\psi_o + \psi)$	

Part B: Given the coordinates of a ground point, find the attitude offsets, the corresponding view angle and the coordinates of the point with the same view angle after the errors are introduced.

Error Sources	Geometric Error Mapping Function	Comments
Altitude Error, Δh	At nominal altitude h, a ground point $P(X_o, Y_o)$ corresponding to view angle λ is given. After elevating Δh, the same view angle λ will aim at another ground point $P'(X'_o, Y'_o)$. The following equations are for obtaining X'_o and Y'_o: $$\lambda = \tan^{-1}\left(\frac{\sqrt{X_o^2 + Y_o^2}}{R + h - \sqrt{R^2 - X_o^2 - Y_o^2}}\right)$$ $$X'_o = \frac{RX_o \sin\lambda}{\sqrt{X_o^2 + Y_o^2}}\left[\left(1 + \frac{h + \Delta h}{R}\right)\cos\lambda - \sqrt{1 - \left(1 + \frac{h + \Delta h}{R}\right)^2 \sin^2\lambda}\right]$$ $$Y'_o = \frac{RY_o \sin\lambda}{\sqrt{X_o^2 + Y_o^2}}\left[\left(1 + \frac{h + \Delta h}{R}\right)\cos\lambda - \sqrt{1 - \left(1 + \frac{h + \Delta h}{R}\right)^2 \sin^2\lambda}\right]$$	R = Earth Radius

Error Sources	Geometric Error Mapping Function	Comments
Roll Error, ϕ	A ground point P(0, Y*) corresponding to roll offset ϕ_o and view angle λ is given. After roll error ϕ is introduced, the same view angle λ will aim at another ground point P'(0, Y*'). The following equations are for obtaining Y*': $$\lambda + \phi_o = -\mathrm{sgn}(Y^*) \tan^{-1}\left(\frac{\lvert Y^*\rvert}{R + h - \sqrt{R^2 - Y^{*2}}}\right)$$ $$Y^{*\prime} = -R \sin(\lambda + \phi_o + \phi)\left[\left(1 + \frac{h}{R}\right)\cos(\lambda + \phi_o + \phi) - \sqrt{1 - \left(1 + \frac{h}{R}\right)^2 \sin^2(\lambda + \phi_o + \phi)}\right]$$	R = Earth Radius h = Nominal Altitude

Error Sources	Geometric Error Mapping Function	Comments
Pitch Error, θ	A ground point P(X*, Y*) corresponding to pitch offset θ_o and view angle λ is given. After pitch error θ is introduced, the same view angle λ will aim at another ground point P'(X*', Y*'). The following equations are for obtaining X*' and Y*':	R = Earth Radius h = Nominal Altitude For ξ, refer to Fig.23.

$$\lambda = \tan^{-1}\left[\frac{Y^*}{\left(R + h - \sqrt{R^2 - X^{*2} - Y^{*2}}\right)\left(\sqrt{1 + \left(\frac{X^*}{R + h - \sqrt{R^2 - X^{*2} - Y^{*2}}}\right)^2}\right)}\right]$$

$$\theta_o = \tan^{-1}\left[\frac{X^*}{R + h - \sqrt{R^2 - X^{*2} - Y^{*2}}}\right]$$

$$\xi = \tan^{-1}\left[\sec(\theta_o + \theta)\sqrt{\sin^2(\theta_o + \theta) + \tan^2\lambda}\right]$$

$$X^{*\prime} = \frac{R \sin(\theta_o + \theta) \sin\xi \left[\left(1 + \frac{h}{R}\right)\cos\xi - \sqrt{1 - \left(1 + \frac{h}{R}\right)^2 \sin^2\xi}\right]}{\sqrt{\sin^2(\theta_o + \theta) + \tan^2\lambda}}$$

$$Y^{*\prime} = -\frac{R \tan\lambda \sin\xi \left[\left(1 + \frac{h}{R}\right)\cos\xi - \sqrt{1 - \left(1 + \frac{h}{R}\right)^2 \sin^2\xi}\right]}{\sqrt{\sin^2(\theta_o + \theta) + \tan^2\lambda}}$$

Error Sources	Geometric Error Mapping Function	Comments
Yaw Error, ψ	A ground point P(X*,Y*) corresponding to yaw offset ψ_o and a certain view angle is given. After yaw error ψ is introduced, the same view angle will aim at another ground point P'(X*',Y*'). The following equations are for obtaining X*' and Y*': $\psi_o = -\tan^{-1}\left(\frac{X^*}{Y^*}\right)$ $\lambda = -\operatorname{sgn}(Y^*)\tan^{-1}\left(\frac{\sqrt{X^{*2}+Y^{*2}}}{R+h-\sqrt{R^2-X^{*2}-Y^{*2}}}\right)$ $X^{*\prime} = \left[\left(1+\frac{h}{R}\right)\cos\lambda - \sqrt{1-\left(1+\frac{h}{R}\right)^2\sin^2\lambda}\right] R\sin\lambda\sin(\psi_o+\psi)$ $Y^{*\prime} = -\left[\left(1+\frac{h}{R}\right)\cos\lambda - \sqrt{1-\left(1+\frac{h}{R}\right)^2\sin^2\lambda}\right] R\sin\lambda\cos(\psi_o+\psi)$	R = Earth Radius h = Nominal Altitude
Earth Rotation	Let Γ be the shuttle orbital inclination at the equator, and ζ be the latitude of the nadir point. A given point P(X,Y), after time period Δt, will move to P'(X',Y'). The following equations are for obtaining X' and Y': $V_e = \omega R\cos\zeta$ $\omega = \frac{2\pi}{86{,}400}$ radians/sec $X' = X + \frac{\cos\Gamma}{\cos\zeta}V_e\Delta t$ $Y' = Y = \sqrt{1-\left(\frac{\cos\Gamma}{\cos\zeta}\right)^2}\,V_e\Delta t$	V_e = Linear Velocity of Ground Point at Latitude ζ ω = Angular Velocity of Earth Rotation Δt is assumed small.

Error Sources	Geometric Error Mapping Function	Comments
Yaw Error ψ followed by Pitch Error θ then Roll Error ϕ	A ground point P(0,Y*) corresponding to view angle λ (with no attitude offset) is given. A yaw error ψ is introduced first, then a pitch error θ, finally a roll error ϕ. The same view angle λ will then aim at another ground point P'(X*',Y*'). The following equations are for obtaining X*' and Y*': $\lambda = -\,\mathrm{sgn}(Y^*)\,\tan^{-1}\left(\frac{\lvert Y^*\rvert}{R + h - \sqrt{R^2 - Y^{*2}}}\right)$ $\xi = \tan^{-1}\left[\sec\theta\sqrt{\sin^2\theta + \tan^2(\lambda+\phi)}\right]$ $X = \frac{R\sin\theta\sin\xi\left[\left(1+\frac{h}{R}\right)\cos\xi - \sqrt{1-\left(1+\frac{h}{R}\right)^2\sin^2\xi}\right]}{\sqrt{\sin^2\theta + \tan^2(\lambda+\phi)}}$ $Y = \frac{-R\tan(\lambda+\theta)\sin\xi\left[\left(1+\frac{h}{R}\right)\cos\xi - \sqrt{1-\left(1+\frac{h}{R}\right)^2\sin^2\xi}\right]}{\sqrt{\sin^2\theta + \tan^2(\lambda+\phi)}}$ $X^{*'} = X\cos\psi - Y\sin\psi$ $Y^{*'} = X\sin\psi + Y\cos\psi$	R = Earth Radius h = Nominal Altitude For ξ, refer to Fig. 23.

APPENDIX B

NAPIER'S RULES FOR RIGHT SPHERICAL TRIANGLES*

A right spherical triangle has five variable parts. If these components and their complements (complement of $\Gamma \equiv 90^\circ - \Gamma$) are arranged in a circle, as illustrated below

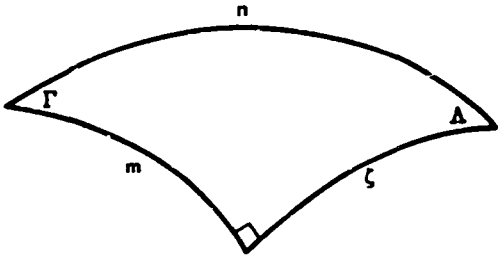

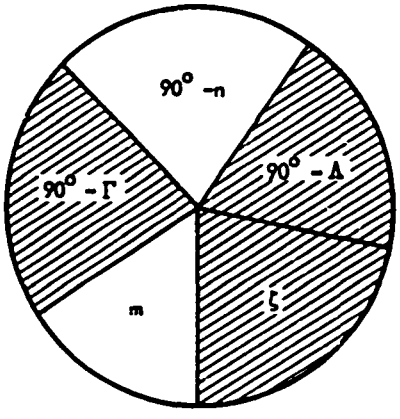

then, the following relationships hold between the five components in the circle:

The sine of any component equals the product of either:

1. The tangents of the adjacent components, or
2. The cosines of the opposite components

For our case, from 2:

$$\sin (90^\circ - \Gamma) = \cos \zeta \cos (90^\circ - A)$$

i.e.,

$$\cos \Gamma = \cos \zeta \sin A$$

*See Ref. 13

APPENDIX C

COMPUTER PROGRAM FOR SHUTTLE IMAGING SPECTROMETER POINTING ERROR POWER SPECTRAL DENSITIES FOR CONFIGURATION A — PAYLOAD-BAY NADIR POINTING

```
ELT  WED-10/20/82-10:20:28-(52,)
12537*IS(1).SRMA/PROG(52)
      1:PROGRAM IMAGING SPECTROMETER SHUTTLE RIGID MOUNT - A
      2:INITIAL
      3:VARIABLE T=0.0
      4:       INTEGER FNUM,NPOINT
      5:
      6:
      7:COMMENT INITIALIZE SOME PARAMETERS
      8:       CONSTANT NPOINT=641
      9:       CONSTANT FNUM=39
     10:       CALL FOPEN(FNUM)
     11:       TFINAL=1.0*NPOINT-1.0
     12:       CONSTANT FACTOR=0.0
     13:       CONSTANT SCAFAC=1.0E+5
     14:       SCFAC2=SCAFAC*SCAFAC
     15:       SCF2DB=10.0*ALOG10(SCFAC2)
     16:
     17:COMMENT SET VARIOUS MATHMATICAL CONSTANTS
     18:       PI=3.14159265
     19:       RSRCC=PI/(180.0*3600.0)
     20:       RSHZCC=1.0/(2.0*PI)
     21:
     22:COMMENT DEFINE MOMENTS OF INERTIA
     23:       CONSTANT IX=1.38E+6
     24:       CONSTANT IY=1.00E+7
     25:       CONSTANT IZ=1.05E+7
     26:       IX2=IX*IX
     27:       IY2=IY*IY
     28:       IZ2=IZ*IZ
     29:       IXYZ=IX-IY+IZ
     30:       IXYZ2=IXYZ*IXYZ
     31:
     32:COMMENT DEFINE WO
     33:       CONSTANT WO=0.0011315
     34:       WO2=WO*WO
     35:       WO4=WO2*WO2
     36:
     37:COMMENT DEFINE INITIAL ANGLES AND RATES
     38:       CONSTANT THO=0.0
     39:       CONSTANT PHIO=0.0
     40:       CONSTANT PSIO=0.0
     41:       CONSTANT THOD=0.0
     42:       CONSTANT PHIOD=0.0
     43:       CONSTANT PSIOD=0.0
     44:       THO2=THO*THO
     45:       THOD2=THOD*THOD
     46:       PHIO2=PHIO*PHIO
     47:       PHIOD2=PHIOD*PHIOD
     48:       PSIO2=PSIO*PSIO
     49:       PSIOD2=PSIOD*PSIOD
     50:
     51:COMMENT DEFINE Q'S
     52:       CONSTANT QX=2.014E-6
     53:       CONSTANT QY=1.251E-3
     54:       CONSTANT QZ=5.438E-4
     55:
     56:COMMENT DEFINE RATE FILTER PARAMETERS
     57:       CONSTANT WD=0.2513
     58:       CONSTANT ZETAD=0.8
     59:       WD2=WD*WD
     60:       WD4=WD2*WD2
     61:       ZD2=ZETAD*ZETAD
     62:
     63:COMMENT DEFINE VARIOUS CONSTANTS
     64:       CONSTANT R=8.55E-10
```

```
 65:       CONSTANT SIGBO=87.32
 66:       SIGBO=SIGBO*ASRCC
 67:       SIGBO2=SIGBO*SIGBO
 68:       CONSTANT TAU=0.023
 69:       TAU2=TAU*TAU
 70:       DELW=1.0
 71:
 72:COMMENT DEFINE W CONSTANTS AND INITIALIZE W
 73:       CONSTANT WLO=6.28318531E-7
 74:       CONSTANT WFACT=1.029200527
 75:       W=WLO/WFACT
 76:
 77:END
 78:DYNAMIC
 79:CINTERVAL CI=1.0
 80:
 81:COMMENT COMPUTE W
 82:       W=W*WFACT
 83:       PROCEDURAL(DELW=W)
 84:         DELW=0.0
 85:         IF(W.LE.0.) DELW=1.0
 86:       END
 87:       WHZ=W*RSHZCC
 88:       FREQ=ALOG10(WHZ)
 89:       W2=W*W
 90:       W4=W2*W2
 91:
 92:COMMENT COMPUTE HW2 AND DW2
 93:       HW2=1.0/(TAU2*W2+1.0)
 94:       HDW2=WD4*W2/((W2-WD2)**2+4.0*ZD2*WD2*W2)
 95:       DW2=IX*IZ*W4-WO2*(IX*IZ+IY2+3.0*IY*IZ-3.0*IZ2)*W2
 96:COMMENT DW2=DW2+4.0*WO4*(IY-IX)*(IY-IZ)
 97:       DW2=DW2/SCAFAC
 98:       DW2=DW2*DW2
 99:
100.COMMENT COMPUTE F'S
101:COMMENT FTHW2=HW2*SCFAC2/((IY*W2+3.0*WO2*(IZ-IX))**2)
102:COMMENT FRW2=(IZ*W2-WO2*(IY-IX))**2*HW2/DW2
103:COMMENT FYW2=(IX*W2+4.0*WO2*(IZ-IY))**2*HW2/DW2
104:       FTHW2=HW2*SCFAC2/((IY*W2)**2)
105:       FRW2=(IZ*W2)**2*HW2/DW2
106:       FRYW2=WO2*IXYZ2*W2*HW2/DW2
107:       FYW2=(IX*W2)**2*HW2/DW2
108:
109:COMMENT COMPUTE PSD'S
110:
111:COMMENT PITCH PSD COMPUTATIONS
112:       PPW1=FTHW2*IY2*THOD2
113:       PPW2=FTHW2*IY2*THO2*W2
114:       PPW3=FTHW2*QY
115:       PPW=R+SIGBO2*DELW+(PPW1+PPW2+PPW3)/SCFAC2
116:       PPWD=PPW*HDW2
117:
118:COMMENT ROLL PSD COMPUTATIONS
119:       PRW1=FRW2*IX2*PHIOD2
120:       PRW2=FRW2*IX2*PHIO2*W2
121:       PRW3=FRW2*WO2*IXYZ2*PSIO2
122:       PRW4=FRW2*QX
123:       PRW5=FRYW2*IZ2*PSIOD2
124:       PRW6=FRYW2*IZ2*PSIO2*W2
125:       PRW7=FRYW2*WO2*IXYZ2*PHIO2
126:       PRW8=FRYW2*QZ
127:       RS=R+SIGBO2*DELW
128:       PRW=RS+(PRW1+PRW2+PRW3+PRW4+PRW5+PRW6+PRW7+PRW8)/SCFAC2
129:       PRWD=PRW*HDW2
130:
```

```
      131:COMMENT YAW PSD COMPUTATIONS
      132:        PYW1=FYW2*IZ2*PSIOD2
      133:        PYW2=FYW2*IZ2*PSIO2*WZ
      134:        PYW3=FYW2*WO2*IXYZ2*PHIOZ
      135:        PYW4=FYW2*OZ
      136.        PYW5=FRYW2*IX2*PHIOD2
      137:        PYW6=FRYW2*IX2*PHIO2*WZ
      138:        PYW7=FRYW2*WO2*IXYZ2*PSIO2
      139:        PYW8=FRYW2*OX
      140:        PYW=RS*(PYW1+PYW2+PYW3+PYW4+PYW5+PYW6+PYW7+PYW8)/SCFAC2
      141:        PYWD=PYW*HDW2
      142:
      143:
      144:COMMENT PREPARE VARIABLES FOR OUTPUT
      145:        RSIG=P+SIGBO2*DELW
      146:        RSIGDB=10.0*ALOG10(RSIG)+FACTOR
      147:        PPW3DB=10.0*ALOG10(PPW3)-SCF2DB+FACTOR
      148:        PPWDB=10.0*ALOG10(PPW)+FACTOR
      149:        PRW4DB=10.0*ALOG10(PRW4)-SCF2DB+FACTOR
      150:        PRW8DB=10.0*ALOG10(PRW8)-SCF2DB+FACTOR
      151:        PRWDB=10.0*ALOG10(PRW)+FACTOR
      152:        PYW4DB=10.0*ALOG10(PYW4)-SCF2DB+FACTOR
      153:        PYW8DB=10.0*ALOG10(PYW8)-SCF2DB+FACTOR
      154:        PYWDB=10.0*ALOG10(PYW)+FACTOR
      155:
      156:        PPWDDB=10.0*ALOG10(PPWD)+FACTOR
      157:        PRWDDB=10.0*ALOG10(PPWD)+FACTOR
      158:        PYWDDB=10.0*ALOG10(PYWD)+FACTOR
      159:
      160:COMMENT SAVE NUMBERS IN FILE
      161:        CALL FSAVE(FREQ,PPWDB,PRWDB,PYWDB,FNUM)
      162:
      163:
      164:        TERMT(T.GE.TFINAL)
      165:DERIVATIVE
      166:ALGORITHM IALG=3
      167:        GQ=INTEG(1.0,0.0)
      168:END
      169:END
      170:TERMINAL
      171:
      172:COMMENT CLOSE FILE
      173:        CALL FCLOSE(FNUM)
      174:END
      175:END
    EOF:175
```

```
0:>ELT  WED-10/20/82-10:30:02-(3,)
12537#IS(1).SRMA/FSUBS(3)
      1:@FOR,IS FF.FOPEN
      2:       SUBROUTINE FOPEN(N)
      3:       REWIND N
      4:       RETURN
      5:       END
      6:@FOR,IS FF.FSAVE
      7:       SUBROUTINE FSAVE(W,P1,P2,P3,N)
      8:       WRITE(N,100)W,P1,P2,P3
      9: 100   FORMAT(4G14.8)
     10:       RETURN
     11:       END
     12:@FOR,IS FF.FCLOSE
     13:       SUBROUTINE FCLOSE(N)
     14:       ENDFILE N
     15:       RETURN
     16:       END
EOF:16
```

APPENDIX D

COMPUTER PROGRAM FOR SHUTTLE IMAGING SPECTROMETER POINTING ERROR POWER SPECTRAL DENSITIES FOR CONFIGURATION B -- NOSE-DOWN NADIR POINTING

```
ELT  WED-10/20/82-10:36:41-(14,)
12537*IS(1).SRMB/PROG(14)
      1:PROGRAM IMAGING SPECTROMETER SHUTTLE RIGID MOUNT - B
      2:INITIAL
      3:VARIABLE T=0.0
      4:       INTEGER FNUM,NPOINT
      5:
      6:
      7:COMMENT INITIALIZE SOME PARAMETERS
      8:       CONSTANT NPOINT=641
      9:       CONSTANT FNUM=39
     10:       CALL FOPEN(FNUM)
     11:       TFINAL=1.0*NPOINT-1.0
     12:       CONSTANT FACTOR=0.0
     13:       CONSTANT SCAFAC=1.0E+10
     14:       SCFAC2=SCAFAC*SCAFAC
     15:       SCF2DB=10.0*ALOG10(SCFAC2)
     16:
     17:COMMENT SET VARIOUS MATHMATICAL CONSTANTS
     18:       PI=3.14159265
     19:       RSRCC=PI/(180.0*3600.0)
     20:       RSHZCC=1.0/(2.0*PI)
     21:
     22:COMMENT DEFINE MOMENTS OF INERTIA
     23:       CONSTANT IX=1.00E+7
     24:       CONSTANT IY=1.05E+7
     25:       CONSTANT IZ=1.38E+6
     26:       IX2=IX*IX
     27:       IY2=IY*IY
     28:       IZ2=IZ*IZ
     29:       IXYZ=IX-IY+IZ
     30:       IXYZ2=IXYZ*IXYZ
     31:
     32:COMMENT DEFINE WO
     33:       CONSTANT WO=0.0011315
     34:       WO2=WO*WO
     35:       WO4=WO2*WO2
     36:
     37:COMMENT DEFINE.INITIAL ANGLES AND RATES
     38:       CONSTANT THO=0.0
     39:       CONSTANT PHIO=0.0
     40:       CONSTANT PSIO=0.0
     41:       CONSTANT THOD=0.0
     42:       CONSTANT PHIOD=0.0
     43:       CONSTANT PSIOD=0.0
     44:       THO2=THO*THO
     45:       THOD2=THOD*THOD
     46:       PHIO2=PHIO*PHIO
     47:       PHIOD2=PHIOD*PHIOD
     48:       PSIO2=PSIO*PSIO
     49:       PSIOD2=PSIOD*PSIOD
     50:
     51:COMMENT DEFINE Q'S
     52:       CONSTANT QX=1.97OE-4
     53:       CONSTANT QY=1.286E-3
     54:       CONSTANT QZ=6.32OE-4
     55:
     56:COMMENT DEFINE RATE FILTER PARAMETERS
     57:       CONSTANT WD=0.2513
     58:       CONSTANT ZETAD=0.8
     59:       WD2=WD*WD
     60:       WD4=WD2*WD2
     61:       ZD2=ZETAD*ZETAD
     62:
     63:COMMENT DEFINE VARIOUS CONSTANTS
     64:       CONSTANT R=8.55E-10
```

```
      CONSTANT SIGBO=87.32
      SIGBO=SIGBO*RSRCC
      SIGBO2=SIGBO*SIGBO
      CONSTANT TAU=0.023
      TAU2=TAU*TAU
      DELW=1.0

COMMENT DEFINE W CONSTANTS AND INITIALIZE W
      CONSTANT WLO=6.28318531E-7
      CONSTANT WFACT=1.029200527
      W=WLO/WFACT

.END
DYNAMIC
CINTERVAL CI=1.0

COMMENT COMPUTE W
      W=W*WFACT
      PROCEDURAL(DELW=W)
        DELW=0.0
        IF(W.LE.0.) DELW=1.0
      END
      WHZ=W*RSHZCC
      FREQ=ALOG10(WHZ)
      W2=W*W
      W4=W2*W2

COMMENT COMPUTE HW2 AND DW2
      HW2=1.0/(TAU2*W2+1.0)
      HDW2=WD4*W2/((W2-WD2)**2+4.0*ZD2*WD2*W2)
      DW2=IX*IZ*W4-WO2*(IX*IZ+IY2+3.0*IY*IZ-3.0*IZ2)*W2
      DW2=DW2+4.0*WO4*(IY-IX)*(IY-IZ)
      DW2=DW2/SCFAC
      DW2=DW2*DW2

COMMENT COMPUTE F'S
      FTHW2=HW2*SCFAC2/((IY*W2+3.0*WO2*(IZ-IX))**2)
      FRW2=(IZ*W2-WO2*(IY-IX))**2*HW2/DW2
      FYW2=(IX*W2+4.0*WO2*(IZ-IY))**2*HW2/DW2
      FRYW2=WO2*IXYZ2*W2*HW2/DW2

COMMENT COMPUTE PSD'S

COMMENT PITCH PSD COMPUTATIONS
      PPW1=FTHW2*IY2*THOD2
      PPW2=FTHW2*IY2*THO2*W2
      PPW3=FTHW2*QY
      PPW=R+SIGBO2*DELW+(PPW1+PPW2+PPW3)/SCFAC2
      PPWD=PPW*HDW2

COMMENT ROLL PSD COMPUTATIONS
      PRW1=FRW2*IX2*PHIOD2
      PRW2=FRW2*IX2*PHIO2*W2
      PRW3=FRW2*WO2*IXYZ2*PSIO2
      PRW4=FRW2*QX
      PRW5=FRYW2*IZ2*PSIOD2
      PRW6=FRYW2*IZ2*PSIO2*W2
      PRW7=FRYW2*WO2*IXYZ2*PHIO2
      PRW8=FRYW2*QZ
      RS=R+SIGBO2*DELW
      PRW=RS+(PRW1+PRW2+PRW3+PRW4+PRW5+PRW6+PRW7+PRW8)/SCFAC2
      PRWD=PRW*HDW2

COMMENT YAW PSD COMPUTATIONS
      PYW1=FYW2*IZ2*PSIOD2
      PYW2=FYW2*IZ2*PSIO2*W2
```

```
      PYW3=FYW2*WO2*IXYZ2*PHIO2
      PYW4=FYW2*OZ
      PYW5=FRYW2*IX2*PHIOD2
      FYW6=FRYW2*IX2*PHIO2*W2
      PYW7=FRYW2*WO2*IXYZ2*PSIO2
      PYW8=FRYW2*OX
      PYW=RS+(PYW1+PYW2+PYW3+PYW4+PYW5+PYW6+PYW7+PYW8)/SCFAC2
      PYWD=PYW*HDW2

COMMENT PREPARE VARIABLES FOR OUTPUT
      RSIG=R+SIGBO2*DELW
      RSIGDB=10.0*PLOG10(RSIG)+FACTOR
      PPW3DB=10.0*ALOG10(PPW3)-SCF2DB+FACTOR
      PPWDB=10.0*ALOG10(PPW)+FACTOR
      PRW4DB=10.0*ALOG10(PRW4)-SCF2DB+FACTOR
      PRW8DB=10.0*ALOG10(PRW8)-SCF2DB+FACTOR
      PRWDB=10.0*ALOG10(PRW)+FACTOR
      PYW4DB=10.0*ALOG10(PYW4)-SCF2DB+FACTOR
      PYW8DB=10.0*ALOG10(PYW8)-SCF2DB+FACTOR
      PYWDB=10.0*ALOG10(PYW)+FACTOR

      PPWDDB=10.0*ALOG10(PPWD)+FACTOR
      PRWDDB=10.0*ALOG10(PRWD)+FACTOR
      PYWDDB=10.0*ALOG10(PYWD)+FACTOR

COMMENT SAVE NUMBERS IN FILE
      CALL FSAVE(FREQ,PPWDB,PRWDB,PYWDB,FNUM)


      TERMT(T.GE.TFINAL)
DERIVATIVE
ALGORITHM IALG=3
      QQ=INTEG(1.0,0.0)
END
END
TERMINAL

COMMENT CLOSE FILE
      CALL FCLOSE(FNUM)
END
END
EOF:172
```

```
ELT  WED-10/20/82-10:30:42-(G,)
12537*IS(1).SRMB/FSUBS(0)
      1:@FOR,IS FF.FOPEN
      2:       SUBROUTINE FOPEN(N)
      3:       REWIND N
      4:       RETURN
      5:       END
      6:@FOR,IS FF.FSAVE
      7:       SUBROUTINE FSAVE(W,P1,P2,P?,N)
      8:       WRITE(N,100)W,P1,P2,P3
      9:  100  FORMAT(4G14.8)
     10:       RETURN
     11:       END
     12:@FOR,IS FF.FCLOSE
     13:       SUBROUTINE FCLOSE(N)
     14:       ENDFILE N
     15:       RETURN
     16:       END
EOF:16
```

APPENDIX E

GEOMETRIC ERROR ANALYSIS PROGRAM LISTINGS

```
)00 D 004552 DOLTA      0000 R 000263 DPITCH    0000 R 000156 DPSA      0000 R 000067 [
)00 R 000064 DPSI2      0000 R 000244 DROLL     0000 D 002262 DSXY      0000 R 000170 [
)00 R 000125 DTETA1     0000 R 000130 DTETA2    0000 R 000213 DTHETA    0000 D 003214 [
)00 D 001240 DY         0000 R 000225 DYAW      0000 D 022676 ERR       0000 D 023102 [
)00 D 013626 FI         0000 D 000352 FI1       0000 D 000360 FI2       0000 R 000000 [
)00 I 030711 J          0000 I 030706 K         0000 D 000302 LAMDA     0000 D 000626 [
)00 D 001536 PDXY       0000 D 013640 PDY       0000 R 030710 PI        0000 D 017166 [
)00 D 004252 PSI        0000 D 001776 PSXY      0000 D 003264 PXY       0000 D 000742 [
)00 D 004266 RA         0000 D 006520 RHO       0000 D 010254 RHO1      0000 D 010436 [
)00 D 026522 RO1        0000 D 002522 S         0000 R 000047 SDH       0000 D 013350 [
)00 D 013166 SHFT       0000 D 022532 SLOMDA    0000 D 015576 SQURT     0000 D 010620 [
)00 D 027614 SQUT1      0000 D 002236 SXY       0000 D 003240 T         0000 D 022502 [
)00 R 000052 TDH2       0000 D 007314 TETA1     0000 D 007322 TETA2     0000 D 014732 [
)00 D 007526 TII2       0000 D 007330 TI1       0000 D 007336 TI2       0000 D 003144 [
)00 D 015552 TI         0000 D 025372 TII       0000 D 005130 T2        0000 D 023206 [
)00 D 022750 VP         0000 D 022736 VPX       0000 D 022734 VS        0000 D 022556 [
)00 D 014756 XI         0000 R 000075 XO        0000 D 000326 XY        0000 R 000133 [
)00 D 012074 X2         0000 D 011530 X22       0000 D 017224 X3        0000 D 000674 [
)00 D 014136 YI         0000 D 005062 YO        0000 D 023140 Y0        0000 D 011346 [
)00 D 011712 Y22        0000 D 020316 Y3
```

```
1*      C     THIS PROGRAM COMPUTES THE ERROR SENSITIVITIES AND GEOMETRIC
2*      C     ERRORS OF GROUND POINTS INDUCED BY ALTITUDE,ROLL,YAW AND
3*      C     PITCH ERRORS AS WELL AS EARTH ROTATION AND SHUTTLE MOTION
4*
5*
6*
7*            PARAMETER NLAMDA=10,NLOMDA=19,NDH=8,NFI=3,NPSI=3,NTETA=3
8*           $,NDT=3,NDETA=5,NDFI=5,NDPSA=10,NDTHE=10,NCOM=15,NSDH=2
9*            REAL H,R,DH(NDH),DLAMDA(NLAMDA),DLOMDA(NLOMDA),SDH(NSDH),
10*          $TDH1,TDH2,DFI1(NFI),DFI2(NFI),DPSI1(NPSI),DPSI2(NPSI),
11*          $DPSI(NPSI),DBETA(NPSI),XO(NLOMDA),DFI(NDFI),
12*          $DTETA1(NTETA),DTETA2(NTETA),XO(NLOMDA),DPSA(NDPSA)
13*          $,DT(NDT),DTAU,DETA(NDETA),DALFA(NDPSA),DTHETA(NDTHE)
14*          $,DYAW(NCOM),DROLL(NCOM),DPITCH(NCOM)
15*           DOUBLE PRECISION LAMDA(NLAMDA),XY(NLAMDA),FI1(NFI),FI2(NFI)
16*          $,DXY(NDH,NLAMDA),LOMDA(NLOMDA),Y(NLOMDA),PY(NDFI,NLOMDA)
17*          $,DY(NDFI,NLOMDA),PDXY(NDH,NLAMDA),PSXY(NLAMDA,NDH),
18*          $BXY(NLAMDA),DBXY(NLAMDA,NDH),B(NLAMDA,NDH),BY1(NFI,NLOMDA),
19*          $TXY1(NLAMDA),TXY2(NLAMDA),DTXY(NLAMDA),T(NLAMDA),PXY(NDH,NLAMD
20*          $A),BY2(NFI,NLOMDA),DBY(NFI,NLOMDA),B(NFI,NLOMDA),PSI(NPSI),
21*          $BETA(NPSI),RA(NLAMDA),DELTA(NPSI,NLAMDA),D(NPSI,NLAMDA),
22*          $PSA(NDPSA),ALFA(NDPSA),DOLTA(NDPSA,NLAMDA),YO(NLOMDA),
23*          $T2(NDTHE,NLOMDA),DEL(NDTHE,NLOMDA),RHO(NDTHE,NLOMDA)
24*          $,TETA1(NTETA),TETA2(NTETA),TI1(NTETA),TI2(NTETA),
25*          $TII1(NTETA,NLOMDA),TII2(NTETA,NLOMDA),DEL1(NTETA,NLOMDA),
26*          $DEL2(NTETA,NLOMDA),RHO1(NTETA,NLOMDA),RHO2(NTETA,NLOMDA),
27*          $SQURT1(NTETA,NLOMDA),SQURT2(NTETA,NLOMDA),X11(NTETA,NLOMDA),
28*          $Y11(NTETA,NLOMDA),X22(NTETA,NLOMDA),Y22(NTETA,NLOMDA)
29*           DOUBLE PRECISION X2(NCOM,NLOMDA),
30*          $SHFT(NTETA,NLOMDA),SEN(NTETA,NLOMDA),YAW(NCOM),ROLL(NCOM),
31*          $FI(NDFI),PDY(NDFI,NLOMDA),YI(NDTHE,NLOMDA),THETA(NDTHE),
32*          $XI(NDTHE,NLOMDA),TI(NDTHE),SQURT(NDTHE,NLOMDA),
33*          $SHF(NDTHE,NLOMDA),PITCH(NCOM),
```

ORIGINAL PAGE IS
OF POOR QUALITY

```
      $X3(NCOM,NLOMDA),Y3(NCOM,NLOMDA)
      $,DIFF(NCOM,NLOMDA),TAU,OMEGA,ETA(NDETA),
      $V(NDETA),ELUMDA(NDETA),CLUMDA(NDETA),VX(NDETA),VY(NDETA),
      $DEX(NDETA,NDT),DEY(NDETA,NDT),ERR(NDETA,NDT),VB,VPX(NDETA),
      $VP(NDETA),ANGL(NDETA),DANGL(NDETA),DELX(NDETA,NDT)
      $,DELY(NDETA,NDT),ERRO(NDETA,NDT),YB(NLOMDA)
      $,T33(NCOM,NLOMDA),DE1(NCOM,NLOMDA),T11(NCOM),
      $Y2(NCOM,NLOMDA),RO1(NCOM,NLOMDA),BOUT1(NCOM,NLOMDA)
       DATA (DH(K),K=1,NDH)/1.,-1.,2.,-2.,3.,-3.,4.,-4./
       DATA H,R,DTAU/400.,6350.,785,85./
       DATA (DFI(K),K=1,NDFI)/18.,19.,20.,21.,22./
       DATA (DPSA(K),K=1,NDPSA)/.5,1.,1.5,2.,2.5,3.,3.5,4.,4.5,5./
       DATA (DTHETA(K),K=1,NDTHE)/20.5,21.5,22.5,23.5,24.5,43.,44.,
      $45.,46.,47./
       DATA (DYAW(K),K=1,NCOM)/0.,0.,0.,1.,-1.,0.,0.,0.,1.,-1.,0.,
      $0.,1.,-1./
       DATA (DPITCH(K),K=1,NCOM)/0.,1.,-1.,0.,0.,22.5,22.5,22.5,22.5,
      $22.5,45.,45.,45.,45.,45./
       DATA (DROLL(K),K=1,NCOM)/20.,20.,20.,20.,20.,0.,1.,-1.,0.,0.,
      $0.,1.,-1.,0.,0./
       DATA (DLAMDA(I),I=1,NLAMDA)/0.,1.,2.,3.,4.,5.,6.,7.,8.,9./
       DATA (DLOMDA(I),I=1,NLOMDA)/-9.,-8.,-7.,-6.,-5.,-4.,-3.,-2.,
      $-1.,0.,1.,2.,3.,4.,5.,6.,7.,8.,9./
       DATA (DDH(I),I=1,NDDH)/.01,.02/
       DATA TDH1,TDH2/.01,-.01/
       DATA (DFI1(K),K=1,NFI),(DFI2(K),K=1,NFI)/.01,.02,.05,-.01,
      $-.02,-.05/
       DATA (DPSI1(K),K=1,NPSI),(DPSI2(K),K=1,NPSI)/.01,.02,.05,
      $-.01,-.02,-.05/
       DATA (DTETA1(K),K=1,NTETA),(DTETA2(K),K=1,NTETA)/.01,.02,
      $.05,-.01,-.02,-.05/
       DATA (XO(K),K=1,NLOMDA)/1990./
       DATA (XO(K),K=1,NLOMDA)/1990./
       DATA (DT(K),K=1,NDT)/1.,.1,.01/
       DATA (DETA(K),K=1,NDETA)/0.,20.,40.,60.,80./
       PI=3.14159265

       DO 100 K=1,NDH
       DO 90 I=1,NLAMDA
       LAMDA(I)=DLAMDA(I)*PI/180.
       XY(I)=R*((1+H/R)*DCOS(LAMDA(I))-DSQRT(1-(1+H/R)*(1+H/R)*
      $DSIN(LAMDA(I))*DSIN(LAMDA(I))))*DSIN(LAMDA(I))
       PXY(K,I)=R*((1+(H+DH(K))/R)*DCOS(LAMDA(I))-DSQRT(1-(1+(H+DH(K
      $))/R)*(1+(H+DH(K))/R)*DSIN(LAMDA(I))*DSIN(LAMDA(I))))*DSIN
      $(LAMDA(I))
       DXY(K,I)=PXY(K,I)-XY(I)
       IF(DXY(K,I).EQ.0.) GO TO 80
       PDXY(K,I)=DABS(DXY(K,I))*100./DABS(XY(I))
       GO TO 90
    80 PDXY(K,I)=0.
    90 CONTINUE
   100 CONTINUE

       DO 102 J=1,NSDH
       DO 101 I=1,NLAMDA
```

```
      LAMDA(I)=DLAMDA(I)*PI/180.
      SXY(I)=R*((1+H/R)*DCOS(LAMDA(I))-DSQRT(1-(1+H/R)*(1+H/R)*
     $DSIN(LAMDA(I))*DSIN(LAMDA(I))))*DSIN(LAMDA(I))
      PSXY(I,J)=R*((1+(H+SDH(J))/R)*DCOS(LAMDA(I))-DSQRT(1-(1+(H+SDH(J))
     $/R)*(1+(H+SDH(J))/R)*DSIN(LAMDA(I))*DSIN(LAMDA(I))))*DSIN(
     $LAMDA(I))
      DSX(I,J)=PSXY(I,J)-SXY(I)
      S(I,J)=DSXY(I,J)/SDH(J)
  101 CONTINUE
  102 CONTINUE


      DO 103 I=1,NLAMDA
      LAMDA(I)=DLAMDA(I)*PI/180.
      TXY1(I)=R*((1+(H+TDH1)/R)*DCOS(LAMDA(I))-DSQRT(1-(1+(H+TDH1)/R)*
     $(1+(H+TDH1)/R)*DSIN(LAMDA(I))*DSIN(LAMDA(I))))*DSIN(LAMDA(I))
      TXY2(I)=R*((1+(H+TDH2)/R)*DCOS(LAMDA(I))-DSQRT(1-(1+(H+TDH2)/R)*
     $(1+(H+TDH2)/R)*DSIN(LAMDA(I))*DSIN(LAMDA(I))))*DSIN(LAMDA(I))
      DTXY(I)=TXY1(I)-TXY2(I)
      T(I)=DTXY(I)/(TDH1-TDH2)
  103 CONTINUE


      DO 111 K=1,NDFI
      FI(K)=DFI(K)*PI/180.
      DO 110 J=1,NLOMDA
      LOMDA(J)=DLOMDA(J)*PI/180.
      Y(J)=-R*((1+H/R)*DCOS(LOMDA(J))-DSQRT(1-(1+H/R)*(1+H/R)*
     $DSIN(LOMDA(J))*DSIN(LOMDA(J))))*DSIN(LOMDA(J))
      PY(K,J)=-R*((1+H/R)*DCOS(LOMDA(J)+FI(K))-DSQRT(1-(1+H/R)*(1+H/R)*
     $DSIN(LOMDA(J)+FI(K))*DSIN(LOMDA(J)+FI(K))))*DSIN(LOMDA(J)+FI(K))
      DY(K,J)=PY(K,J)-Y(J)
      IF(Y(J).EQ.0.) GO TO 109
      PDY(K,J)=DABS(DY(K,J))*100./DABS(Y(J))
      GO TO 110
  109 PDY(K,J)=10.D100
  110 CONTINUE
  111 CONTINUE


      DO 130 K=1,NFI
      FI1(K)=DFI1(K)*PI/180.
      FI2(K)=DFI2(K)*PI/180.
      DO 120 J=1,NLOMDA
      LOMDA(J)=DLOMDA(J)*PI/180.
      BY1(K,J)=-R*((1+H/R)*DCOS(LOMDA(J)+FI1(K))-DSQRT(1-(1+H/R)*
     $(1+H/R)*DSIN(LOMDA(J)+FI1(K))*DSIN(LOMDA(J)+FI1(K))))*
     $DSIN(LOMDA(J)+FI1(K))
      BY2(K,J)=-R*((1+H/R)*DCOS(LOMDA(J)+FI2(K))-DSQRT(1-(1+H/R)*
     $(1+H/R)*DSIN(LOMDA(J)+FI2(K))*DSIN(LOMDA(J)+FI2(K))))*
     $DSIN(LOMDA(J)+FI2(K))
      DBY(K,J)=BY1(K,J)-BY2(K,J)
      B(K,J)=DBY(K,J)/(DFI1(K)-DFI2(K))
  120 CONTINUE
  130 CONTINUE


```

```
148*          DO 132 K=1,NDPSA
149*          DALFA(K)=(180.-DPSA(K))/2.
150*          PSA(K)=DPSA(K)*PI/180.
151*          ALFA(K)=DALFA(K)*PI/180.
152*          DO 131 J=1,NLAMDA
153*          LAMDA(J)=DLAMDA(J)*PI/180.
154*          RA(J)=R*((1+H/R)*DCOS(LAMDA(J))-DSQRT(1-(1+H/R)*(1+H/R)
155*         $*DSIN(LAMDA(J))*DSIN(LAMDA(J))))*DSIN(LAMDA(J))
156*          DOLTA(K,J)=(RA(J)*DSIN(PSA(K)))/DSIN(ALFA(K))
157*      131 CONTINUE
158*      132 CONTINUE
159*
160*
161*          DO 136 K=1,NPSI
162*          DPSI(K)=DPSI1(K)-DPSI2(K)
163*          DBETA(K)=(180.-DPSI(K))/2.
164*          PSI(K)=DPSI(K)*PI/180.
165*          BETA(K)=DBETA(K)*PI/180.
166*          DO 135 J=1,NLAMDA
167*          LAMDA(J)=DLAMDA(J)*PI/180.
168*          RA(J)=R*((1+H/R)*DCOS(LAMDA(J))-DSQRT(1-(1+H/R)*(1+H/R)*
169*         $DSIN(LAMDA(J))*DSIN(LAMDA(J))))*DSIN(LAMDA(J))
170*          DELTA(K,J)=(RA(J)*DSIN(PSI(K)))/DSIN(BETA(K))
171*          D(K,J)=DELTA(K,J)/DPSI(K)
172*      135 CONTINUE
173*      136 CONTINUE
174*
175*
176*          DO 206 K=1,NDTHE
177*          THETA(K)=DTHETA(K)*PI/180.
178*          DO 205 J=1,NLOMDA
179*          LOMDA(J)=DLOMDA(J)*PI/180.
180*          YO(J)=R*((1+H/R)*DCOS(LOMDA(J))-DSQRT(1-(1+H/R)*(1+H/R)*DSIN
181*         $(LOMDA(J))*DSIN(LOMDA(J))))*DSIN(LOMDA(J))
182*          T1(K)=H*DTAN(THETA(K))
183*          T2(K,J)=-DABS(H/DCOS(THETA(K)))*DTAN(LOMDA(J))
184*          DEL(K,J)=DSQRT(T1(K)*T1(K)+T2(K,J)*T2(K,J))
185*          RHO(K,J)=DATAN(DEL(K,J)/H)
186*          SQURT(K,J)=R*((1+H/R)*DCOS(RHO(K,J))-DSQRT(1-(1+H/R)*(1+H/R)*DSIN
187*         $(RHO(K,J)))*DSIN(RHO(K,J))))*DSIN(RHO(K,J))
188*          XI(K,J)=(SQURT(K,J)*T1(K))/DEL(K,J)
189*          YI(K,J)=(SQURT(K,J)*T2(K,J))/DEL(K,J)
190*          SHF(K,J)=DSQRT(XI(K,J)*XI(K,J)+(YI(K,J)-YO(J))*(YI(K,J)-YO(J)))
191*      205 CONTINUE
192*      206 CONTINUE
193*
194*
195*          DO 208 K=1,NTETA
196*          TETA1(K)=DTETA1(K)*PI/180.
197*          TETA2(K)=DTETA2(K)*PI/180.
198*          DO 207 J=1,NLOMDA
199*          LOMDA(J)=DLOMDA(J)*PI/180.
200*          TI1(K)=H*DTAN(TETA1(K))
201*          TI2(K)=H*DTAN(TETA2(K))
202*          TII1(K,J)=-DABS(H/DCOS(TETA1(K)))*DTAN(LOMDA(J))
203*          TII2(K,J)=-DABS(H/DCOS(TETA2(K)))*DTAN(LOMDA(J))
204*          DEL1(K,J)=DSQRT(TI1(K)*TI1(K)+TII1(K,J)*TII1(K,J))
```

ORIGINAL PAGE IS
OF POOR QUALITY

```
      DEL2(K,J)=DSQRT(TI2(K)*TI2(K)+TII2(K,J)*TII2(K,J))
      RHO1(K,J)=DATAN(DEL1(K,J)/H)
      RHO2(K,J)=DATAN(DEL2(K,J)/H)
      SQURT1(K,J)=R*((1+H/R)*DCOS(RHO1(K,J))-DSQRT(1-(1+H/R)*
     $(1+H/R)*DSIN(RHO1(K,J))*DSIN(RHO1(K,J))))*DSIN(RHO1(K,J))
      SQURT2(K,J)=R*((1+H/R)*DCOS(RHO2(K,J))-DSQRT(1-(1+H/R)*
     $(1+H/R)*DSIN(RHO2(K,J))*DSIN(RHO2(K,J))))*DSIN(RHO2(K,J))
      X11(K,J)=(SQURT1(K,J)*TI1(K))/DEL1(K,J)
      Y11(K,J)=(SQURT1(K,J)*TII1(K,J))/DEL1(K,J)
      X22(K,J)=(SQURT2(K,J)*TI2(K))/DEL2(K,J)
      Y22(K,J)=(SQURT2(K,J)*TII2(K,J))/DEL2(K,J)
      SHFT(K,J)=DSQRT((X11(K,J)-X22(K,J))*(X11(K,J)-X22(K,J))+
     $(Y11(K,J)-Y22(K,J))*(Y11(K,J)-Y22(K,J)))
      SEN(K,J)=SHFT(K,J)/(DTETA1(K)-DTETA2(K))
  207 CONTINUE
  208 CONTINUE


      DO 211 K=1,NCOM
      YAW(K)=DYAW(K)*PI/180.
      ROLL(K)=DROLL(K)*PI/180.
      PITCH(K)=DPITCH(K)*PI/180.
      DO 210 J=1,NLOMDA
      LOMDA(J)=DLOMDA(J)*PI/180.
      Y0(J)=R*((1+H/R)*DCOS(LOMDA(J))-DSQRT(1-(1+H/R)*(1+H/R)*
     $DSIN(LOMDA(J))*DSIN(LOMDA(J))))*DSIN(LOMDA(J))
      T11(K)=H*DTAN(PITCH(K))
      T33(K,J)=-DABS(H/DCOS(PITCH(K)))*DTAN(LOMDA(J)+ROLL(K))
      DE1(K,J)=DSQRT(T11(K)*T11(K)+T33(K,J)*T33(K,J))
      RO1(K,J)=DATAN(DE1(K,J)/H)
      SQUT1(K,J)=R*((1+H/R)*DCOS(RO1(K,J))-DSQRT(1-(1+H/R)*(1+H/R)
     $*DSIN(RO1(K,J))*DSIN(RO1(K,J))))*DSIN(RO1(K,J))
      X2(K,J)=(SQUT1(K,J)*T11(K))/DE1(K,J)
      Y2(K,J)=(SQUT1(K,J)*T33(K,J))/DE1(K,J)
      X3(K,J)=X2(K,J)*DCOS(YAW(K))-Y2(K,J)*DSIN(YAW(K))
      Y3(K,J)=X2(K,J)*DSIN(YAW(K))+Y2(K,J)*DCOS(YAW(K))
      DIFF(K,J)=DSQRT((X3(K,J)-X0(J))*(X3(K,J)-X0(J))+(Y3(K,J)-Y0(J))*
     $(Y3(K,J)-Y0(J)))
  210 CONTINUE
  211 CONTINUE


      TAU=DTAU*PI/180.
      OMEGA=2.*PI/86400.
      DO 220 K=1,NDETA
      ETA(K)=DETA(K)*PI/180.
      V(K)=OMEGA*R*DCOS(ETA(K))
      SLUMDA(K)=DCOS(TAU)/DCOS(ETA(K))
      CLUMDA(K)=DSQRT(1-SLUMDA(K)*SLUMDA(K))
      VX(K)=V(K)*SLUMDA(K)
      VY(K)=V(K)*CLUMDA(K)
      DO 215 J=1,NDT
      DEX(K,J)=VX(K)*DT(J)
      DEY(K,J)=VY(K)*DT(J)
      ERR(K,J)=DSQRT(DEX(K,J)*DEX(K,J)+DEY(K,J)*DEY(K,J))
  215 CONTINUE
  220 CONTINUE
```

```
*
*
*         VS=2.*PI*R/5545.484
*         TAU=DTAU*PI/180.
*         OMEGA=2.*PI/86400.
*         DO 222 K=1,NDETA
*         ETA(K)=DETA(K)*PI/180.
*         V(K)=OMEGA*R*DCOS(ETA(K))
*         SLUMDA(K)=DCOS(TAU)/DCOS(ETA(K))
*         CLUMDA(K)=DSQRT(1-SLUMDA(K)*SLUMDA(K))
*         VX(K)=V(K)*SLUMDA(K)
*         VY(K)=V(K)*CLUMDA(K)
*         VPX(K)=VX(K)-VS
*         VP(K)=DSQRT(VPX(K)*VPX(K)+VY(K)*VY(K))
*         ANGL(K)=DATAN(VPX(K)/VY(K))
*         DANGL(K)=ANGL(K)*180./PI
*         DO 221 J=1,NDT
*         DELX(K,J)=VPX(K)*DT(J)
*         DELY(K,J)=VY(K)*DT(J)
*         ERRO(K,J)=DSQRT(DELX(K,J)*DELX(K,J)+DELY(K,J)*DELY(K,J))
*      221 CONTINUE
*      222 CONTINUE
*
*
*         DO 237 I=1,NDH
*         WRITE(6,236) R,H,DH(K),(DLAMDA(I),I=1,NLAMDA),(XY(I),I=1,NLAMD
*        $A),(PXY(K,I),I=1,NLAMDA),(DXY(K,I),I=1,NLAMDA),(PDXY(K,I),I=1,
*        $NLAMDA)
*      236 FORMAT(1H1,'********************* GEOMETRIC ERROR INDUCED BY'
*        $' ALTITUDE ERROR **********************',//////////,
*        $' EARTH RADIUS R =',F9.4,'KM',///,' NOMINAL ALTITUDE',
*        $' H=',F4.0,'KM',///,' ALTITUDE ERROR DH =',F3.0,'KM',
*        $//////////,' VIEW',5X,'ANGLE',/,' DLAMDA(DEGREES)',
*        $12X,F2.0,9(9X,F2.0),///,' NOMINAL LOCATION (KM)',10D11.4,
*        $///,' SHIFTED LOCATION (KM)',10D11.4,///,7X,'ERROR',6X,
*        $'(KM)',10D11.4,///,4X,'ABS(ERROR)',3X,'(%)',2X,F5.3,
*        $8X,F5.3,8(6X,F5.3))
*      237 CONTINUE
*
*
*         DO 239 J=1,NSDH
*         WRITE(6,238) R,H,SDH(J),(DLAMDA(I),I=1,NLAMDA),(SXY(I),I=
*        $1,NLAMDA),(PSXY(I,J),I=1,NLAMDA),(DSXY(I,J),I=1,NLAMDA),(S(I,J)
*        $,I=1,NLAMDA)
*      238 FORMAT(1H1,'********************* GEOMETRIC ERROR SENSITIVITY'
*        $' WITH RESPECT TO ALTITUDE ERROR **********',////////
*        $//,' EARTH RADIUS R =',F9.4,'KM',///,' NOMINAL ALTITUDE H =',
*        $F4.0,'KM',///,' ALTITUDE ERROR SDH =',F4.2,'KM',//////////,' VIEW'
*        $,5X,'ANGLE',/,' DLAMDA(DEGREES)',12X,F2.0,9(9X,F2.0),///,
*        $' NOMINAL LOCATION (KM)',10D11.4,///,' SHIFTED LOCATION (KM)',
*        $10D11.4,///,7X,'ERROR',6X,'(KM)',10D11.4,///6X,'ERROR',/,
*        $'   SENSITIVITY (KM/KM)',10D11.4)
*      239 CONTINUE
*
*
*         WRITE(6,240) R,H,TDH1,TDH2,(DLAMDA(I),I=1,NLAMDA),(TXY1(I),I=
*        $1,NLAMDA),(TXY2(I),I=1,NLAMDA),(DTXY(I),I=1,NLAMDA),(T(I),I=
```

ORIGINAL PAGE IS
OF POOR QUALITY

```
     $1,NLAMDA)
240 FORMAT(1H1,'********************* GEOMETRIC ERROR SENSITIVITY'
   $' WITH RESPECT TO ALTITUDE ERROR ********************',
   $//////////,' EARTH RADIUS R =',F9.4,'KM',///,' NOMINAL'
   $' ALTITUDE H =',F8.0,'KM',///,' ALTITUDE ERROR 1 TDH1 =',
   $F8.2,'KM',///,' ALTITUDE ERROR 2 TDH2 =',F5.2,'KM',
   $/////////,' VIEW',5X,'ANGLE',/,' DLAMDA(DEGREES)',12X,
   $F2.0,9(9X,F2.0),///,' SHIFTED LOCATION',/,' DUE TO ERROR'
   $' 1   (KM)',10D11.4,///,' SHIFTED LOCATION',/,' DUE TO'
   $' ERROR 2   (KM)',10D11.4,///,'    DIFFERENCE    (KM)',
   $10D11.4,///,6X,'ERROR',/,'   SENSITIVITY (KM/KM)',10
   $D11.4)


      DO 246 K=1,NOFI
      WRITE(6,245) R,H,DFI(K),(DLOMDA(J),J=1,10),(Y(J),J=1,10),
   $(PY(K,J),J=1,10),(DY(K,J),J=1,10),(PDY(K,J),J=1,10),(DLOMDA(J),
   $J=11,NLOMDA),(Y(J),J=11,NLOMDA),(PY(K,J),J=11,NLOMDA),(DY(K,J),
   $J=11,NLOMDA),(PDY(K,J),J=11,NLOMDA)
245 FORMAT(1H1,'********************* GEOMETRIC ERROR INDUCED BY'
   $' ROLL ERROR ********************',///////,
   $' EARTH RADIUS R =',F9.4,'KM',///,' NOMINAL ALTITUDE H =',
   $F8.0,'KM',///,' ROLL ERROR DFI =',F8.0,'DEGREE',//////,
   $' VIEW',5X,'ANGLE',/,' DLOMDA(DEGREES)',12X,F3.0,9(8X,F3.0),
   $///,' NOMINAL LOCATION (KM)',10D11.4,///,' SHIFTED',
   $' LOCATION (KM)',10D11.4,///,7X,'ERROR',6X,'(KM)',10D11.4,
   $///,4X,'ABS(ERROR)',5X,'(%)',F10.4,8F11.4,3X,F5.2,
   $//////,' VIEW',5X,'ANGLE',/,' DLOMDA(DEGREES)',13X,F2.0,
   $8(9X,F2.0),///,' NOMINAL LOCATION (KM)',9D11.4,///,' SHIFTED'
   $' LOCATION (KM)',9D11.4,///,7X,'ERROR',6X,'(KM)',9D11.4,
   $///,4X,'ABS(ERROR)',5X,'(%)',F10.4,8F11.4)
246 CONTINUE


      DO 300 K=1,NFI
      WRITE(6,250) R,H,DFI1(K),DFI2(K),(DLOMDA(J),J=1,10),(BY1(K
   $,J),J=1,10),(BY2(K,J),J=1,10),(DBY(K,J),J=1,10),(B(K,J),J=
   $1,10),(DLOMDA(J),J=11,NLOMDA),(BY1(K,J),J=11,NLOMDA),(BY2
   $(K,J),J=11,NLOMDA),(DBY(K,J),J=11,NLOMDA),(B(K,J),J=11,NLOM
   $DA)
250 FORMAT(1H1,'********************* GEOMETRIC ERROR SENSITIVI'
   $'TY WITH RESPECT TO ROLL ERROR **********************',/////
   $,' EARTH RADIUS R =',F9.4,'KM',///,' NOMINAL ALTITUDE H =',
   $F8.0,'KM',///,' ROLL ERROR 1 DFI1 =',F5.2,'DEGREE',///,
   $' ROLL ERROR 2 DFI2 =',F5.2,'DEGREE',/////,' VIEW',5X,
   $'ANGLE',/,' DLOMDA(DEGREES)',12X,F3.0,9(8X,F3.0),///,
   $' SHIFTED LOCATION',/,' DUE TO ERROR 1   (KM)',10D11.4
   $//,' SHIFTED LOCATION',/,' DUE TO ERROR 2   (KM)',
   $10D11.4,///,'    DIFFERENCE    (KM)',10D11.4,//,6X,
   $'ERROR',/,'   SENSITIVITY(KM/DEG)',10D11.4,/////,
   $' VIEW',5X,'ANGLE',/,' DLOMDA(DEGREES)',12X,F3.0,8(8X,
   $F3.0),///,' SHIFTED LOCATION',/,' DUE TO ERROR 1   (KM)',
   $9D11.4,///,' SHIFTED LOCATION',/,' DUE TO ERROR 2   (KM)',
   $9D11.4,///,'    DIFFERENCE    (KM)',9D11.4,//,6X,
   $'ERROR',/,'   SENSITIVITY(KM/DEG)',9D11.4)
300 CONTINUE
```

```
376*
377*          DO 321 K=1,NDPSA
378*          WRITE(6,320) R,M,DPSA(K),(DLAMDA(I),I=1,NLAMDA),
379*         $(DDLTA(K,J),J=1,NLAMDA)
380*      320 FORMAT(1H1,'*********************** GEOMETRIC ERROR INDUCED'
381*         $' BY YAW ERROR **********************',/////////,' EARTH '
382*         $'RADIUS R =',F9.4,'KM',///,' NOMINAL ALTITUDE M =',F4.0,
383*         $'KM',///,' YAW ERROR DPSA =',F3.1,'DEGREE',//////////,
384*         $' VIEW',5X,'ANGLE',/,' DLAMDA(DEGREES)',12X,F2.0,9(9X,F2.0),
385*         $,////,7X,'ERROR',6X,'(KM)',10D11.4)
386*      321 CONTINUE
387*
388*
389*          DO 400 K=1,NPSI
390*          WRITE(6,350) R,M,DPSI1(K),DPSI2(K),(DLAMDA(I),I=1,NLAMDA),
391*         $(DELTA(K,J),J=1,NLAMDA),(D(K,J),J=1,NLAMDA)
392*      350 FORMAT(1H1,'*********************** GEOMETRIC ERROR SENSITIVITY'
393*         $' WITH RESPECT TO YAW ERROR **********************',/////////,
394*         $' EARTH RADIUS R =',F9.4,'KM',///,' NOMINAL ALTITUDE M =',
395*         $F4.0,'KM',///,' YAW ERROR 1 DPSI1 =',F5.2,'DEGREE',///,
396*         $' YAW ERROR 2 DPSI2 =',F5.2,'DEGREE',/////////,' VIEW',5X,
397*         $'ANGLE',/,' DLAMDA(DEGREES)',12X,F2.0,9(9X,F2.0),////,
398*         $'     TOTAL SHIFT   (KM)',10D11.4,///,6X,'ERROR',//,
399*         $'   SENSITIVITY(KM/DEG)',10D11.4)
400*      400 CONTINUE
401*
402*
403*          DO 451 K=1,NDTHE
404*          WRITE(6,450) R,M,DTHETA(K),(DLOMDA(J),J=1,10),(XO(J),J=1,10),
405*         $(YO(J),J=1,10),(XI(K,J),J=1,10),(YI(K,J),J=1,10),(SHF(K,J),J=1,10)
406*         $,(DLOMDA(J),J=11,NLOMDA),(XO(J),J=11,NLOMDA),(YO(J),J=11,
407*         $NLOMDA),(XI(K,J),J=11,NLOMDA),(YI(K,J),J=11,NLOMDA),(SHF(K,J),J=
408*         $11,NLOMDA)
409*      450 FORMAT(1H1,'*********************** GEOMETRIC ERROR INDUCED BY'
410*         $' PITCH ERROR **********************',/////,' EARTH RADIUS R ='
411*         $,F9.4,'KM',///,' NOMINAL ALTITUDE M =',F4.0,'KM',///,' PITCH'
412*         $' ERROR DTHETA =',F5.1,'DEGREE',/////,' VIEW',5X,'ANGLE',/,
413*         $' DLOMDA(DEGREES)',12X,F3.0,9(8X,F3.0),///,' NOMINAL X COORD'
414*         $,' (KM)',7X,F2.0,9(9X,F2.0),///,' NOMINAL Y COORD. (KM)',
415*         $10D11.4,///,' SHIFTED X COORD. (KM)',10D11.4,///,' SHIFTED'
416*         $' Y COORD. (KM)',10D11.4,///,7X,'ERROR',6X,'(KM)',10D11.4,
417*         $/////,' VIEW',5X,'ANGLE',/,' DLOMDA(DEGREES)',12X,F3.0,
418*         $8(8X,F3.0),///,' NOMINAL X COORD. (KM)',7X,F2.0,8(9X,F2.0),
419*         $///,' NOMINAL Y COORD. (KM)',9D11.4,///,' SHIFTED X COORD.'
420*         $' (KM)',9D11.4,///,' SHIFTED Y COORD. (KM)',9D11.4,///,7X,
421*         $'ERROR',6X,'(KM)',9D11.4)
422*      451 CONTINUE
423*
424*
425*          DO 500 K=1,NTETA
426*          WRITE(6,480) R,M,DTETA1(K),DTETA2(K),(DLOMDA(J),J=1,10),
427*         $(X11(K,J),J=1,10),(Y11(K,J),J=1,10),(X22(K,J),J=1,10),
428*         $(Y22(K,J),J=1,10),(SHFT(K,J),J=1,10),(SEN(K,J),J=1,10),
429*         $(DLOMDA(J),J=11,NLOMDA),(X11(K,J),J=11,NLOMDA),
430*         $(Y11(K,J),J=11,NLOMDA),(X22(K,J),J=11,NLOMDA),
431*         $(Y22(K,J),J=11,NLOMDA),(SHFT(K,J),J=11,NLOMDA),
432*         $(SEN(K,J),J=11,NLOMDA)
```

ORIGINAL PAGE IS
OF POOR QUALITY

```
      400 FORMAT(1H1,'********************* GEOMETRIC ERROR SENSITIVI'
     $'TY WITH RESPECT TO PITCH ERROR ********************',////,
     $' EARTH RADIUS R =',F9.4,'KM',///,' NOMINAL ALTITUDE H =',
     $F4.0,'KM',//,' PITCH ERROR 1 DTETA1 =',F5.2,'DEGREE',//,
     $' PITCH ERROR 2 DTETA2 =',F5.2,'DEGREE',////,' VIEW',5X,
     $'ANGLE',/,' DLOMDA(DEGREES)',12X,F3.0,9(8X,F3.0),///,
     $' SHIFTED X COORD.',/,' DUE TO ERROR 1   (KM)',10D11.4,//,
     $' SHIFTED Y COORD.',/,' DUE TO ERROR 1   (KM)',10D11.4,//,
     $' SHIFTED X COORD.',/,' DUE TO ERROR 2   (KM)',10D11.4,//,
     $' SHIFTED Y COORD.',/,' DUE TO ERROR 2   (KM)',10D11.4,///,
     $'    DIFFERENCE    (KM)',10D11.4,//,6X,'ERROR',/,'   SENSI'
     $'TIVITY(KM/DEG)',10D11.4,////,' VIEW',5X,'ANGLE',/,
     $' DLOMDA(DEGREES)',12X,F3.0,8(8X,F3.0),///,
     $' SHIFTED X COORD.',/,' DUE TO ERROR 1   (KM)',9D11.4,//,
     $' SHIFTED Y COORD.',/,' DUE TO ERROR 1   (KM)',9D11.4,//,
     $' SHIFTED X COORD.',/,' DUE TO ERROR 2   (KM)',9D11.4,//,
     $' SHIFTED Y COORD.',/,' DUE TO ERROR 2   (KM)',9D11.4,///,
     $'    DIFFERENCE    (KM)',9D11.4,//,6X,'ERROR',/,'   SENSI'
     $'TIVITY(KM/DEG)',9D11.4)
      500 CONTINUE


       DO 601 K=1,NCOM
       WRITE(6,600) R,H,DYAW(K),DPITCH(K),DROLL(K),(DLOMDA(J),J=1,10),
     $(X0(J),J=1,10),(Y0(J),J=1,10),(X3(K,J),J=1,10),(Y3(K,J),J=1,10),
     $(DIFF(K,J),J=1,10),(DLOMDA(J),J=11,NLOMDA),(X0(J),J=11,NLOMDA)
     $,(Y0(J),J=11,NLOMDA),(X3(K,J),J=11,NLOMDA),(Y3(K,J),J=11,NLOMDA)
     $,(DIFF(K,J),J=11,NLOMDA)
      600 FORMAT(1H1,'********************* GEOMETRIC ERROR INDUCED BY'
     $' YAW,PITCH AND ROLL ERRORS ********************',////,
     $' EARTH RADIUS R =',F9.4,'KM',///,' NOMINAL ALTITUDE H =',
     $F4.0,'KM',////,' YAW ERROR DYAW =',F4.1,'DEGREE',///,
     $' PITCH ERROR DPITCH =',F4.1,'DEGREE',///,' ROLL ERROR'
     $' DROLL =',F4.1,'DEGREE',////,' VIEW',5X,'ANGLE',/,' DLOMDA'
     $'(DEGREES)',12X,F3.0,9(8X,F3.0),///,' NOMINAL X COORD. (KM)'
     $,7X,F2.0,9(9X,F2.0),///,' NOMINAL Y COORD. (KM)',10D11.4,
     $///,' SHIFTED X COORD. (KM)',10D11.4,///,' SHIFTED Y COORD.'
     $' (KM)',10D11.4,///,7X,'ERROR',6X,'(KM)',10D11.4,////,
     $' VIEW',5X,'ANGLE',/,' DLOMDA(DEGREES)',12X,F3.0,8(8X,F3.0),
     $///,' NOMINAL X COORD. (KM)',7X,F2.0,8(9X,F2.0),///,
     $' NOMINAL Y COORD. (KM)',9D11.4,///,' SHIFTED X COORD. (KM)'
     $,9D11.4,///,' SHIFTED Y COORD. (KM)',9D11.4,///,7X,'ERROR',
     $6X,'(KM)',9D11.4)
      601 CONTINUE


       DO 705 K=1,NDETA
       WRITE(6,700) R,DTAU,DETA(K),V(K),(DT(J),J=1,NDT),(DEX(K,J),
     $J=1,NDT),(DEY(K,J),J=1,NDT),(ERR(K,J),J=1,NDT)
      700 FORMAT(1H1,'********************* GEOMETRIC ERROR INDUCED BY'
     $' EARTH ROTATION ********************',//////////,' EARTH'
     $' RADIUS =',F9.4,'KM',////,' ORBIT INCLINATION =',F4.0,
     $'DEGREE',////,' LATITUDE =',F4.0,'DEGREE',/////////,
     $' GROUND POINT SHIFT VELOCITY DUE TO EARTH ROTATION =',
     $D10.4,'KM/SEC',////,
     $' TIME INTERVAL   (SEC)',3F15.2,///,'     SHIFT IN',/,
     $'   X DIRECTION    (KM)',3X,3D15.4,///,'     SHIFT IN',/,
```

```
      $'   Y DIRECTION    (KM)',3X,3D15.4,////,'    TOTAL SHIFT'
      $'   (KM)',3X,3D15.4)
  705 CONTINUE


       DO 707 K=1,NDETA
       WRITE(6,706) R,DTAU,DETA(K),V(K),VS,VP(K),DANGL(K),(DT(J),
      $J=1,NDT),(DELX(K,J),J=1,NDT),(DELY(K,J),J=1,NDT),(ERRO(K,J),
      $J=1,NDT)
  706 FORMAT(1H1,'********************* GROUND POINT SHIFT INDUCED
      $' BY SHUTTLE MOTION AND EARTH ROTATION *********************
      $,//////////,' EARTH RADIUS =',F9.4,'KM',////,' ORBIT
      $' INCLINATION =',F4.0,'DEGREE',////,' LATITUDE =',F4.0,
      $'DEGREE',////,' GROUND POINT SHIFT VELOCITY DUE TO EARTH
      $' ROTATION =',D10.4,'KM/SEC',////,' SHUTTLE GROUND SPEED =',
      $D10.4,'KM/SEC',////,' GROUND POINT SHIFT VELOCITY RELATIVE
      $' TO NADIR POINT =',D10.3,
      $'KM/SEC',////,' ANGLE OF VELOCITY VECTOR WITH Y-AXIS =',
      $D10.4,'DEGREE',////,' TIME INTERVAL    (SEC)',3F15.2,///,
      $'     SHIFT IN',/,'   X DIRECTION    (KM)',3X,3D15.4,////,
      $'     SHIFT IN',/,'   Y DIRECTION    (KM)',3X,3D15.4,////,
      $'    TOTAL SHIFT   (KM)',3X,3D15.4)
  707 CONTINUE


       STOP
       END


41   CTP=.134   SUPS=10.789

.A SHUTEXP.IMAGE/ABS
283-JB  04/27/83  10:31:21

2  SUPS=.736  CPU=.050  IO=.302  CC-ER=.433
```

ORIGINAL PAGE IS
OF POOR QUALITY

********************* GEOMETRIC ERROR INDUCED BY ALTITUDE ERROR *********************

'ARTH RADIUS R =6350.7850KM

NOMINAL ALTITUDE H=400.KM

\LTITUDE ERROR DH = 1.KM

VIEW ANGLE PLANDA(DEGREES)		0.	1.	2.	3.	4.	5.	6.	7.	8.	9.
NOMINAL LOCATION	(KM)	.0000	.6982+001	.1397+002	.2096+002	.2796+002	.3500+002	.4206+002	.4916+002	.5629+002	.6348+002
SHIFTED LOCATION	(KM)	.0000	.7000+001	.1400+002	.2102+002	.2804+002	.3509+002	.4216+002	.4926+002	.5639+002	.6358+002
ERROR	(KM)	.0000	.1746-001	.3492-001	.5243-001	.6995-001	.8753-001	.1052+000	.1229+000	.1407+000	.1588+000
ABS(ERROR)	(%)	.000	.250	.250	.250	.250	.250	.250	.250	.250	.250

********************* GEOMETRIC ERROR SENSITIVITY WITH RESPECT TO ALTITUDE ERROR *********************

EARTH RADIUS R =6350.7850KM

NOMINAL ALTITUDE H =400.KM

ALTITUDE ERROR 1 TDH1 = .01KM

ALTITUDE ERROR 2 TDH2 = -.01KM

VIEW ANGLE PLANDA(DEGREES)		0.	1.	2.	3.	4.	5.	6.	7.	8.	9.
SHIFTED LOCATION DUE TO ERROR 1	(KM)	.0000	.6982+001	.1397+002	.2097+002	.2798+002	.3503+002	.4209+002	.4918+002	.5629+002	.6341+00
SHIFTED LOCATION DUE TO ERROR 2	(KM)	.0000	.6982+001	.1397+002	.2096+002	.2797+002	.3500+002	.4206+002	.4916+002	.5625+002	.6348+00
DIFFERENCE	(KM)	.0000	.3491-003	.6983-003	.1048-002	.1399-002	.1751-002	.2104-002	.2458-002	.2814-002	.3173-00
ERROR SENSITIVITY	(KM/KM)	.0000	.1746-001	.3492-001	.5243-001	.6995-001	.8753-001	.1052+000	.1229+000	.1407+000	.1588+00

ORIGINAL PAGE IS
OF POOR QUALITY

•••••••••••••••••••• GEOMETRIC ERROR INDUCED BY ROLL ERROR ••••••••••••••••••••

EARTH RADIUS R =6356.7050KM

NOMINAL ALTITUDE H =600.KM

ROLL ERROR DFI =1.DEGREE

VIEW ANGLE DLOMDA(DEGREES)	-9.	-8.	-7.	-6.	-5.	-4.	-3.	-2.	-1.	0.
NOMINAL LOCATION (KM)	.6340E+002	.5825E+002	.4914E+002	.4286E+002	.3500E+002	.2798E+002	.2096E+002	.1397E+002	.6982E+001	.0000
SHIFTED LOCATION (KM)	.5825E+002	.4914E+002	.4286E+002	.3500E+002	.2798E+002	.2096E+002	.1397E+002	.6982E+001	.0000	-.6982E+001
ERROR (KM)	-.7153E+001	-.7114E+001	-.7081E+001	-.7052E+001	-.7029E+001	-.7010E+001	-.6997E+001	-.6987E+001	-.6982E+001	-.6982E+001
ABS(ERROR) (%)	11.2809	12.6671	14.4103	16.7699	20.0802	25.0584	33.3784	50.0107	100.0000	*****

VIEW ANGLE DLOMDA(DEGREES)	1.	2.	3.	4.	5.	6.	7.	8.	9.
NOMINAL LOCATION (KM)	-.6982E+001	-.1397E+002	-.2096E+002	-.2798E+002	-.3500E+002	-.4286E+002	-.4914E+002	-.5825E+002	-.6340E+002
SHIFTED LOCATION (KM)	-.1397E+002	-.2096E+002	-.2798E+002	-.3500E+002	-.4286E+002	-.4914E+002	-.5825E+002	-.6340E+002	-.7000E+002
ERROR (KM)	-.6987E+001	-.6998E+001	-.7016E+001	-.7029E+001	-.7052E+001	-.7081E+001	-.7114E+001	-.7153E+001	-.7198E+001
ABS(ERROR) (%)	100.0007	50.0035	33.4373	25.1295	20.1175	16.8305	14.4784	12.7153	11.3496

•••••••••••••••••••• GEOMETRIC ERROR SENSITIVITY WITH RESPECT TO ROLL ERROR ••••••••••••••••••••

EARTH RADIUS R =6356.7050KM

NOMINAL ALTITUDE H =600.KM

ROLL ERROR 1 DFI1 = .01DEGREE

ROLL ERROR 2 DFI2 = -.01DEGREE

VIEW ANGLE DLOMDA(DEGREES)	-9.	-8.	-7.	-6.	-5.	-4.	-3.	-2.	-1.	0.
SHIFTED LOCATION DUE TO ERROR 1 (KM)	.6333E+002	.5818E+002	.4907E+002	.4199E+002	.3493E+002	.2790E+002	.2089E+002	.1390E+002	.6912E+001	-.6981E+001
SHIFTED LOCATION DUE TO ERROR 2 (KM)	.6348E+002	.5832E+002	.4921E+002	.4213E+002	.3507E+002	.2805E+002	.2103E+002	.1404E+002	.7052E+001	-.6981E+001
DIFFERENCE (KM)	-.1435E+000	-.1427E+000	-.1419E+000	-.1413E+000	-.1408E+000	-.1404E+000	-.1400E+000	-.1398E+000	-.1397E+000	-.1396E+000
ERROR SENSITIVITY(KM/DEG)	-.7173E+001	-.7133E+001	-.7097E+001	-.7066E+001	-.7040E+001	-.7018E+001	-.7002E+001	-.6991E+001	-.6986E+001	-.6981E+001

VIEW ANGLE DLOMDA(DEGREES)	1.	2.	3.	4.	5.	6.	7.	8.	9.
SHIFTED LOCATION DUE TO ERROR 1 (KM)	-.6982E+001	-.1404E+002	-.2103E+002	-.2805E+002	-.3507E+002	-.4213E+002	-.4921E+002	-.5832E+002	-.6348E+002
SHIFTED LOCATION DUE TO ERROR 2 (KM)	-.6912E+001	-.1390E+002	-.2089E+002	-.2790E+002	-.3493E+002	-.4199E+002	-.4907E+002	-.5818E+002	-.6333E+002
DIFFERENCE (KM)	-.1397E+000	-.1398E+000	-.1400E+000	-.1404E+000	-.1408E+000	-.1413E+000	-.1419E+000	-.1427E+000	-.1435E+000
ERROR SENSITIVITY(KM/DEG)	-.6981E+001	-.6991E+001	-.7002E+001	-.7018E+001	-.7040E+001	-.7066E+001	-.7097E+001	-.7133E+001	-.7173E+001

ORIGINAL PAGE IS
OF POOR QUALITY

EARTH RADIUS R 6356.7850KM

NOMINAL ALTITUDE H 8000.KM

PITCH ERROR DTHETA 01.DEGREE

VIEW ANGLE ALPHA(DEGREES)	-9.	-8.	-7.	-6.	-5.	-4.	-3.	-2.	-1.	0.
NOMINAL X COORD. (KM)	0.	0.	0.	0.	0.	0.	0.	0.	0.	0.
NOMINAL Y COORD. (KM)	.6340E+02	.5025E+02	.4014E+02	.3200E+02	.2588E+02	.2170E+02	.1907E+02	.1782E+02	.1761E+02	.1838E+02
SHIFTED X COORD. (KM)	.6968E+01	.6980E+01	.6985E+01	.6984E+01	.6978E+01	.6963E+01	.6943E+01	.6918E+01	.6882E+01	.6838E+01
SHIFTED Y COORD. (KM)	.6341E+02	.5026E+02	.4015E+02	.3200E+02	.2588E+02	.2170E+02	.1907E+02	.1782E+02	.1761E+02	.1838E+02
ERROR (KM)	.6968E+01	.6980E+01	.6985E+01	.6984E+01	.6978E+01	.6963E+01	.6943E+01	.6918E+01	.6882E+01	.6838E+01

VIEW ANGLE ALPHA(DEGREES)	1.	2.	3.	4.	5.	6.	7.	8.	9.
NOMINAL X COORD. (KM)	0.	0.	0.	0.	0.	0.	0.	0.	0.
NOMINAL Y COORD. (KM)	-.6982E+01	-.1907E+02	-.2698E+02	-.3288E+02	-.3788E+02	-.4170E+02	-.4414E+02	-.4525E+02	-.4504E+02
SHIFTED X COORD. (KM)	.6982E+01	.6982E+01	.6983E+01	.6984E+01	.6978E+01	.6965E+01	.6965E+01	.6966E+01	.6966E+01
SHIFTED Y COORD. (KM)	-.6983E+01	-.1907E+02	-.2697E+02	-.3288E+02	-.3788E+02	-.4170E+02	-.4414E+02	-.4525E+02	-.4504E+02
ERROR (KM)	.6982E+01	.6982E+01	.6983E+01	.6984E+01	.6978E+01	.6965E+01	.6965E+01	.6966E+01	.6966E+01

GEOMETRIC ERROR SENSITIVITY WITH RESPECT TO PITCH ERROR

EARTH RADIUS R 6356.7850KM

NOMINAL ALTITUDE H 8000.KM

PITCH ERROR 1 DTETA1 = .01DEGREE

PITCH ERROR 2 DTETA2 = -.01DEGREE

VIEW ANGLE ALPHA(DEGREES)	-9.	-8.	-7.	-6.	-5.	-4.	-3.	-2.	-1.	0.
SHIFTED X COORD. DUE TO ERROR 1 (KM)	.6967E+01	.6980E+01	.6985E+01	.6984E+01	.6978E+01	.6963E+01	.6943E+01	.6918E+01	.6882E+01	.6838E+01
SHIFTED Y COORD. DUE TO ERROR 1 (KM)	.6340E+02	.5025E+02	.4014E+02	.3200E+02	.2588E+02	.2170E+02	.1907E+02	.1782E+02	.1761E+02	.1838E+02
SHIFTED X COORD. DUE TO ERROR 2 (KM)	-.6967E+01	-.6980E+01	-.6985E+01	-.6984E+01	-.6978E+01	-.6963E+01	-.6943E+01	-.6918E+01	-.6882E+01	-.6838E+01
SHIFTED Y COORD. DUE TO ERROR 2 (KM)	.6340E+02	.5025E+02	.4014E+02	.3200E+02	.2588E+02	.2170E+02	.1907E+02	.1782E+02	.1761E+02	.1838E+02
DIFFERENCE (KM)	.1397E+00	.1397E+00	.1397E+00	.1397E+00	.1397E+00	.1396E+00	.1396E+00	.1396E+00	.1396E+00	.1396E+00
ERROR SENSITIVITY(KM/DEG)	.6967E+01	.6980E+01	.6985E+01	.6984E+01	.6978E+01	.6982E+01	.6982E+01	.6982E+01	.6981E+01	.6981E+01

VIEW ANGLE ALPHA(DEGREES)	1.	2.	3.	4.	5.	6.	7.	8.	9.
SHIFTED X COORD. DUE TO ERROR 1 (KM)	.6981E+01	.6982E+01	.6982E+01	.6982E+01	.6983E+01	.6984E+01	.6985E+01	.6986E+01	.6987E+01
SHIFTED Y COORD. DUE TO ERROR 1 (KM)	-.6982E+01	-.1907E+02	-.2698E+02	-.3288E+02	-.3788E+02	-.4170E+02	-.4414E+02	-.4525E+02	-.4504E+02
SHIFTED X COORD. DUE TO ERROR 2 (KM)	-.6981E+01	-.6982E+01	-.6982E+01	-.6982E+01	-.6983E+01	-.6984E+01	-.6985E+01	-.6986E+01	-.6987E+01
SHIFTED Y COORD. DUE TO ERROR 2 (KM)	-.6982E+01	-.1907E+02	-.2698E+02	-.3288E+02	-.3788E+02	-.4170E+02	-.4414E+02	-.4525E+02	-.4504E+02
DIFFERENCE (KM)	.1396E+00	.1396E+00	.1396E+00	.1396E+00	.1397E+00	.1397E+00	.1397E+00	.1397E+00	.1397E+00
ERROR SENSITIVITY(KM/DEG)	.6981E+01	.6982E+01	.6982E+01	.6982E+01	.6983E+01	.6984E+01	.6985E+01	.6986E+01	.6987E+01

********** GEOMETRIC ERROR INDUCED BY YAW ERROR **********

EARTH RADIUS R =6356.7650KM

NOMINAL ALTITUDE H =400.KM

YAW ERROR DPSA =1.DEGREE

VIEW ANGLE DLAMDA(DEGREES)	0.	1.	2.	3.	4.	5.	6.	7.	8.	9.
ERROR (KM)	.0000	.1219E+000	.2436E+000	.3650E+000	.4863E+000	.6076E+000	.7288E+000	.8500E+000	.9710E+000	.1092E+001

********** GEOMETRIC ERROR SENSITIVITY WITH RESPECT TO YAW ERROR **********

EARTH RADIUS R =6356.7650KM

NOMINAL ALTITUDE H =400.KM

YAW ERROR 1 DPSI1 = .01DEGREE

YAW ERROR 2 DPSI2 = -.01DEGREE

VIEW ANGLE DLAMDA(DEGREES)	0.	1.	2.	3.	4.	5.	6.	7.	8.	9.
TOTAL SHIFT (KM)	.0000	.2437E-002	.4872E-002	.7318E-002	.9765E-002	.1222E-001	.1468E-001	.1715E-001	.1960E-001	.2213E-00
ERROR SENSITIVITY(KM/DEG)	.0000	.1219E+000	.2436E+000	.3659E+000	.4883E+000	.6109E+000	.7340E+000	.8576E+000	.9818E+000	.1107E+00

ORIGINAL PAGE IS
OF POOR QUALITY

******************** CUMULATIVE ERROR INDUCED BY YAW, PITCH AND ROLL ERRORS ********************

EARTH RADIUS R =6356.785KM

NOMINAL ALTITUDE H =400.KM

YAW ERROR DYAW =1.DEGREE

PITCH ERROR DPITCH =1.DEGREE

ROLL ERROR DROLL =1.DEGREE

VIEW ANGLE DLOMDA(DEGREES)	-9.	-8.	-7.	-6.	-5.	-4.	-3.	-2.	-1.	0.
NOMINAL X COORD. (KM)	0.	0.	0.	0.	0.	0.	0.	0.	0.	0.
NOMINAL Y COORD. (KM)	.6340E+002	.5625E+002	.4914E+002	.4204E+002	.3500E+002	.2797E+002	.2096E+002	.1397E+002	.6982E+001	.0000
SHIFTED X COORD. (KM)	.6005E+001	.6128E+001	.6250E+001	.6372E+001	.6494E+001	.6616E+001	.6738E+001	.6859E+001	.6981E+001	.7104E+001
SHIFTED Y COORD. (KM)	.5637E+002	.4920E+002	.4214E+002	.3515E+002	.2816E+002	.2109E+002	.1409E+002	.7105E+001	.1230E+000	-.6859E+001
ERROR (KM)	.8245E+001	.8296E+001	.8353E+001	.8414E+001	.8480E+001	.8550E+001	.8625E+001	.8704E+001	.8787E+001	.8874E+001

VIEW ANGLE DLOMDA(DEGREES)	1.	2.	3.	4.	5.	6.	7.	8.	9.
NOMINAL X COORD. (KM)	0.	0.	0.	0.	0.	0.	0.	0.	0.
NOMINAL Y COORD. (KM)	-.6982E+001	-.1397E+002	[illegible]	-.2797E+002	-.3500E+002	-.4204E+002	[illegible]	-.5625E+002	-.6340E+002
SHIFTED X COORD. (KM)	.7225E+001	.7347E+001	.7470E+001	.7593E+001	.7717E+001	.7841E+001	.7966E+001	.8092E+001	.8219E+001
SHIFTED Y COORD. (KM)	-.1305E+002	-.2004E+002	-.2705E+002	-.3408E+002	-.4113E+002	-.4901E+002	-.5013E+002	-.6320E+002	[illegible]
ERROR (KM)	.9966E+001	.1006E+002	.1016E+002	.1026E+002	.1037E+002	.1048E+002	.1059E+002	.1072E+002	[illegible]

******************** GROUND POINT SHIFT INDUCED BY SHUTTLE MOTION AND EARTH ROTATION ********************

EARTH RADIUS R=6356.785KM

ORBIT INCLINATION = 85.DEGREE

LATITUDE = 0.DEGREE

GROUND POINT SHIFT VELOCITY DUE TO EARTH ROTATION = .4623E+000KM/SEC

SHUTTLE GROUND SPEED = .7202E+001KM/SEC

GROUND POINT SHIFT VELOCITY RELATIVE TO NADIR POINT = .7177E+001KM/SEC

ANGLE OF VELOCITY VECTOR WITH Y-AXIS =-.8032E+002DEGREE

TIME INTERVAL (SEC)	1.00	.10	.01
SHIFT IN X DIRECTION (KM)	-.7162E+001	-.7162E+000	-.7162E-001
SHIFT IN Y DIRECTION (KM)	.4605E+000	.4605E-001	.4605E-002
TOTAL SHIFT (KM)	.7177E+001	.7177E+000	.7177E-001

********** GROUND POINT SHIFT INDUCED BY SHUTTLE MOTION AND EARTH ROTATION **********

EARTH RADIUS =6350.7850KM

ORBIT INCLINATION = 85.DEGREE

LATITUDE = 20.DEGREE

GROUND POINT SHIFT VELOCITY DUE TO EARTH ROTATION = .4344+000KM/SEC

SHUTTLE GROUND SPEED = .7202+001KM/SEC

GROUND POINT SHIFT VELOCITY RELATIVE TO NADIR POINT = .7175+001KM/SEC

ANGLE OF VELOCITY VECTOR WITH Y-AXIS =-.6054+002DEGREE

TIME INTERVAL (SEC)	1.00	.10	.01
SHIFT IN X DIRECTION (KM)	-.7162+001	-.7162+000	-.7162+001
SHIFT IN Y DIRECTION (KM)	.6325+000	.6325-001	.6325-002
TOTAL SHIFT (KM)	.7175+001	.7175+000	.7175-001

********** GROUND POINT SHIFT INDUCED BY SHUTTLE MOTION AND EARTH ROTATION **********

EARTH RADIUS =6350.7850KM

ORBIT INCLINATION = 85.DEGREE

LATITUDE = 40.DEGREE

GROUND POINT SHIFT VELOCITY DUE TO EARTH ROTATION = .3341+000KM/SEC

SHUTTLE GROUND SPEED = .7202+001KM/SEC

GROUND POINT SHIFT VELOCITY RELATIVE TO NADIR POINT = .7171+001KM/SEC

ANGLE OF VELOCITY VECTOR WITH Y-AXIS =-.8719+002DEGREE

TIME INTERVAL (SEC)	1.00	.10	.01
SHIFT IN X DIRECTION (KM)	-.7162+001	-.7162+000	-.7162+001
SHIFT IN Y DIRECTION (KM)	.3516+000	.3516-001	.3516-002
TOTAL SHIFT (KM)	.7171+001	.7171+000	.7171-001

********** GROUND POINT SHIFT INDUCED BY SHUTTLE MOTION AND EARTH ROTATION **********

EARTH RADIUS =6356.7650KM

ORBIT INCLINATION = 85.DEGREE

LATITUDE = 00.DEGREE

GROUND POINT SHIFT VELOCITY DUE TO EARTH ROTATION = .2311+000KM/SEC

SHUTTLE GROUND SPEED = .7282+001KM/SEC

GROUND POINT SHIFT VELOCITY RELATIVE TO NADIR POINT = .7165+001KM/SEC

ANGLE OF VELOCITY VECTOR WITH Y-AXIS =-.8818+0020EGREE

TIME INTERVAL (SEC)	1.00	.10	.01
SHIFT IN X DIRECTION (KM)	-.7162+001	-.7162+000	-.7162+001
SHIFT IN Y DIRECTION (KM)	.2270+000	.2270-001	.2270-002
TOTAL SHIFT (KM)	.7166+001	.7166+000	.7166+001

********** GROUND POINT SHIFT INDUCED BY SHUTTLE MOTION AND EARTH ROTATION **********

EARTH RADIUS =6356.7650KM

ORBIT INCLINATION = 85.DEGREE

LATITUDE = 80.DEGREE

GROUND POINT SHIFT VELOCITY DUE TO EARTH ROTATION = .8027+001KM/SEC

SHUTTLE GROUND SPEED = .7282+001KM/SEC

GROUND POINT SHIFT VELOCITY RELATIVE TO NADIR POINT = .7162+001KM/SEC

ANGLE OF VELOCITY VECTOR WITH Y-AXIS =-.8948+0020EGREE

TIME INTERVAL (SEC)	1.00	.10	.01
SHIFT IN X DIRECTION (KM)	-.7162+001	-.7162+000	-.7162+001
SHIFT IN Y DIRECTION (KM)	.8943+001	.8943+002	.8943+003
TOTAL SHIFT (KM)	.7162+001	.7162+000	.7162+001

ORIGINAL PAGE IS
OF POOR QUALITY

APPENDIX F

GROUND PATTERN AND IMAGING

DISTORTIONS GENERATION PROGRAM LISTINGS

0000	I	006010	IM	0000	I	006021	IM1	0000	I	005706	IPT
0000	I	005712	J	0000	I	006045	JDD	0000	I	005742	JG
0000	I	006011	JM	0000	I	006022	JM1	0000	I	005723	JR
0000	I	005714	L	0000	R	000000	LAMDA	0000	I	003030	LFLAG
0000	R	000003	LKMDA	0000	R	000002	LYMDA	0000	I	001747	MFLAG
0000	I	005673	NGX	0000	I	005674	NGY	0000	I	006050	NLIN
0000	I	006065	NLIN3	0000	I	006070	NLIN4	0000	I	006073	NLIN5
0000	I	006047	NTIC	0000	I	006053	NTIC1	0000	I	006056	NTIC2
0000	I	006072	NTIC5	0000	I	006061	NTIC6	0000	I	006075	NTIC7
0000	R	006024	PEGA	0000	R	005646	PD	0000	R	005631	PI
0000	R	005630	R	0000	R	005767	RA	0000	R	006037	RAA
0000	R	005751	RHO1	0000	R	006000	ROLL	0000	R	005656	RS
0000	R	005752	SQURT1	0000	R	006023	TAU	0000	R	005743	TEHTA
0000	R	006052	TIC1	0000	R	006055	TIC2	0000	R	006063	TIC3
0000	R	006060	TIC6	0000	R	006074	TIC7	0000	R	005730	T1
0000	R	005747	T21	0000	R	006026	V	0000	R	005636	VS
0000	R	006034	VTY	0000	R	006031	VX	0000	R	006032	VY
0000	R	005740	YB	0000	R	006040	XBB	0000	R	005756	XB1
0000	R	005664	XCENT	0000	R	005757	XC1	0000	R	005220	XDD
0000	R	003262	XF	0000	R	000612	XG	0000	R	004610	XG1
0000	R	005754	XI1	0000	R	005770	XJ	0000	R	006005	XK
0000	R	005675	XLEFT	0000	R	005667	XLEN	0000	R	006017	XL1
0000	R	005707	XNOM	0000	R	000202	XP	0000	R	002140	XP1
0000	R	003221	XP4	0000	R	003015	XP5	0000	R	005172	XP6
0000	R	005661	XSTA	0000	R	006001	XSTA0	0000	R	005774	XT
0000	R	005720	XZ	0000	R	000421	Y	0000	R	005725	YA
0000	R	005651	YAWD	0000	R	005652	YAWS	0000	R	005745	YA1
0000	R	005700	YBOT	0000	R	005755	YB1	0000	R	005703	YC
0000	R	005760	YC1	0000	R	005764	YD	0000	R	005411	YDD
0000	R	003453	YF	0000	R	001003	YG	0000	R	005001	YG1
0000	R	005753	YI1	0000	R	005771	YJ	0000	R	006002	YK
0000	R	005670	YLEN	0000	R	006020	YL1	0000	R	001365	YM
0000	R	000215	YP	0000	R	002153	YP1	0000	R	002201	YP2
0000	R	003247	YP5	0000	R	005205	YP6	0000	R	005615	YP7
0000	R	005644	YSTAP	0000	R	005645	YSTAP1	0000	R	005634	YSTAR
0000	R	005701	YTOP	0000	R	005713	YW	0000	R	000200	YY

```
100      1*      C     DECLARE PARAMETERS
101      2*            PARAMETER NLINES=11,NDT=400,NLAMDA=460,NLPMDA=310,
101      3*           $NLYMDA=450,NLKMDA=480
103      4*
103      5*            REAL LAMDA,LFFDA,LYMDA,LRMDA
104      6*            INTEGER FLAG,AFLAG
105      7*
106      8*      C     DIMENSION OF VARIABLES
106      9*            DIMENSION XX(2),YY(2),XP(NLINES),YP(NLINES),X(NLINES,NLINES)
105     10*           $,Y(NLINES,NLINES),XG(NLINES,NLINES),YG(NLINES,NLINES),
105     11*           $XP(NLINES,NLINES),YM(NLINES,NLINES),MFLAG(NLINES,NLINES),
106     12*           $MFLAG(NLINES,NLINES),XP1(NLINES),YP1(NLINES)
106     13*           $,XP2(NLINES),YP2(NLINES),YM(NLINES,NLINES),YM(NLINES,NLINES)
106     14*           $XFLAG(NLINES,NLINES),YP3(NLINES),YP3(NLINES),XP5(NLINES),
105     15*           $LFLAG(NLINES,NLINES),YP4(NLINES),YP4(NLINES),YP5(NLINES),
105     16*           $XF(NLINES,NLINES),YF(NLINES,NLINES),LFLAG1(NLINES,NLINES),
105     17*           $XM1(NLINES,NLINES),YM1(NLINES,NLINES),MFLAG1(NLINES,NLINES),
```

ORIGINAL PAGE IS
OF POOR QUALITY

```
C0105    18*          $(G1(NLINES,NLINES),YG1(NLINES,NLINES),XP6(NLINES),
00105    19*          $YP6(NLINES),XDD(NLINES,NLINES),YDD(NLINES,NLINES),
00105    20*          $AFLAG(NLINES,NLINES),XP7(NLINES),YP7(NLINES)
00106    21*
C0106    22*           DATA R,PI,F,D,YSTAR,DT,VS,H,DD,DS/6356.785,3.141592654,
00106    23*          $1000000.,400.,-5.5,.0C9,7.1389,440.,.0039,.3/
00121    24*           DATA EPS1,DET,YSTAP,YSTAP1,PD,PS,FLAG/.02,1.,
00121    25*          $-5.,-434.7,.0055,.65,2/
00131    26*           DATA YSTAY,YAWD,YAWS/-5.,.0037,.825/
C0135    27*           DATA DROLL,YSTAO,RD,RS/0.,-5.0,.0042,1./
00142    28*           DATA DTAU,DETA,XSTA,YSTA,VS4/85.,40.,0.,-5.,7.202/
C0150    29*
C0150    30*     C     INITIALIZE THE PLOTTER
00150    31*           CALL PGNPLT
C0151    32*
C0151    33*     C     CENTER PLOT
00151    34*           XCENT=C.0
C0152    35*           YCENT=1.0
C0153    36*           CALL ORIGIN(XCENT,YCENT)
00154    37*
C0154    38*     C     DEFINE THE FORM OF THE PLOT
G0154    39*           PTYPE='LINLIN'
00155    40*           XLEN=P.0
C0156    41*           YLEN=P.0
00157    42*           CALL PLFORM(PTYPE,XLEN,YLEN)
00160    43*
00160    44*     C     SCALE THE PLOT
00160    45*           XX(1)=-8
G0161    46*           XX(2)=8
C0162    47*           YY(1)=-8
00163    48*           YY(2)=8
C0164    49*           NXX=2
00165    50*           NYY=2
00166    51*           NGX=-1
C0167    52*           NGY=-1
C0170    53*           CALL PLSCAL(XX,NXX,NGX,YY,NYY,NGY)
00171    54*
C0171    55*     C     TO START PLOTTING
00171    56*           CALL PLGRAF
C0172    57*
00172    58*     C     DEFINE GRID LIMITS
C0172    59*           XLEFT=-5
00173    63*           XRIGHT=5
00174    61*           XDEL=(XRIGHT-XLEFT)/(NLINES-1)
00175    62*           YBOT=-5
00176    63*           YTOP=5
C0177    64*           YDEL=(YTOP-YBOT)/(NLINES-1)
00203    65*
00200    66*     C     CONSTRUCT DATA
00200    67*           YC=YTOP
00201    68*           DO 150 INOR=1,NLINES
00204    69*           XC=XLEFT
00205    70*           DO 100 IPT=1,NLINES
00210    71*           XNOM=R*SIN(XC/R)
00210    72*     C     XD=(XC-XNOM)*F
00210    73*     C     XNOM=XC-XD
00211    74*           YNOM=YC
```

```
0212      75.           X(IHOR,IPT)=XHOM
0213      76.           Y(IHOR,IPT)=YHOM
0214      77.           XC=XC+XDEL
0215      78.       100 CONTINUE
0217      79.           YC=YC-YDEL
0220      80.       150 CONTINUE
0222      81.           IF(FLAG.EQ.1) GO TO 200
0224      82.           IF(FLAG.EQ.2) GO TO 208
0226      83.           IF(FLAG.EQ.3) GO TO 231
0230      84.           IF(FLAG.EQ.4) GO TO 251
0232      85.           GO TO 261
0233      86.
0233      87.       200 CONTINUE
0234      88.           DO 202 I=1,NLINES
0237      89.           DO 201 J=1,NLINES
0242      90.           NFLAG(I,J)=0
0243      91.       201 CONTINUE
0245      92.       202 CONTINUE
0247      93.           YW=YSTAR
0250      94.           DO 206 L=1,NDT
0253      95.           DLAMDA=DS
0254      96.           DO 205 K=1,NLAMDA
0257      97.           LAMDA=DLAMDA*PI/180.
0260      98.           XW=-R*((1+H/R)*COS(LAMDA)-SQRT(1-((1+H/R)*(1+H/R)*
0260      99.          $SIN(LAMDA)*SIN(LAMDA)))*SIN(LAMDA)
0261     100.           DO 90 I=1,NLINES
0264     101.           DO 70 J=1,NLINES
0267     102.           XZ=XW-X(I,J)
0270     103.           YZ=YW-Y(I,J)
0271     104.           IR=I
0272     105.           JR=J
0273     106.           IF(ABS(XZ).LE.EPSI.AND.ABS(YZ).LE.EPSI) GO TO 204
0275     107.        70 CONTINUE
0277     108.        80 CONTINUE
0301     109.           GO TO 99
0302     110.       204 NFLAG(IR,JR)=1
0303     111.           XF(IR,JR)=D*(-TAN(LAMDA))
0304     112.           YF(IR,JR)=YSTAR+(L-1)*.0285
0305     113.           WRITE(6,98) XW,YW,IR,JR,DLAMDA,XF(IR,JR),YF(IR,JR)
0316     114.        98 FORMAT(/,2F10.5,2I4,3F10.5)
0317     115.        99 DLAMDA=DLAMDA-DD
0320     116.       205 CONTINUE
0322     117.           YW=YSTAR+L*DT*VS
0323     118.       206 CONTINUE
0325     119.           GO TO 299
0326     120.
0326     121.       208 CONTINUE
0327     122.           DO 2 I=1,NLINES
0332     123.           DO 1 J=1,NLINES
0335     124.           NFLAG(I,J)=0
0336     125.         1 CONTINUE
0340     126.         2 CONTINUE
0342     127.           DTHETA=0.
0343     128.           YA=YSTAR
0344     129.           DO 217 L=1,NDT
0347     130.           THETA=DTHETA*PI/180.
0350     131.           DLPMDA=PS
```

ORIGINAL PAGE IS
OF POOR QUALITY

```
 0351    132.          DO 216 K=1,NLPMDA
 0354    133.          LPMDA=DLPMDA*PI/180.
 0355    134.          T1=D*TAN(THETA)
 0356    135.          T2=-ABS(D/COS(THETA))*TAN(LPMDA)
 0357    136.          DEL=SQRT(T1*T1+T2*T2)
 0360    137.          RHO=ATAN(DEL/D)
 0361    138.          SQURT=R*((1+D/R)*COS(RHO)-SQRT(1-(1+D/R)*(1+D/R)*SIN
 0361    139.         $(RHO)*SIN(RHO)))*SIN(RHO))
 0362    140.          YI=(SQURT*T1)/DEL
 0363    141.          XI=(SQURT*T2)/DEL
 0364    142.          YB=YI+YA
 0365    143.          XB=XI
 0366    144.          DO 22 I=1,NLINES
 0371    145.          DO 11 J=1,NLINES
 0374    146.          XC=XB-X(I,J)
 0375    147.          YC=YB-Y(I,J)
 0376    148.          IG=I
 0377    149.          JG=J
 0400    150.          IF(ABS(YC).LE.EPSI.AND.ABS(YC).LE.EPSI) GO TO 210
 0402    151.       11 CONTINUE
 0404    152.       22 CONTINUE
 0406    153.          GO TO 215
 0407    154.      210 NFLAG(IG,JG)=1
 0410    155.          XG(IG,JG)=D*(-TAN(LPMDA))
 0411    156.          YG(IG,JG)=YBOT+(L-1)*.0288
 0412    157.          WRITE(6,212) XB,YB,IG,JG,DLPMDA,XG(IG,JG),YG(IG,JG)
 0423    158.      212 FORMAT(/,2F10.5,2I4,3F10.5)
 0424    159.      215 DLPMDA=DLPMDA-PD
 0425    160.      216 CONTINUE
 0427    161.          YA=YSTAP+L*.0288
 0430    162.          DTHETA=L/2500.
 0431    163.      217 CONTINUE
 0433    164.          GO TO 299

 0434    165.
 0434    166.          DO 220 I=1,NLINES
 0437    167.          DO 219 J=1,NLINES
 0442    168.          NFLAG1(I,J)=0
 0443    169.      219 CONTINUE
 0445    170.      220 CONTINUE
 0447    171.          THETA=DTHETA*PI/180.
 0450    172.          ET=DET*PI/180.
 0451    173.          YA1=YSTAP1
 0452    174.          DO 227 L=1,NDT
 0455    175.          DLPMDA=PS
 0456    176.          DO 226 K=1,NLPMDA
 0461    177.          LPMDA=DLPMDA*PI/180.
 0462    178.          T11=D*TAN(THETA+ET)
 0463    179.          T21=-ABS(D/COS(THETA+ET))*TAN(LPMDA)
 0464    180.          DEL1=SQRT(T11*T11+T21*T21)
 0465    181.          RHO1=ATAN(DEL1/D)
 0466    182.          SQURT1=R*((1+D/R)*COS(RHO1)-SQRT(1-(1+D/R)*(1+D/R)*
 0466    183.         $SIN(RHO1)*SIN(RHO1)))*SIN(RHO1)
 0467    184.          YI1=(SQURT1*T11)/DEL1
 0470    185.          XI1=(SQURT1*T21)/DEL1
 0471    186.          YB1=YI1+YA1
 0472    187.          XB1=XI1
```

```
0473    188*          DO 222 I=1,NLINES
0476    189*          DO 221 J=1,NLINES
0501    190*          XC1=XB1-X(I,J)
0502    191*          YC1=YB1-Y(I,J)
0503    192*          IG1=I
0504    193*          JG1=J
0505    194*          IF(ABS(YC1).LE.EPSI.AND.ABS(YC1).LE.EPSI) GO TO 223
0507    195*      221 CONTINUE
0511    196*      222 CONTINUE
0513    197*          GO TO 225
0514    198*      223 KFLAG1(IG1,JG1)=1
0515    199*          XG1(IG1,JG1)=D*(-TAN(LPMDA))
0516    200*          YG1(IG1,JG1)=YSTAP1+(L-1)*.0288+YI1
0517    201*          WRITE(6,224) YB1,YB1,IG1,JG1,DLPMDA,XG1(IG1,JG1),
0517    202*         $YG1(IG1,JG1)
0530    203*      224 FORMAT(/,2F10.5,2I4,3F10.5)
0531    204*      225 DLPMDA=DLPMDA-PD
0532    205*      226 CONTINUE
0534    206*          YA1=YSTAP1+L*.0288
0535    207*      227 CONTINUE
0537    209*          GO TO 605
0540    209*
0540    210*      231 CONTINUE
0541    211*          DO 4 I=1,NLINES
0544    212*          DO 3 J=1,NLINES
0547    213*          KFLAG(I,J)=0
0550    214*        3 CONTINUE
0552    215*        4 CONTINUE
0554    216*          DYAW=0.
0555    217*          YD=YSTAY
0556    218*          DO 240 L=1,NDT
0561    219*          YAW=DYAW*PI/180.
0562    220*          DLYMDA=YAWS
0563    221*          DO 238 K=1,NLYMDA
0566    222*          LYMDA=DLYMDA*PI/180.
 567    223*          RA=-R*((1+D/R)*COS(LYMDA)-SQRT(1-(1+D/R)*(1+D/R)*SIN(LYMDA)
 567    224*         $*SIN(LYMDA)))*SIN(LYMDA)
 570    225*          XJ=RA*COS(YAW)
 571    226*          YJ=-RA*SIN(YAW)
 572    227*          XE=XJ
 573    228*          YE=YJ+YD
 574    229*          DO 44 I=1,NLINES
 577    230*          DO 33 J=1,NLINES
 602    231*          XT=XE-X(I,J)
 603    232*          YT=YE-Y(I,J)
 604    233*          IH=I
 605    234*          JH=J
 606    235*          IF(ABS(YT).LE.EPSI.AND.ABS(YT).LE.EPSI) GO TO 233
 610    236*       33 CONTINUE
 612    237*       44 CONTINUE
 614    238*          GO TO 235
 615    239*      233 KFLAG(IH,JH)=1
 616    240*          XH(IH,JH)=D*(-TAN(LYMDA))
 617    241*          YH(IH,JH)=YROT+(L-1)*.0288
 620    242*          WRITE(6,234) XE,YE,IH,JH,DLYMDA,XH(IH,JH),YH(IH,JH)
 631    243*      234 FORMAT(/,2F10.5,2I4,3F10.5)
 632    244*      235 DLYMDA=DLYMDA-YAWD
```

ORIGINAL PAGE IS
OF POOR QUALITY

```
0633    245*        238 CONTINUE
0635    246*            YD=YSTAY+L*.0288
0636    247*            DYAW=5.*SIN((L*PI)/174.)
0637    248*        240 CONTINUE
0641    249*            GO TO 299

0642    250*
0642    251*        241 CONTINUE
0643    252*            DO 6 I=1,NLINES
0646    253*            DO 5 J=1,NLINES
0651    254*            LFLAG(I,J)=0
0652    255*          5 CONTINUE
0654    256*          6 CONTINUE
0656    257*            ROLL=DROLL*PI/180.
0657    258*            XSTAO=R*((1+D/R)*(COS(ROLL)-SQRT(1-(1+D/R)*(1+D/R)*SIN(ROLL)
0657    259*           $*SIN(ROLL)))*SIN(ROLL)
0660    260*            YK=YSTAO
0661    261*            DO 250 L=1,NDT
0664    262*            DLRMDA=RS
0665    263*            DO 245 K=1,NLRMDA
0670    264*            LRMDA=DLRMDA*PI/180.
0671    265*            DIS=-R*((1+D/R)*COS(LRMDA+ROLL)-SQRT(1-(1+D/R)*(1+D/R)*SIN
0671    266*           $(LRMDA+ROLL)*SIN(LRMDA+ROLL)))*SIN(LRMDA+ROLL)
0672    267*            XK=DIS+XSTAO
0673    268*            DO 66 I=1,NLINES
0676    269*            DO 55 J=1,NLINES
0701    270*            XL=XK-X(I,J)
0702    271*            YL=YK-Y(I,J)
0703    272*            IM=I
0704    273*            JM=J
0705    274*            IF(ABS(XL).LE.EPSI.AND.ABS(YL).LE.EPSI) GO TO 242
0707    275*         55 CONTINUE
0711    276*         66 CONTINUE
0713    277*            GO TO 244
0714    278*        242 LFLAG(IM,JM)=1
0715    279*            XM(IM,JM)=D*(-TAN(LRMDA))
0716    280*            YM(IM,JM)=YSTAO+(L-1)*.0288
0717    281*            WRITE(6,243) XK,YK,IM,JM,DLRMDA,XM(IM,JM),YM(IM,JM)
 730    282*        243 FORMAT(/,2F10.5,2I4,3F10.5)
 731    283*        244 DLRMDA=DLRMDA-RD
 732    284*        245 CONTINUE
 734    285*            YK=YSTAO+L*.0288
 735    286*        250 CONTINUE
 737    287*
 737    288*        251 CONTINUE
 740    289*            DO 8 I=1,NLINES
 743    290*            DO 7 J=1,NLINES
 746    291*            LFLAG1(I,J)=0
 747    292*          7 CONTINUE
 751    293*          8 CONTINUE
 753    294*            ROLL=DROLL*PI/180.
 754    295*            DER=0.
 755    296*            XSTAO=R*((1+D/R)*(COS(ROLL)-SQRT(1-(1+D/R)*(1+D/R)*SIN(ROLL)
 755    297*           $*SIN(ROLL)))*SIN(ROLL)
 756    298*            YK1=YSTAO
 757    299*            DO 260 L=1,NDT
 762    300*            ER=DER*PI/180.
```

```
0763    301*            DLRMDA=RS
0764    302*            DO 255 K=1,NLRMDA
0767    303*            LRMDA=DLRMDA*PI/180.
0770    304*            DIS1=-R*((1+D/R)*COS(LRMDA+ROLL+ER)-SQRT(1-(1+D/R)*(1+D/R)
0770    305*           $*SIN(LRMDA+ROLL+ER))*SIN(LRMDA+ROLL+ER)))*SIN(LRMDA+ROLL+ER)
0771    306*            XK1=DIS1+XSTAO
0772    307*            DO 98 I=1,NLINES
0775    308*            DO 77 J=1,NLINES
1000    309*            XL1=XK1-X(I,J)
1001    310*            YL1=YK1-Y(I,J)
1002    311*            IM1=I
1003    312*            JM1=J
1004    313*            IF(ABS(XL1).LE.EPSI.AND.ABS(YL1).LE.EPSI) GO TO 252
1006    314*         77 CONTINUE
1010    315*         98 CONTINUE
1012    316*            GO TO 254
1013    317*        252 LFLAG1(IM1,JM1)=1
1014    318*            XM1(IM1,JM1)=D*(-TAN(LRMDA))
1015    319*            YM1(IM1,JM1)=YBOT+(L-1)*.0288
1016    320*            WRITE(6,253) XK1,YK1,IM1,JM1,DLRMDA,XM1(IM1,JM1),
1016    321*           $YM1(IM1,JM1)
1027    322*        253 FORMAT(/,2F10.5,2I4,3F10.5)
1030    323*        254 DLRMDA=DLRMDA-RD
1031    324*        255 CONTINUE
1033    325*            YK1=YSTAO+L*.0288
1034    326*            DER=D.2*SIN((L*PI)/174.)
1035    327*        260 CONTINUE
1037    328*            GO TO 299
1040    329*
1040    330*        261 CONTINUE
1041    331*            DO 263 I=1,NLINES
1044    332*            DO 262 J=1,NLINES
1047    333*            AFLAG(I,J)=0
1050    334*        262 CONTINUE
1052    335*        263 CONTINUE
1054    336*            TAU=DTAU*PI/180.
1055    337*            OMEGA=2.*PI/86400.
1056    338*            ETA=DETA*PI/180.
1057    339*            V=OMEGA*R*COS(ETA)
1060    340*            SLUMDA=COS(TAU)/COS(ETA)
1061    341*            CLUMDA=SQRT(1-SLUMDA*SLUMDA)
1062    342*            VX=V*CLUMDA
1063    343*            VY=V*SLUMDA
1064    344*            VTX=-VX
1065    345*            VTY=VS4-VY
1066    346*            XAA=XSTA
1067    347*            YAA=YSTA
1070    348*            DO 270 L=1,NDT
1073    349*            DLYMDA=YAWS
1074    350*            DO 269 F=1,NLYMDA
1077    351*            LYMDA=DLYMDA*PI/180.
1100    352*            RAA=-R*((1+D/R)*COS(LYMDA)-SQRT(1-(1+D/R)*(1+D/R)*SIN
1100    353*           $(LYMDA)*SIN(LYMDA)))*SIN(LYMDA)
1101    354*            XBB=XAA+FAA
1102    355*            YBB=YAA
1103    356*            DO 265 I=1,NLINES
1106    357*            DO 264 J=1,NLINES
```

ORIGINAL PAGE IS
OF POOR QUALITY

```
1111    358.          XCC=XBB-X(I,J)
1112    359.          YCC=YBB-Y(I,J)
1113    360.          IDD=I
1114    361.          JDD=J
1115    362.          IF(ABS(XCC).LE.EPSI.AND.ABS(YCC).LE.EPSI) GO TO 266
1117    363.       264 CONTINUE
1121    364.       265 CONTINUE
1123    365.          GO TO 268
1124    366.       266 AFLAG(I,J)=1
1125    367.          XDD(IDD,JDD)=D*(-TAN(LYMDA))
1126    368.          YDD(IDD,JDD)=YSTA+(L-1)*.028
1127    369.          WRITE(6,267) XBB,YBB,IDD,JDD,DLYMDA,XDD(IDD,JDD),
1127    370.         $YDD(IDD,JDD)
1140    371.       267 FORMAT(/,2F10.5,2I4,3F10.5)
1141    372.       268 DLYMDA=DLYMDA-DD
1142    373.       269 CONTINUE
1144    374.          XAA=XSTA+L*DT*VTX
1145    375.          YAA=YSTA+L*DT*VTY
1146    376.       270 CONTINUE
1150    377.
1150    378.     C     PLOT HORIZONTAL LINES
1150    379.
1150    380.       299 CONTINUE
1151    381.          TIC=0.0
1152    382.          NTIC=-1
1153    383.          NLIN=NLINES
1154    384.          DO 400 IHOR=1,NLINES
1157    385.          DO 300 IPT=1,NLINES
1162    386.          XP(IPT)=X(IHOR,IPT)
1163    387.          YP(IPT)=Y(IHOR,IPT)
1164    388.       300 CONTINUE
1166    389.          CALL PLCURV(XP,YP,NLIN,NTIC,TIC)
1167    390.       400 CONTINUE
1171    391.
1171    392.     C     PLOT VERTICAL LINES
1171    393.          DO 500 IVERT=1,NLINES
1174    394.          CALL PLCURV(X(1,IVERT),Y(1,IVERT),NLIN,NTIC,TIC)
1175    395.       500 CONTINUE
1177    396.          IF(FLAG.EQ.1) GO TO 655
1201    397.          IF(FLAG.EQ.2) GO TO 805
1203    398.          IF(FLAG.EQ.3) GO TO 901
1205    399.          IF(FLAG.EQ.4) GO TO 909
1207    400.          GO TO 921
1210    401.
1210    402.     C     PLOT HORIZONTAL LINES
1210    403.
1210    404.       655 CONTINUE
1211    405.          TIC1=0
1212    406.          NTIC1=0
1213    407.          NLIN1=NLINES
1214    408.          DO 750 IHOR=1,NLINES
1217    409.          DO 700 IPT=1,NLINES
1222    410.          XP1(IPT)=XF(IHOR,IPT)
1223    411.          YP1(IPT)=YF(IHOR,IPT)
1224    412.       700 CONTINUE
1226    413.          CALL PLCURV(XP1,YP1,NLIN1,NTIC1,TIC1)
1227    414.       750 CONTINUE
```

```
1231    415.
1231    416.      C     PLOT VERTICAL LINES
1231    417.            DO 800 IVERT=1,NLINES
1234    418.            CALL PLCURV(XP61,IVERT),YP(1,IVERT),NLIN1,NTIC1,TIC1)
1235    419.          800 CONTINUE
1237    420.            GO TO 9999
1240    421.
1240    422.      C     PLOT HORIZONTAL LINES
1240    423.          805 CONTINUE
1241    424.            TIC2=0
1242    425.            NTIC2=0
1243    426.            NLIN2=NLINES
1244    427.            DO 850 IHOR=1,NLINES
1247    428.            DO 820 IPT=1,NLINES
1252    429.            XP2(IPT)=XG(IHOR,IPT)
1253    430.            YP2(IPT)=YG(IHOR,IPT)
1254    431.          820 CONTINUE
1256    432.            CALL PLCURV(XP2,YP2,NLIN2,NTIC2,TIC2)
1257    433.          850 CONTINUE
1261    434.
1261    435.      C     PLOT VERTICAL LINES
1261    436.            DO 851 IVERT=1,NLINES
1264    437.            CALL PLCURV(XG(1,IVERT),YG(1,IVERT),NLIN2,NTIC2,TIC2)
1265    438.          851 CONTINUE
1267    439.            GO TO 9999

1270    440.
1270    441.      C     PLOT HORIZONTAL LINES
1270    442.            TIC6=0
1271    443.            NTIC6=0
1272    444.            NLIN6=NLINES
1273    445.            DO 854 IHOR=1,NLINES
1276    446.            DO 853 IPT=1,NLINES
1301    447.            XP6(IPT)=XG1(IHOR,IPT)
1302    448.            YP6(IPT)=YG1(IHOR,IPT)
1303    449.          853 CONTINUE
1305    450.            CALL PLCURV(XP6,YP6,NLIN6,NTIC6,TIC6)
1306    451.          854 CONTINUE
1310    452.
1310    453.      C     PLOT VERTICAL LINES
1310    454.            DO 855 IVERT=1,NLINES
1313    455.            CALL PLCURV(XG1(1,IVERT),YG1(1,IVERT),NLIN6,NTIC6,TIC6)
1314    456.          855 CONTINUE
1316    457.            GO TO 9999
1317    458.
1317    459.      C     PLOT HORIZONTAL LINES
1317    460.          901 CONTINUE
1320    461.            TIC3=0
1321    462.            NTIC3=0
1322    463.            NLIN3=NLINES
1323    464.            DO 905 IHOR=1,NLINES
1326    465.            DO 903 IPT=1,NLINES
1331    466.            XP3(IPT)=XH(IHOR,IPT)
1332    467.            YP3(IPT)=YH(IHOR,IPT)
1333    468.          903 CONTINUE
1335    469.            CALL PLCURV(XP3,YP3,NLIN3,NTIC3,TIC3)
1336    470.          905 CONTINUE
```

ORIGINAL PAGE IS
OF POOR QUALITY

```
01340    471*
01340    472*      C     PLOT VERTICAL LINES
01340    473*            DO 907 IVERT=1,NLINES
01343    474*            CALL PLCURV(XM(1,IVERT),YM(1,IVERT),NLIN3,NTIC3,TIC3)
01345    475*          907 CONTINUE
01346    476*            GO TO 9999
01347    477*
01347    478*      C     PLOT HORIZONTAL LINES
01347    479*          911 CONTINUE
                     **
01350    480*            TIC4=0.0
01351    481*            NTIC4=-1
01352    482*            NLIN4=NLINES
01353    483*            DO 915 IHOR=1,NLINES
 1356    484*            DO 913 IPT=1,NLINES
 1361    485*            XP4(IPT)=XM(IHOR,IPT)
01362    486*            YP4(IPT)=YM(IHOR,IPT)
01363    487*          913 CONTINUE
 1365    488*            CALL PLCURV(XP4,YP4,NLIN4,NTIC4,TIC4)
 1366    489*          915 CONTINUE
 1370    490*
 1370    491*      C     PLOT VERTICAL LINES
 1370    492*            DO 917 IVERT=1,NLINES
 1373    493*            CALL PLCURV(XM(1,IVERT),YM(1,IVERT),NLIN4,NTIC4,TIC4)
 1374    494*          917 CONTINUE
 1376    495*
 1376    496*      C     PLOT HORIZONTAL LINES
 1376    497*          909 CONTINUE
 1377    498*            TIC5=0
 1400    499*            NTIC5=0
 1401    500*            NLIN5=NLINES
 1402    501*            DO 919 IHOR=1,NLINES
 1405    502*            DO 918 IPT=1,NLINES
 1410    503*            XP5(IPT)=XM1(IHOR,IPT)
 1411    504*            YP5(IPT)=YM1(IHOR,IPT)
 1412    505*          918 CONTINUE
 1414    506*            CALL PLCURV(XP5,YP5,NLIN5,NTIC5,TIC5)
 1415    507*          919 CONTINUE
 1417    508*
 1417    509*      C     PLOT VERTICAL LINES
 1417    510*            DO 920 IVERT=1,NLINES
 1422    511*            CALL PLCURV(XM1(1,IVERT),YM1(1,IVERT),NLIN5,NTIC5,TIC5)
 1423    512*          920 CONTINUE
 1425    513*            GO TO 9999
 1426    514*
 1426    515*      C     PLOT HORIZONTAL LINES
 1426    516*          921 CONTINUE
 1427    517*            TIC7=0
 1430    518*            NTIC7=0
 1431    519*            NLIN7=NLINES
 1432    520*            DO 923 IHOR=1,NLINES
 1435    521*            DO 922 IPT=1,NLINES
 1440    522*            XP7(IPT)=YDD(IHOR,IPT)
 1441    523*            YP7(IPT)=YDD(IHOR,IPT)
 1442    524*          922 CONTINUE
 1444    525*            CALL PLCURV(XP7,YP7,NLIN7,NTIC7,TIC7)
 1445    526*          923 CONTINUE
```

```
1447    527*
1447    528*        C       PLOT VERTICAL LINES
1447    529*                DO 924 IVERT=1,NLINES
1452    530*                CALL PLCURV(XDD(1,IVERT),YDD(1,IVERT),NLIN7,NTIC7,TIC7)
1453    531*          924   CONTINUE
1455    532*
1455    533*        C       TO FINISH PLOTTING
1455    534*         9999   CALL ENDPLT
1456    535*
1456    536*          *      STOP
1457    537*                 END


NO FLR:
PU:1.399   CTP:.115   SUPS:9.131

DELETE.A SHUTEVP.IMAGE-1/ABS
URPUR 2-3-JB  05/19/83  11:56:41

TP=.333  SUP=.737  CPU=.000  IO=.302  CC-ER=.433
```


NASA—JPL—Comm, LA, Calif.

End of Document